DOKUZ EYLÜL UNIVERSITY

GRADUATE SCHOOL OF NATURAL AND APPLIED SCIENCES

PRODUCTION OF ANTIBACTERIAL, BIODEGRADABLE AND BIOCOMPATIBLE MATERIALS FOR TISSUE ENGINEERING APPLICATIONS

by

Oylum ÇOLPANKAN GÜNEŞ

September, 2019

İZMİR

PRODUCTION OF ANTIBACTERIAL, BIODEGRADABLE AND BIOCOMPATIBLE MATERIALS FOR TISSUE ENGINEERING APPLICATIONS

A Thesis Submitted to the
Graduate School of Natural and Applied Sciences of Dokuz Eylül University
In Partial Fulfillment of the Requirements for the Degree of Doctor of
Philosophy in Metallurgical and Materials Engineering

by
Oylum ÇOLPANKAN GÜNEŞ
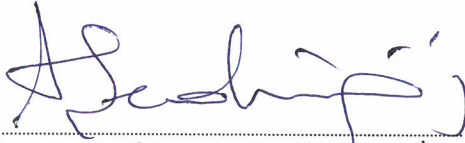
September, 2019
İZMİR

Ph.D. THESIS EXAMINATION RESULT FORM

We have read the thesis entitled **"PRODUCTION OF ANTIBACTERIAL, BIODEGRADABLE AND BIOCOMPATIBLE MATERIALS FOR TISSUE ENGINEERING APPLICATIONS"** completed by **OYLUM ÇOLPANKAN GÜNEŞ** under supervision of **ASSOC. PROF. DR. AYLİN ZİYLAN** and we certify that in our opinion it is fully adequate, in scope and in quality, as a thesis for the degree of Doctor of Philosophy.
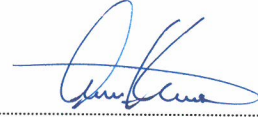
Assoc. Prof. Dr. Aylin ZİYLAN

Supervisor
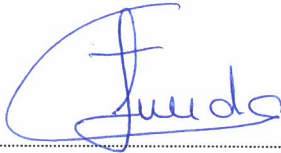
Assoc. Prof. Dr. Aylin ŞENDEMİR

Thesis Committee Member

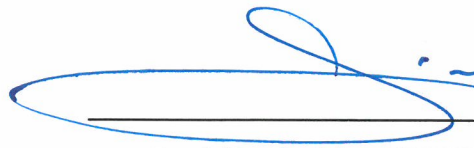Assist. Prof. Dr. Işıl BİRLİK

Thesis Committee Member

Prof. Dr. Funda Tıhmınlıoğlu

Examining Committee Member

Prof. Dr. M. Nalan DEMİR

Examining Committee Member

Prof. Dr. Kadriye ERTEKİN

Director

Graduate School of Natural and Applied Sciences

ACKNOWLEDGMENT

I would like to express my gratitude to my advisor, Assoc. Prof. Dr. Aylin ZİYLAN, for her supervision, guidance, support, understanding and encouragement during my thesis. I would also like to show my great appreciation to Assoc. Prof. Dr. Aylin ŞENDEMİR for her invaluable advice, guidance and support. I also wish to thank to my thesis committee member, Assist. Prof. Dr. Işıl BİRLİK for her fruitful discussions in the thesis.

I would like to express my gratitude to Dr. Berivan ÇEÇEN and Dr. Şeyma TAŞDEMİR for their assistance in biocompatibility studies and evaluation of the corresponding results obtained. I am also thankful to İrem ÜNALAN for her help at the very beginning of this thesis.

I would like to express my gratitude to Prof. Dr. Metin TANOĞLU from the Department of Mechanical Engineering, Izmir Institute of Technology for his assistance in the measurements of viscolelastic properties by dynamic mechanical analyzer. I would like to thank to Research Assistant Pelin BARIŞ KAVUR and Prof. Dr. Ahmet YEMENİCİOĞLU from the Department of Food Engineering, Izmir Institute of Technology for their help in use of texture profile analysis. I wish to thank to Evrim PAŞIK from Biotechnology and Bioengineering Application and Research Center, Izmir Institute of Technology for assisting me in performing antibacterial tests and in evaluation of the corresponding results obtained. I am also thankful to Middle East Technical University, Central Laboratory for porosity measurements.

I would like to appreciate Tülay KOÇ DELİCE for her encouragement, help and the moments that we shared together. I am also grateful to my colleagues.

Finally, I would like to express my special thanks to my mother Şengül

ÇOLPANKAN and my father Recep ÇOLPANKAN for providing me with inspiration and constant encouragement during my graduate work and all my life. I offer sincere thanks my husband, Mehmet Deniz GÜNEŞ for his incredible patience, selfless love and support during this thesis. I am grateful for their invaluable love and understanding for all my life. Without them, this dissertation would not have been materialized. I need them always by my side.

Oylum ÇOLPANKAN GÜNEŞ

PRODUCTION OF ANTIBACTERIAL, BIODEGRADABLE AND BIOCOMPATIBLE MATERIALS FOR TISSUE ENGINEERING APPLICATIONS

ABSTRACT

Tissue engineering aims to restore, maintain, or improve damaged tissue functions. Cells, biochemical factors, and scaffolds are referred to as the key components of tissue engineering. The scaffold has a crucial role in tissue regeneration process by providing a microenvironment for cell attachment, proliferation, and differentiation, and new tissue formation by mimicking an extracellular matrix. This thesis aimed to produce biodegradable and biocompatible materials for bone and cartilage tissue engineering as well as wound healing applications.

In the bone tissue engineering part, three dimensional and porous hydroxyapatite (HAP) incorporated and silk impregnated poly(3-hydroxybutyrate-co-3-hydroxy valerate) (PHBV) nanofibrous cotton wool-like scaffolds were fabricated by wet-electrospinning followed by freeze-drying techniques. The produced scaffolds exhibited improved bioactivity and biomineralization tendency and therefore, it can be evaluated as a candidate filling material for bone regeneration.

In the cartilage regeneration part, PHBV nanofiber reinforced carboxymethyl chitosan (CMCht) - silk hydrogel scaffolds that were cross-linked by poly (ethylene glycol) diglycidyl ether (PEGDE) were prepared. The designed scaffolds demonstrated good properties in terms of damping capability, thermal stability, compressive strength, and chondrogenic differentiation as an indication of being a promising material for cartilage tissue regeneration.

In the wound healing part, modified cotton hydrogel wound dressings were produced by antibacterial nisin incorporation and CMCht-alginate impregnation. It was concluded that the produced dressings would be used as wound dressings for acute wounds due to the fact that they retained their porous structures after modification, had

high water up-take capacity, exhibited viscoelastic properties and antibacterial activity against gram-positive *Staphylococcus aureus* bacteria.

Keywords: Bone tissue engineering, cartilage tissue engineering, wound dressing, biomaterial, biocompatible, antibacterial

DOKU MÜHENDİSLİĞİ UYGULAMALARI İÇİN ANTİBAKTERİYEL, BİYOBOZUNUR VE BİYOUYUMLU MALZEME ÜRETİMİ

ÖZ

Doku mühendisliği, bozulan doku işlevlerini geri kazandırmayı, korumayı veya iyileştirmeyi amaçlamaktadır. Hücre, biyokimyasal faktörler ve doku iskelesi doku mühendisliğinin anahtar bileşenleri olarak ifade edilmektedir. Doku iskelesi, hücre tutunması, çoğalması, farklılaşması ve hücre dışı matrisi taklit ederek yeni doku oluşumu için bir ortam sağlamasından dolayı doku onarımında çok önemli bir role sahiptir. Bu tezin amacı, kemik ve kıkırdak doku mühendisliği ve yara iyileşmesi uygulamaları için biyobozunur ve biyouyumlu malzemeler üretmektir.

Kemik doku mühendisliği bölümünde, hidroksiapatit (HAP) katkılandırılmış ve ipek emdirilmiş üç boyutlu ve gözenekli pamuksu yapıdaki poli (3-hidroksibutirat-ko-3-hidroksi valerat) (PHBV) nanofiber doku iskeleleri ıslak elektro-eğirme ve ardından liyofilizasyon ile üretilmiştir. Üretilen doku iskeleleri, gelişmiş biyoaktivite ve biyo-mineralizasyon eğilimi göstermesi sebebi ile kemik rejenerasyonu için aday bir dolgu malzemesi olarak değerlendirilebilir.

Kıkırdak onarımı bölümünde, poli (etilen glikol) diglisidil eter (PEGDE) ile çapraz bağlanmış PHBV nanofiber takviyeli karboksimetil kitosan (CMCht) - ipek hidrojel doku iskeleleri hazırlanmıştır. Tasarlanan doku iskeleleri darbe sönümleme kabiliyeti, termal kararlılık, basma dayanımı ve kondrojenik farklılaşma açısından iyi özellikler sergilemiş ve kıkırdak dokusu onarımı için umut verici bir malzeme olduğu gösterilmiştir.

Yara iyileşmesi bölümünde, modifiye pamuk hidrojel yara örtüleri antibakteriyel nisin ilave edilmesi ve CMCht-aljinat emdirilmesi ile üretilmiştir. Yara örtülerinin modifikasyon sonrasında gözenekli yapılarını korumaları, yüksek su tutma kapasitesine sahip olmaları, viskoelastik özellik ve gram-pozitif *Staphylococcus aureus* bakterilerine karşı antibakteriyel aktivite göstermelerinden dolayı, akut yaralar

için yara örtüsü olarak kullanılabileceği sonucuna varılmıştır.

Anahtar kelimeler: Kemik doku mühendisliği, kıkırdak doku mühendisliği, yara örtüsü, biyomalzeme, biyouyumlu, antibakteriyel

CONTENTS

LIST OF FIGURES

Page

LIST OF TABLES

CHAPTER ONE
INTRODUCTION

Tissue engineering is an interdisciplinary field that aims to restore damaged tissue and maintain or improve its function. The fundamental principle of tissue engineering approaches involves using cells, biochemical factors, and scaffolds as the key components of tissue engineering either alone or in combination. The scaffold has a crucial role in the repair process by providing a microenvironment for cell attachment, proliferation, differentiation, and new tissue formation by mimicking extracellular matrix. It should mimic the structure, morphology, and bioactivity of the extracellular matrix to modulate cell behavior. Therefore, it should be made from biocompatible and biodegradable materials. It should also have an appropriate surface property and a porous structure with an adequate mechanical property consistent with the implanted site.

This thesis focuses on establishing fundamental science research to produce biomaterials with desired biocompatibility, biodegradability and antibacterial features for bone and cartilage tissue engineering and wound healing applications. For this purpose, the materials, as well as the production techniques, were specifically chosen for the intended uses.

Fundamentally, this thesis consists of three different studies in itself. Each study comprises an introduction, experimental, results and discussion, and conclusion parts. The relevant literature regarding the structure and properties of the selected materials and the related tissue, summary of some recent studies, and objective of the work were presented in the introduction part. The materials, experimental procedures, and characterization techniques used were described in the experimental part. The findings were evaluated in the results and discussion part, and finally, whether the objective of the study was achieved or not was discussed in the conclusion part.

In Chapter 2, the background information consisting of a tissue engineering approach, properties, materials, and fabrication techniques of the scaffold for tissue engineering applications are given in detail.

Chapter 3 includes the study done to design a scaffold for bone tissue engineering application. HAP incorporated and silk impregnated PHBV nanofibrous cotton wool-like scaffolds were produced *via* wet-electrospinning followed by freeze-drying. The suitability of the produced scaffolds as a filling material for bone tissue regeneration was evaluated. Scanning Electron Microscopy (SEM) was used to examine the fibrous and porous structure of the produced scaffolds. Several analytical techniques including Fourier Infrared Spectroscopy (FTIR), X-Ray diffraction (XRD) and thermogravimetric differential thermal analysis (DTA/TGA) were conducted to characterize the chemical and crystalline structures, and thermal behavior of the scaffolds, respectively. Biomineralization studies were performed to evaluate the Ca-P mineralization tendency of the scaffolds in simulated body fluid (SBF). The *in-vitro* biocompatibility tests of the scaffolds were performed using MG-63 osteoblast-like cells and bioactivity of the scaffolds was evaluated by resazurin assay, alkaline phosphatase (ALP) activity, total protein assay (BCA), and histological and immunohistochemical analyses.

In chapter 4, hydrogel composite scaffolds were developed for the cartilage tissue engineering applications. PHBV nanofiber reinforced CMCht-SF hydrogel composite scaffolds that can mimic the structure and mechanical properties of the cartilaginous ECM were produced. Hydrogel scaffolds were chemically cross-linked by PEGDE at different CMCht-SF and PEGDE ratios. The morphology of the three-dimensional porous scaffolds was examined by SEM. The chemical structures and cross-linking behavior of the hydrogel scaffolds were evaluated by FTIR. Swelling ratios and water contents of the swollen hydrogel scaffolds were obtained. Thermal behavior and viscoelastic properties of the scaffolds were also evaluated by DTA/TGA and DMA, respectively. Texture profile analyzer was used in two-cycle compression mode to examine the mechanical properties of the scaffolds in a swollen state. Compressive mechanical properties were also presented in a dry state. The attachment, viability and

proliferation, and chondrogenic differentiation of rat bone marrow-derived mesenchymal stem cells on the scaffolds were investigated by SEM, Alamar assay, and histological analysis by alcian blue staining, respectively.

In chapter 5, antibacterial hydrogel composite wound dressings were produced by modifying the natural textile material, cotton. In line with this objective, the CMCht-alginate polymers were integrated into the cotton and freeze-dried. Then, nisin was impregnated to the modified cotton and after the cross-linking reaction, antibacterial hydrogel composite wound dressings were obtained. Morphological, chemical structure and thermal behavior characterization of the wound dressings were performed by SEM, FTIR, and DTA/TGA, respectively. Swelling ratios and water contents of the hydrogel wound dressings were presented. The viscoelastic properties of the hydrogel wound dressings were examined by DMA. Antibacterial activity of the hydrogel wound dressings was evaluated against gram-positive *S. aureus* and gram-negative *E. coli*.

Finally, conclusions of the studies and future work of the thesis were given in chapter 6.

CHAPTER TWO
THEORETICAL BACKGROUND

2.1 Tissue Engineering

Tissue damage and loss arising from disease, injury or trauma are one of the major health care problems in all over the world (Chapekar, 2000). In order to reconstruct the devastated tissues, tissue transplantation and implantation of biomedical devices are the most commonly used treatment strategies (Sahithi, Swetha, Ramasamy, Srinivasan, & Selvamurugan, 2010). In the tissue transplantation strategy, autografts (tissue transplantation from one site to another on the body of a patient) are a promising and lifesaving solution, but they have limited donor availability and also harvesting autografts is expensive and painful. Allografts (tissue transplantations from one person to another) do not limit by a donor and could be alternatives to autografts. However, they have the potential risk of immune response and carrying the infection or disease from the donor to the patient (O'brien, 2011; Vasita & Katti, 2006). On the other hand, biomedical devices are generally used for temporary solutions because they do not repair all the functions of damaged tissue. Infection and potential rejection of the implant are other important disadvantages of this procedure. The rapid increment in the need for tissue treatment has elicited the development of alternative treatments to overcome the disadvantages of traditional treatment strategies (Chen, Ushida, & Tateishi, 2002; Mikos & Temenoff, 2000).

Even though the tissue engineering term was first defined in a National Science Foundation workshop in 1988, the common and widely used definition was made by Robert Langer and Joseph P. Vacanti in 1993 as the 'an interdisciplinary field that applies the principles of engineering and life sciences toward the development of biological substitutes that restore, maintain or improve tissue or organ function' (Chapekar, 2000; O'brien, 2011; Smith, Liu, & Ma, 2008).

2.2 Components of Tissue Engineering

Cells, biochemical factors, and scaffolds are designated as the key components of tissue engineering strategy and the fundamental principle of tissue engineering approaches is to use these components of either alone or in combination (Chan & Leong, 2008).

Basically, tissue engineering strategies involve three approaches. The first strategy, cell transplantation, involves the direct injection of healthy cells removed from donor tissue into the damaged tissue but the probability of new tissue formation is about 10% in this technique (Ebnesajjad, 2012). The second strategy is related to delivering biochemical factors to the damaged tissue. These two strategies are more suitable for the treatment of smaller defects. In addition, the need for producing the tissue with practical size scale and predetermined shapes limits the use of these approaches (Ma, 2004). Therefore, the third approach, implanting the scaffold into the damaged area has become more important and more relevant with the concept of tissue engineering. This scaffold-guided regeneration involves using the scaffold into the damaged area to improve tissue regeneration. In addition, cell loaded scaffold implantation are the basis of most current tissue engineering strategy. In this approach, isolated healthy cells from a patient are subjected to an *in-vitro* environment for their expansion first and then, they were seeded onto a scaffold. These cell-scaffold constructs are implanted into the defect area, scaffold gradually degrades over time and meanwhile, new tissue forms (Dhandayuthapani, Yoshida, Maekawa, & Kumar, 2011; Ebnesajjad, 2012; Martina & Hutmacher, 2007; Shin, Jo, & Mikos, 2003).

In the last approach, cell-scaffold constructs, it is aimed to produce an artificial extracellular matrix (ECM) that is a suitable environment for cell growth just like in their native tissue. ECM is the non-cellular and three-dimensional network that surrounds cells and present in all tissues. It gives mechanical support for the cellular constituents and also serves to regulate many cellular behaviors (Frantz, Stewart, & Weaver, 2010; Kim et al., 2011). The scaffold provides a microenvironment for cell attachment, proliferation, and differentiation, and new tissue formation by mimicking

extracellular matrix. Also, it helps in carrying the biomolecular signals for cells. Therefore, scaffold plays a vital role in tissue regeneration and repair process (Liu, Xia, & Czernuszka, 2007; Ma, 2008).

2.2.1 Properties of the Tissue Engineering Scaffold

Since the design and fabrication of the biomimetic scaffolds are a compelling process, physicochemical, biological and mechanical properties, structure and degradation kinetics should be considered (Chen, Ushida, & Tateishi, 2002; Smith, Liu, & Ma, 2008).

Irrespective of the tissue type, there are several critical design requirements that the suitable scaffold for use in tissue engineering needs to meet:

a) Biocompatibility is the first and very important criterion of the scaffold. It is defined as the "ability to be in contact with a living system without producing an adverse effect" according to IUPAC Recommendations (Vert et al., 2012). The scaffold must be biocompatible that cells could attach and migrate through the structure, and proliferate to form new tissue. In addition, scaffold material should not induce any inflammation or adverse response after implantation (O'brien, 2011).

b) Scaffolds are not permanent implants and they act only as temporary ECM until the new tissue formation is completed in the damaged area. Therefore, biodegradability of the scaffolds is a critical requirement. Since in the regeneration process, scaffold degradation allows cells to produce their own extracellular matrix and eventually grown tissue replace the scaffold, it is important that the degradation rate of the scaffold should match the rate of new tissue formation. In addition, the degradation products of the scaffolds should be non-toxic and can be removed from the body (Ma, 2004; O'brien, 2011).

c) The scaffold should have appropriate surface properties that permit cell attachment, promote cell growth and differentiation. Surface wettability is one of the

important surface properties and hydrophilic surfaces improve cell attachment and spreading (Unalan, Colpankan, Albayrak, Gorgun, & Urkmez, 2016). Surface topography and roughness are other important properties but their effects depend on the on the targeted tissue (Chang & Wang, 2011).

d) The architecture of the scaffold is of critical importance for the scaffold design. The scaffold should possess interconnecting pore structure and high porosity to transport of nutrients and metabolic wastes to the cells and to improve cell adhesion, extracellular matrix regeneration, tissue integration, and vascularization. In the cell attachment stage, cells interact with the scaffold by the help of chemical groups, ligand, on the material surface. Cell-scaffold affinity is closely related to ligand density which is influenced by a specific surface area. Therefore, it is critical to determine the optimum pore size of the scaffold, it should be large enough to allow migration of cells towards the deeper layer of the scaffold and also be small enough to supply sufficient ligand density for cell adhesion (Haugh, Murphy, & O'Brien, 2009; O'brien, 2011; Sachlos & Czernuszka, 2003; Sun, Zhou, & Lee, 2011)

e) The scaffold must have adequate mechanical properties consistent with the implanted site to ensure support to the tissue growth. For example, scaffold could deform when the compressive strength of the scaffold is too low and do not allow tissue growth. Besides, very high compressive strength can lead to inadequate conditions to support cell growth in vivo. In addition, if the difference of elastic moduli value between the scaffold and natural tissue is too high, delamination of the scaffold from the surrounding tissue can occur. The scaffold must be handled without any deformation during the implantation and it is also very important that it should maintain its mechanical integrity until new tissue formation is occurred (Ebnesajjad, 2012; Ma, 2004; Sachlos & Czernuszka, 2003).

f) Scaffolds are three-dimensional porous solid tissue engineering constructs and in the production of the scaffold, cost-effective manufacturing technology become important. The scaffold should be easily fabricated into the desired three-dimensional

structure with different shapes and sizes (Dhandayuthapani, Yoshida, Maekawa, & Kumar, 2011; O'brien, 2011; Sachlos & Czernuszka, 2003)

2.3 Scaffolds for Tissue Engineering

Biomaterials, materials contact with living tissues, used to produce tissue engineering scaffold should enable the cell attachment, proliferation and eventually new tissue formation by the help of the interaction with cells. Therefore, the selection of these materials offers significant importance for the success of the practice. In the biomaterial selection, various criteria of the biomaterials should be considered, for example; their chemistry, solubility, wettability, degradation mechanism etc. A variety of biomaterials such as biopolymers, bioceramics or their combination, biocomposites, have been used for different tissue engineering applications (Armentano, Dottori, Fortunati, Mattioli, & Kenny, 2010; Dhandayuthapani, Yoshida, Maekawa, & Kumar, 2011; O'brien, 2011).

2.3.1 Biopolymers

Biopolymers have gained great interest for different tissue engineering applications and they are generally considered as the primary choice for the production of scaffolds due to their unique properties such as good biocompatibility, ability to promote the new tissue formation prior to biodegradation and ease in tailoring composition and structure for the desired purpose easily. They can be classified as natural and synthetic biopolymers according to their origin (Dhandayuthapani, Yoshida, Maekawa, & Kumar, 2011; Liu & Ma, 2004; Liu, Lim, & Teoh, 2013).

2.3.1.1 Natural Biopolymers

Natural biopolymers include polysaccharides, e.g. chitosan, alginate, cellulose, starch; proteins, e.g. collagen, silk, gelatin and polynucleotides (DNA, RNA) (Dhandayuthapani, Yoshida, Maekawa, & Kumar, 2011). These polymers are from renewable resources, environmentally-friendly polymers and they can be mentioned

as the first biodegradable biomaterials used for tissue regeneration (Dhandayuthapani, Yoshida, Maekawa, & Kumar, 2011; Okamoto & John, 2013).

They have been widely used for different tissue engineering applications due to their superior biocompatible and biodegradable properties. Natural biopolymers are the main constitutes of the native extracellular matrix of the body and therefore, the structural similarity of the scaffolds made of natural biopolymers allows them to have biological recognition that improves the cell adhesion and function (Basha & Doble, 2015; Swetha et al., 2010). They are degraded by the enzymes in the body and the degradation products are non-toxic; therefore, they can be utilized by the cells. Despite their advantages, they have poor mechanical properties and they may exhibit an adverse immunological response. The control of the degradation rate is hard due to the possible differences in host enzyme level. In addition, they do not have batch-to-batch uniformity, they are limited in supply and leading to high cost (Armentano, Dottori, Fortunati, Mattioli, & Kenny, 2010; Liu & Ma, 2004).

Collagen is the main structural element in bone, cartilage, and skin and among the natural biopolymers, it is the most studied one for tissue engineering scaffolds with the aim to mimic the natural extracellular matrix. It is the most abundant protein in the mammals and is in the nanofibrous form. The triple-helical structure of collagen arises from an unusual abundance of glycine, proline, and hydroxyproline amino acids. They make up the characteristic repeating unit of Gly-Pro-X, where X can be any amino acid. There are 28 different types of collagen and among them, type-I collagen is more suitable for bone and skin regeneration, whereas type-II collagen is mostly used for cartilage regeneration. However, there are some drawbacks of collagen such as poor mechanical properties, possible pathogen transmission, adverse immune reaction, high cost, a challenge in the control of biodegradability and in the production (Liu, Xia, & Czernuszka, 2007; Ma, 2004; Ma & Zhang, 1999; Shoulders & Raines, 2009).

Another well-known and mostly used fibrous protein is silk. It is characterized by a highly repetitive primary sequence, β-sheet structure, just like the triple helices of the collagen. It can be produced by different insect larvae, including silkworm

(Bombyx mori). The silk obtained from the cocoon of Bombyx mori composed of a major protein, fibroin, and a glue-like protein, sericin. Fibroin has an amino acid sequence of alanine–glycine with serine or tyrosine. It forms the filaments of silk with giving the silk unique physical and chemical properties. Sericin holds the fibroin fibers together to form the cocoon case to protect the growing worm. It has been widely used in the textile industry as high-performance fiber and biomedical applications as sutures. In addition, it has been introduced and frequently used in the different tissue engineering fields in various forms such as film, hydrogel, porous sponge or fibrous mat. It has advantages over other proteins such as good biocompatibility, high mechanical properties, and low-cost production (Altman et al., 2003; Kim, Nam, Lee, & Park, 2003; Kundu, Rajkhowa, Kundu, & Wang, 2013; Vepari & Kaplan, 2007). Yang et al., (2015), produced silk-based scaffolds and concluded that the biocompatibility and the cell proliferation of these scaffolds were better than the collagen one.

Polysaccharides are another group of natural biopolymers. Chitosan, alginate, hyaluronate are common examples of polysaccharides. They have been used as tissue engineering scaffolds, especially for cartilage regeneration due to the structural similarity of native cartilage extracellular matrix (Eslahi, Simchi, Mehrjoo, Shokrgozar, & Bonakdar, 2016; Ma, 2004).

Chitosan is a linear polysaccharide produced from the partial deacetylation of chitin which is one of the main structural components of the exoskeleton of crustaceans. Chitosan is composed of D-glucosamine and N-acetyl-D-glucosamine units linked by β-(1-4). The chemical structures of the chitin and chitosan are shown in Figure 2.1. The ratio of glucosamine to N-acetyl glucosamine of chitosan is the degree of deacetylation (DD). The DD is an important parameter that affects the crystallinity as well as the solubility of the polymer. The intermediate degrees of DD caused the minimum crystallinity. Chitosan has the generally recognized as safe (GRAS) approval from the Food and Drug Administration (FDA). The application area of chitosan varies from the food and cosmetic to the biomedical and biotechnological fields due to its favorable properties such as low toxicity, good biocompatibility, and

high biodegradability. The presence of positively charged amino groups in the backbone results in chitosan being a natural polycation at acidic pH. The antimicrobial activity of chitosan is strongly related with the interaction of these positively charged amino groups with a negatively charged microbial cell membrane, leading to osmotic damage with the leakage of proteins and other constitutes of the microorganism (Bhattarai, Gunn, & Zhang, 2010; Perinelli et al., 2018; Pranoto, Rakshit, & Salokhe, 2005) Despite the fact that chitosan is widely used in different forms such as beads, films, fibers, membranes, hydrogels for different fields, its solubility only in acid limits its biological applications. Therefore, recently chemically modified chitosan derivatives have been proposed to eliminate this drawback of chitosan.
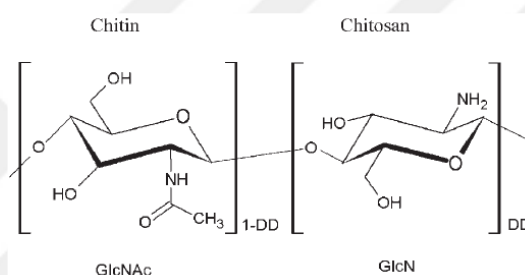
Figure 2.1 Chemical structures of chitin and chitosan (Thein-Han, Kitiyanant, & Misra, 2008)

Carboxymethyl chitosan (CMCht) is the most commonly used chitosan derivative. It is produced by carboxymethylation of chitosan which introduced the carboxymethyl (-COOCH$_3$) group in the primary or secondary hydroxyl groups and the amino groups bonded to the glucopyranose unit. Derivatives of CMCht can be amino substituted (N-CMC), hydroxyl substituted (O-CMC) or both amino and hydroxyl substituted (N, O-CMC). A schematic representation of the synthesis of these derivatives are shown in Figure 2.2. CMCht has desirable water-solubility due to carboxymethyl groups on hydroxyl sites of the glucosamine units. It also maintains the advantages of chitosan such as low toxicity and high biocompatibility in addition to its good water-solubility (Bhattarai, Gunn, & Zhang, 2010; Gonçalves, da Silva, Signini, & Naves, 2017; LogithKumar et al., 2016).
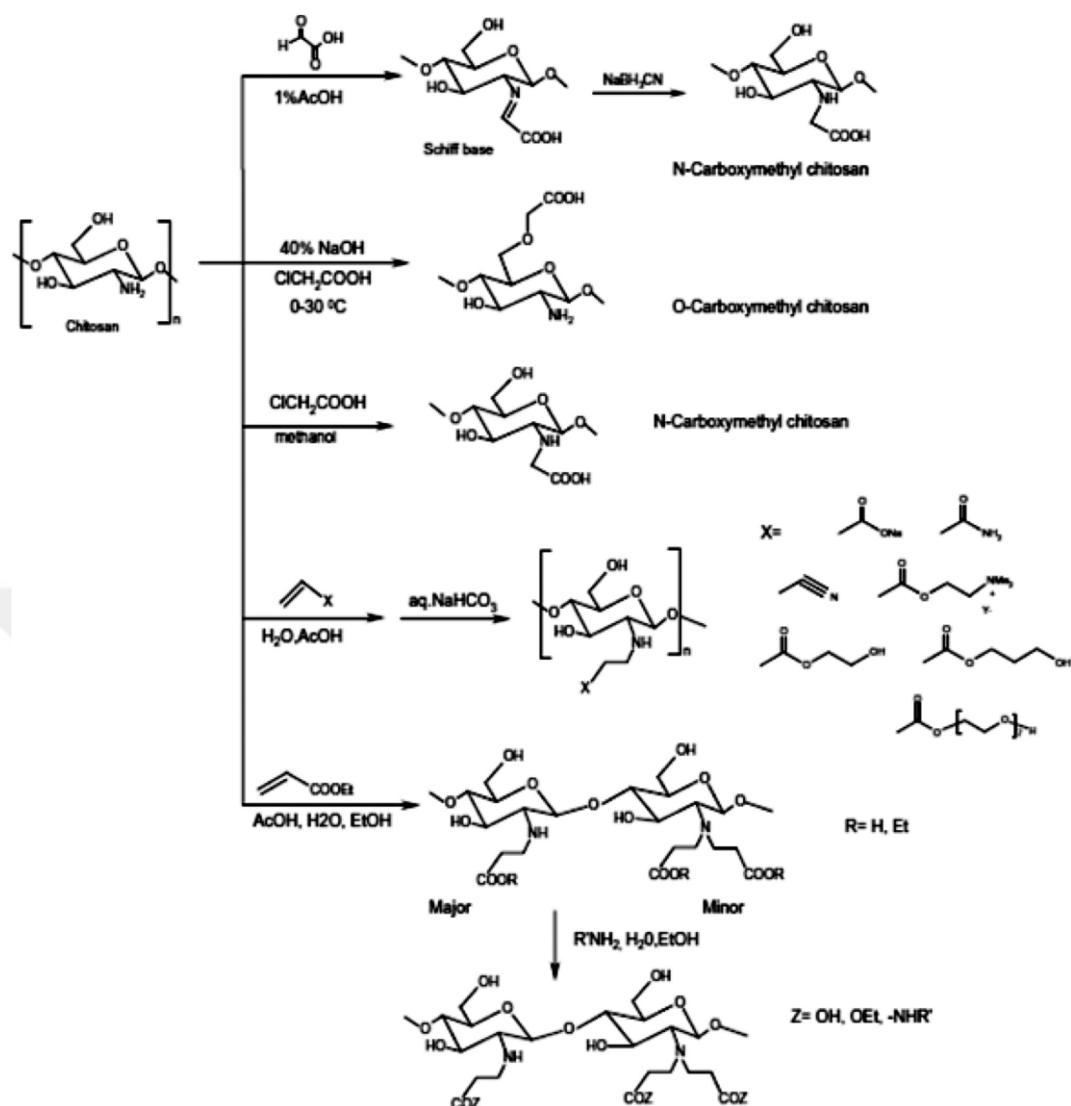
Figure 2.2 Carboxymethylation of chitosan (LogithKumar et al., 2016)

Alginate is the other important and most commonly used linear polysaccharide. It is obtained by the extraction from brown algae with alkali treatment, followed by addition of sodium or calcium chloride in order to precipitate the alginate, and then the alginate salt is transformed into alginic acid by treatment with dilute HCl. Alginate is a linear copolymer composed of 1,4-linked β-d-mannuronic acid (monomer M) and α-l-guluronic acid (monomer G) residues. The chain can be composed of homopolymeric regions of M or G, and heteropolymeric regions where G and M exist in alternating sequence. It contains unbound carboxyl and hydroxyl groups and they allow to combine with other polymers and compounds. The most common method to obtain alginate hydrogels is ionic cross-linking of alginate solution with ionic cross-linking

agents, such as divalent cations such as Ca^{2+}, Sr^{+2}, Ba^{+2}. Only the G-blocks of alginate are participated in cross-linking with divalent cations. In the presence of these cations, chains undergo rearrangement, G-blocks form junctions with the G-blocks of adjacent polymer chains in what is termed the egg-box model of cross-linking. The physical properties of the obtained alginate hydrogels are affected by M/G ratio and sequence, G-block length, and molecular weight. The increased length and molecular weight of G-block result in the enhanced mechanical properties of alginate hydrogels due to the fact that G-block is stiffer than M-block. In recent decades, alginate hydrogels have been adopted in a broad range of biomedical applications such as wound dressings, drug delivery, cell immobilization, and tissue engineering due to its low toxicity after purification, highly hydrophilic, good biocompatible and biodegradable properties (da Silva, Vidart, da Silva, Gimenes, & Vieira, 2017; Lee & Mooney, 2012; Lewandowska-Łańcucka et al., 2017; Zhang, Liu, Yang, & Zhu, 2015).

2.3.1.2 Synthetic Biopolymers

Synthetic biopolymers have attracted great attention in the biomedical field, including tissue engineering due to their advantages over natural biopolymers. Even though, natural biopolymers have the advantage of biological recognition, they have important drawbacks such as possible adverse immune responses and transportation of pathogenic impurities, poor mechanical properties, uncontrollable biodegradability, batch-to-batch non-uniformity and high cost (Armentano, Dottori, Fortunati, Mattioli, & Kenny, 2010; Liu & Ma, 2004). Synthetic biodegradable polymers, approved by US Food and Drug Administration (FDA), have relatively good mechanical strength and more predictable properties with batch-to-batch uniformity properties. They also have the unique advantage having tailored property profiles for specific applications (Armentano, Dottori, Fortunati, Mattioli, & Kenny, 2010; Liu, Xia, & Czernuszka, 2007; Nair & Laurencin, 2007).

Poly(α-ester)s, poly(carbonate)s, poly(fumarate)s and poly(hydroxy alkanoate)s are the common examples of synthetic biodegradable polymers and among them, poly(α-ester)s are the most widely used group in tissue engineering applications (Liu, Xia, &

Czernuszka, 2007). Figure 2.3 shows the most common poly(α-ester)s with their chemical structures.

Poly(glycolic acid)
(PGA)

Poly(lactic acid)
(PLA)

Poly(lactic acid-co-glycolic acid)
(PLGA)

Poly(caprolactone)
(PCL)

Poly(3-hydroxybutyrate)
(PHB)

Poly(3-hydroxyvalerate)
(PHV)
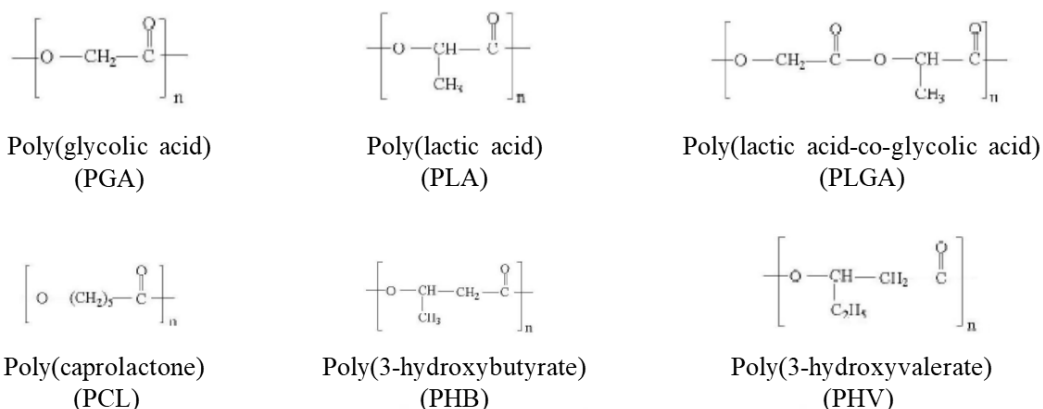
Figure 2.3 Chemical structures of the most common used poly(α-ester)s (Gunatillake & Adhikari, 2003)

Poly(glycolic acid) (PGA), poly(lactic acid) (PLA) and their copolymer poly(lactic acid-co-glycolic acid) (PLGA) are the most extensively used linear aliphatic poly(α-ester)s for the production of tissue engineering scaffolds in different forms such as non-woven fibrous mats, sponges, or films (Liu, Xia, & Czernuszka, 2007; Sachlos & Czernuszka, 2003). They are hydrolytically degradable polymers due to the hydrolytically labile ester bonds in their backbone and their degradation products are already present in the human body and are eliminated easily from the body. PGA degrades between two and four weeks due to its relatively hydrophilic property. Since PLA has an extra methyl group giving it more hydrophobic nature, its degradation rate is much lower than PGA. It takes approximately a year to lose its mechanical integrity. The copolymers of these two polymers, PLGA, is used to obtain the intermediate degradation profile for the intended use. The rate of degradation can be tailored by using different ratios of LA/GA. PCL has similar biocompatibility to PLA and PGA, however, it degrades more slowly (Liu, Xia, & Czernuszka, 2007; Ma, 2004).

Polyhydroxyalkanoates (PHA)s have been recently used for tissue engineering. They are a family of natural biodegradable polyesters and produced by microorganism as their energy source, therefore they are called as bacterial polyesters. Poly(3-hydroxybutyrate) (PHB), poly(3-hydroxy valerate) (PHV) and their copolymer poly(3-hydroxybutyrate-co-3-hydroxy valerate) (PHBV), poly(3-hydroxyoctanoate) (PHO),

poly(3-hydroxynonanoate) (PHN) are typical examples of this family. Among them, only PHBV is produced commercially and used for different biomedical applications including wound dressing, drug delivery, and tissue engineering. It is a non-toxic and biocompatible polymer. However, it is a hydrophobic polyester, by combining with other polymers its hydrophilicity and so biocompatibility can be improved. The degradation time of PHBV is longer than PLA and PGA which allows to maintain the mechanical integrity until the tissue formation occurs in long-term applications. In addition, it can be easily formed into a nanofibrous structure which is a very important factor for the tissue engineering scaffold so as to mimic the natural extracellular matrix (Ai et al., 2011; Li, Yang, & Loh, 2016; Sultana & Wang, 2008).

2.3.2 Bioceramics

Bioceramics are classified into three groups; bioinert (e.g. alumina and zirconia), bioactive (e.g. bioactive glasses) and bioresorbable ceramics (e.g. calcium phosphates). Bioinert ceramics are defined as materials that do not initiate any response with the host while maintains its structure after implantation (Patel & Gohil, 2012). Therefore, bioactive glasses and calcium phosphates are preferred in hard tissue engineering applications. Among them, β-tricalcium phosphate (β-TCP) and hydroxyapatite (HAP) are the most commonly used examples (Ma, 2004). They possess excellent biocompatibility with hard tissues without giving any cytotoxic or antigenic effect. They are also very important for their regeneration ability that they are considered as both osteoconductive and osteoinductive (Liu, Xia, & Czernuszka, 2007; Ma, 2004). Hydroxyapatite, with a general formula $Ca_{10}(OH)_2(PO_4)_6$, is the main inorganic element of natural bone and therefore, synthetic HAPs have been widely used in bone tissue engineering scaffolds (Sun, Zhou, & Lee, 2011; Swetha et al., 2010; Zhou & Lee, 2011). However, the use of these bioceramics by themselves for tissue engineering applications has been limited due to their mechanically brittle properties and difficulty in the processing into a desired porous structure (O'brien, 2011).

2.3.3 Biocomposites

Composites comprise matrix and reinforcement phases so that desirable properties of these phases can be combined. Biocomposites, containing biopolymer matrix and bioceramic reinforcement, have attracted great attention in the biomedical field since they have the advantages of both components and they can meet all the desired requirements for the intended use. Biocomposites are commonly used in bone tissue regeneration studies to develop synthetic bone ECM which comprises collagen fibrils containing embedded hydroxyapatite nanoparticles. The brittle nature and difficulty of processing of the bioceramics are overcomed when they are combined with natural or synthetic biopolymers. In this manner, the mechanical properties and integration ability with hard tissues of natural biopolymers are also enhanced. As a conclusion, biocomposites designed for bone healing possess good biocompatibility with osteoconductive and osteoinductive properties and improved mechanical strength (Liu, Lim, & Teoh, 2013; Sun, Zhou, & Lee, 2011; Zhou & Lee, 2011).

2.4 Commonly Used Fabrication Techniques of the Scaffolds

The tissue engineering scaffold morphology is an important factor for the tissue regeneration process. Among the requirements of the scaffolds, high interconnected porous structure and appropriate surface properties are related to the morphology of the scaffold and the scaffold structure is determined by the used fabrication techniques. The commonly used fabrication techniques in order to produce porous and/or fibrous scaffolds are given in this section (Dhandayuthapani, Yoshida, Maekawa, & Kumar, 2011; Weigel, Schinkel, & Lendlein, 2006).

In tissue engineering applications, porous scaffolds have been extensively used due to their help on the metabolic by products and nutrients transportation to the cells as well as providing a 3D environment for tissue growth and formation. In this approach, pore architecture and porosity value of the scaffolds for each intended use have a significant importance for determining the cellular activity of the scaffolds (Haugh, Murphy, & O'Brien, 2009).

It is very important that the tissue engineering scaffolds could mimic the native ECM which consists of mainly fibrous proteins to improve the regeneration process. Therefore, nanofibrous scaffolds have gained increasing attention in the tissue engineering applications due to this structural similarity of the ECM (Frantz, Stewart, & Weaver, 2010; Holzwarth & Ma, 2011b; Vasita & Katti, 2006).

2.4.1 Solvent Casting-Particulate Leaching (SC/PL) Technique

This technique is a combination of solvent casting and particulate leaching. In the solvent casting technique, polymer solution casts into a predefined 3D mold and solvent evaporates. It is a simple and inexpensive technique to operate, whereas the obtained porosity (~70%) is not enough for tissue engineering applications. Therefore, in order to create porous scaffolds solvent casting is used together with a particulate leaching technique (Sun, Zhou, & Lee, 2011).

Initially, in the SC/PL technique, polymer solution uniformly mixed with water-soluble particles, porogens, such as inorganic salts or crystals of saccharose is prepared and casted. After that, the solvent is evaporated and the particle integrated polymer matrix is immersed in water to remove the water-soluble particles from the matrix so as to create a porous structure. The schematic illustration of the SC/PL technique is seen in Figure 2.4 (Mikos & Temenoff, 2000; Zhu & Chen, 2013).

This SC/PL technique is simple and allows to produce highly porous structure (up to 97%). Controllability of the porosity and pore size of the scaffolds by the amount and size of the added water-soluble particles is the advantage of this technique. However, this technique is not suitable to produce thicker 3D scaffolds, the thickness of the materials produced is limited to 2 mm due to the difficulty of removing the particles from the polymer matrix. In addition, the limited pore connectivity and residual toxic organic solvents are the other disadvantages of this technique (Ebnesajjad, 2012; Liu & Ma, 2004).
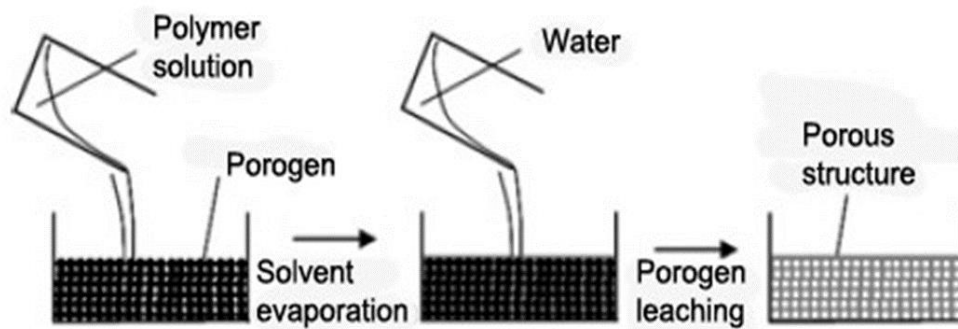
Figure 2.4 Schematic illustration of SC/PL technique (Zhu & Chen, 2013)

2.4.2 Gas Foaming Technique

Gas foaming technique has been developed by Mooney's group, in order to produce porous scaffolds without using toxic organic solvents (Mooney, Baldwin, Suh, Vacanti, & Langer, 1996). In this technique, contrarily to SC/PL technique gas-foaming agents such as carbon dioxide or nitrogen is used to make porous structures. The initial step of this technique is the formation of solid discs of polymers obtained by compression molding. After that, these discs are exposed to gas-foaming agents at high pressures until they saturate. Then, the pressure is decreased rapidly to atmospheric pressure and it initiates a thermodynamic instability which results in nucleation and growth of the pores. The schematic illustration of the gas foaming technique is seen in Figure 2.5 (Mikos & Temenoff, 2000; Sachlos & Czernuszka, 2003).

This technique allows obtaining scaffolds to have up to 97% porosity with pore sizes ranges between 100 to 500 µm. Although these values can be obtained without using any organic solvent and leaching process, a non-porous layer at the surface is formed after the process. Also, it is difficult to obtain interconnected pores and control pore sizes. This layer and unconnected pores make the cell adhesion and spread difficult throughout the scaffold (Ebnesajjad, 2012; Zhu & Chen, 2013).
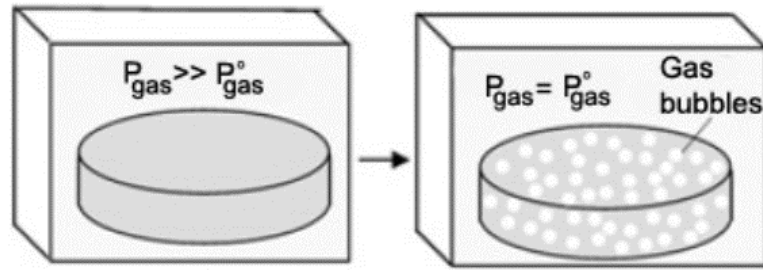
Figure 2.5 Schematic illustration of gas foaming technique (Zhu & Chen, 2013)

2.4.3 Freeze-Drying Technique

The freeze-drying technique has been widely used for the fabrication of tissue engineering scaffolds due to its promising results in the formation of highly porous structure. This technique consists of basically two steps. In the freezing step which is the first one, a polymer solution is cooled down to low temperatures, it freezes and solvent forms ice crystals. After that in the drying step, frozen sample is subjected to lower pressures in order to remove ice crystals in the structure by sublimation and it leads to a porous scaffold at the end of the process. By altering the cooling regime in this technique, the percent porosity value and the pore size distribution of the scaffold can be adjusted (Lu, Li, & Chen, 2013; Zhu & Chen, 2013).

2.4.4 Phase Separation Technique

Phase separation techniques has been used to fabricate porous scaffolds for tissue engineering applications since 1990s, and separation can be induced thermally or by a non-solvent. However, non-solvent induced phase separation technique is not very common for the fabrication of tissue engineering scaffolds due to the heterogeneous pore structure of the obtained scaffolds. Thermally induced phase separation technique (TIPS) can produce the scaffolds with a desired homogeneous porous structure by using thermal energy to induce phase separation. It consists of cooling the homogenous polymer solution leading to thermodynamically unstable which induces into a multiphase system, comprising a polymer-poor and polymer-rich phases. Subsequently, the polymer-rich phase solidifies to form a matrix and the polymer-poor phase turns into pores as a result of solvent removal. The morphology of the scaffolds

produced by the TIPS technique can be controlled by manipulating the process parameters (Akbarzadeh & Yousefi, 2014; Lu, Li, & Chen, 2013; Nam & Park, 1999). It is also possible to produce fibrous structures under the right conditions. Ma & Zhang, 1999 obtained nanofibrous foams in order to mimic the structure of collagen fibrous in the ECM. In their study, PLLA was dissolved in THF and the solvent is exchanged with water, and they were freeze-dried. In this technique, the polymer-rich phase forms the nanofibrous matrix and the polymer-poor phase is extracted, leaving behind nanofibers ranging from 50 to 500 nm (Holzwarth & Ma, 2011b; Smith, Liu, & Ma, 2008; Vasita & Katti, 2006).

Although the use of harsh organic solvents, uncontrollable fiber diameters, long production times, and being a small-scale technique that is suitable only for limited polymers are the disadvantages of TIPS technique, it is a relatively simple technique and has the advantage of simultaneous production of nano and macro-architecture (Holzwarth & Ma, 2011a; Lu, Li, & Chen, 2013; Vasita & Katti, 2006).

2.4.5 Electrospinning Technique

Electrospinning is an attractive, important and most widely studied technique that is utilized for the production of porous and nanofibrous polymeric tissue engineering scaffolds by using natural and synthetic polymers (Pham, Sharma, & Mikos, 2006; Vasita & Katti, 2006).

The history of electrospinning, also known as electrostatic spinning, dates back to more than 100 years ago. It was started with Lord Rayleigh in 1882 by his studies about the charges to overcome the surface tension of a drop. The first devices were developed to spray liquids through the application of an electrical charge in the early 1900s by Cooley and Morton for the applications in textiles and filters. However, the production of fibers by electrospinning was materialized by Antonin Formhals. Between 1934 and 1944, he published a series of patents describing the process and apparatus to obtain polymer filaments by means of electrostatic force. The technique has improved a lot from that years to this time and since the 1980s, electrospinning

process has attracted more attention in nanotechnology due to the processability of ultrafine polymeric fibers in nanoscale (Bhardwaj & Kundu, 2010; Greiner & Wendorff, 2007; Sill & von Recum, 2008; Zhu & Chen, 2013).

Electrospinning technique utilizes electrostatic forces in order to produce fibers or fibrous structures from a polymer solution (Smith, Liu, & Ma, 2008) The schematic illustration of the electrospinning setup is seen in Figure 2.6. Basically, there are three main components of the setup; syringe pump, a high voltage source, and a collector (Zhu & Chen, 2013). A metallic needle is connected to a syringe which is full of a polymer solution and by using a syringe pump, the polymer solution can be fed towards the needle at a constant feeding rate. When a high voltage is applied, the drop of the polymer solution at the nozzle of the metallic needle becomes a positively charged. It has experienced the electrostatic repulsion within the polymer solution as well as the electrostatic attraction between an oppositely charged collector and the polymer drop. These interactions become stronger as the electric field increase and the droplet is distorted into a conical shape, known as Taylor cone. A further increase in the voltage results in a threshold value of the electric field, at which electrostatic forces overcome the surface tension of polymer solution and the fiber jet is formed. Instability in the jet causes whipping motion that elongate and thin the jet with solvent evaporation while travelling to the collector. Eventually, fibers are formed onto the collector (Li & Xia, 2004; Pham, Sharma, & Mikos, 2006; Sill & von Recum, 2008).
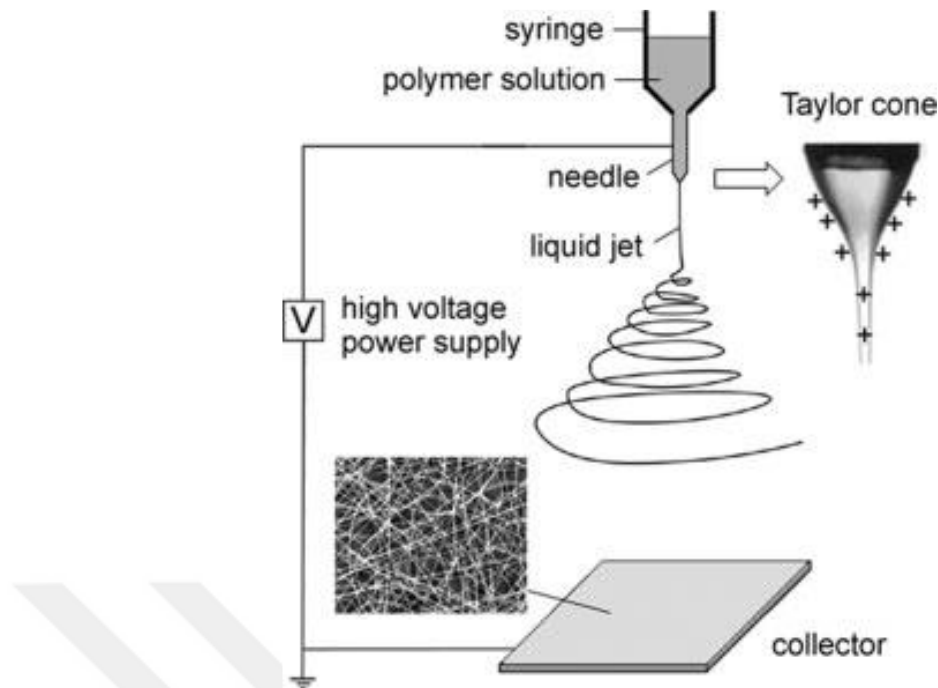
Figure 2.6 Schematic illustration of the electrospinning setup (Li & Xia, 2004)

Electrospinning is a quite simple and effective technique to produce polymeric nanofibers for various application areas. Electrospun nanofibers are widely used for tissue engineering scaffolds due to their similar morphology that mimics the natural ECM as well as features that improve cell-scaffold interaction such as high surface area and high porosity. Simple processing technique, ability to produce nanofibers from various synthetic and natural polymers, and control over fiber diameter by altering the parameters are other advantages of this technique. However, the obtained electrospun membranes are two-dimensional and it is difficult to produce three-dimensional scaffolds by electrospinning technique. This major disadvantage of electrospinning limits its use for many applications (Smith, Liu, & Ma, 2008; Tamayol et al., 2013; Vasita & Katti, 2006).

2.4.5.1 Electrospinning Parameters

It is very important that the electrospinning process becomes continuous and the obtained fibers are uniform and bead-free. In this technique, there are some parameters that greatly affect the morphology and diameter of the fibers as well as the continuous

spinning: solution, processing, and environmental parameters (Martins, Reis, & Neves, 2008).

2.4.5.1.1 Solution Parameters. Polymer solution parameters such as concentration, viscosity, surface tension, and conductivity have an important role for the formation of uniform fiber without any beads, as well as determining the diameter of the obtained fibers (Vasita & Katti, 2006).

Polymer concentration is very important for determining the formation of fiber by affecting the viscosity and surface tension. The increase in the polymer concentration in the solution results in an increase in the viscosity of the solution. It must have high enough to occur chain entanglements. However, there should be an optimum solution concentration for the electrospinning process. If the concentration is too low, polymer fiber will break up into droplets before reaching the collector. Besides, beads are formed instead of fibers and as concentration increases the spherical beads turn to spindle-like shaped and finally uniform fibers. At higher polymer concentrations, it become difficult to maintain the flow of the solution and fibers could not be formed or even if obtained, it resulted in larger diameters (Bhardwaj & Kundu, 2010; Pham, Sharma, & Mikos, 2006; Sill & von Recum, 2008). For example, Katti, Robinson, Ko, & Laurencin, 2004 demonstrated the effect of the polymer solution concentration to the morphology of the electrospun nanofibers. They prepared a PLGA solutions at different concentrations by dissolving in a solvent mixture of tetrahydrofuran (THF): dimethylformamide (DMF) (3:1). At the polymer concentration of 0.1, 0.15 and 2 g /ml beaded structures were obtained, but upon increasing polymer concentration bead density decreased and nanofibers without beads were obtained after the concentrations of 0.25 g/ml. The same spinning parameters were used as an applied voltage of 20 kV cm^{-1}, a flow rate of 2 ml/h. The SEM images of the obtained electrospun nanofibers at different polymer concentration are shown in Figure 2.7.
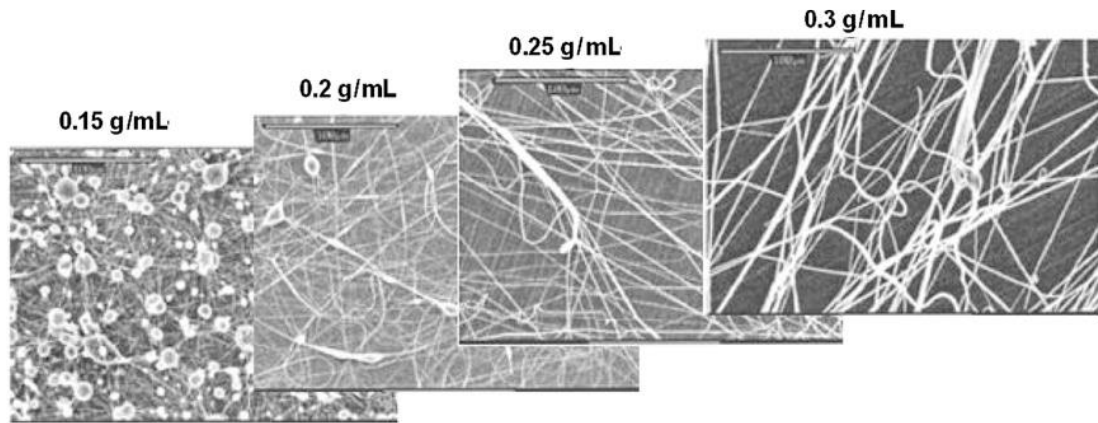
Figure 2.7 SEM images of electrospun PLGA fibers at different polymer solution concentrations (Kumbar, James, Nukavarapu, & Laurencin, 2008)

Surface tension, a function of the solvent composition in the polymer solution, has a crucial role in the fiber formation without beads in the electrospinning process. In the electrospinning process if electrostatic forces can overcome the surface tension force, fibers are obtained. The surface tension of the polymer solution changes according to the solvent used in the polymer solution. The solution viscosity and surface tension changes in the polymer solution consisting ethanol and dimethyl formaldehyde (DMF) are shown in Figure 2.8. The high surface tension of the solution cause the instability of the jet and spray droplets are obtained. Using the polymer solution with a lower surface tension can help to produce fibers without beads. However, the decrement in the surface tension of the solvent is not enough alone and always for a successful fiber formation during the electrospinning (Bhardwaj & Kundu, 2010; Ramakrishna, 2005).
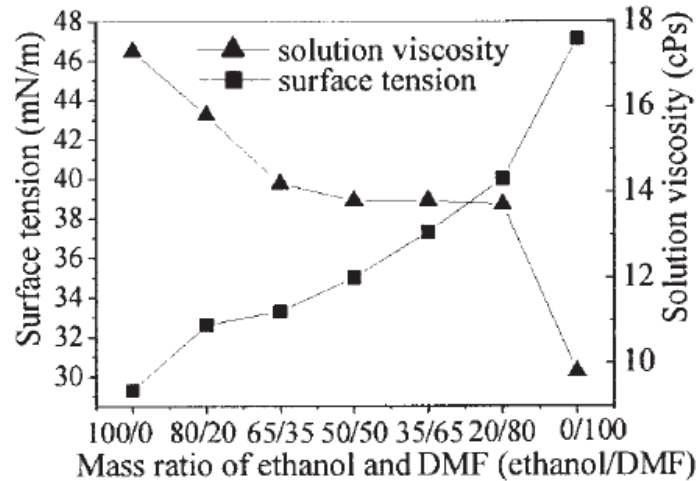
Figure 2.8 Surface tension and viscosity changes as a function of mass ratio of ethanol and DMF (Yang et al., 2004)

The charged ions in the polymer solution which determines the conductivity of the solution are important for the fiber jet formation during the electrospinning. The conductivity of the solution is determined by the used polymer, solvent, and the presence of the ionizable salts. It has been stated that electrospinning of the polymer solution with a high electrical conductivity results in smaller fiber diameter. Mainly there are two approaches to increase the conductivity of the polymer solution; addition of salt or surfactants (Bhardwaj & Kundu, 2010; Huang, Zhang, Kotaki, & Ramakrishna, 2003). The addition of ionic salts to the polymer solution such as sodium chloride (NaCl), potassium chloride (KCl), monopotassium phosphate (KH_2PO_4), monosodium phosphate (NaH_2PO_4), and benzyl triethylammonium chloride (BTEAC) increase the solution conductivity, and allow to obtain uniform bead-free fibers with smaller diameters by electrospinning. For example, Zong et al., 2002 obtained bead-free PLA and PLLA nanofibers with smaller diameters by adding KH_2PO_4 and NaCl ionic salts. Yang, Wang, Zhang, Liu, & Jiang, 2009 dissolved polycarbonate in chloroform with anionic, zwitterionic, nonionic and cationic surfactants, and subjected to electrospinning. They only obtained a successful fiber formation with a solution including cationic surfactant by leading to increase solution conductivity.

25

2.4.5.1.2 Processing Parameters. Processing parameters include applied voltage, flow rate, and distance between needle tip and collector, known as working distance. It is very important to obtain optimum processing parameters to determine ultrafine fibers with a diameter in nanoscale.

In the electrospinning process, for the formation of fiber jet and eventually fiber with solvent evaporation, a threshold value of the electric field at which electrostatic forces overcome the surface tension of polymer solution and the fiber jet is formed should be passed. Therefore, an applied voltage is a crucial parameter in the electrospinning process. At relatively lower voltages, pendant drop of the solution is formed at the tip of the needle and then, Taylor cone forms at the tip of the pendant drop. However, at higher voltages, until the formation of Taylor cone the volume of the pendant drop decreases (Figure 2.9). Further increment in the voltage causes the formation of fiber jet directly which is related with the beads in the fibers. Besides, even though, there are different interpretations, applied voltage has an effect on the fiber diameter. Some researchers reported that higher voltages in the electrospinning process results in the formation larger diameter fibers due to its higher polymer injection. As in the most cases, other researches have suggested that higher applied voltages allow to enhance the electrical field and increase the electrostatic forces in the fiber jet which results in the formation of fibers with smaller diameters. In conclusion, applied voltage affects the fiber diameter and bead formation, it is more accurate to evaluate all the parameters together to obtain uniform and bead-free nanofibers in the electrospinning process (Bhardwaj & Kundu, 2010; Sill & von Recum, 2008).
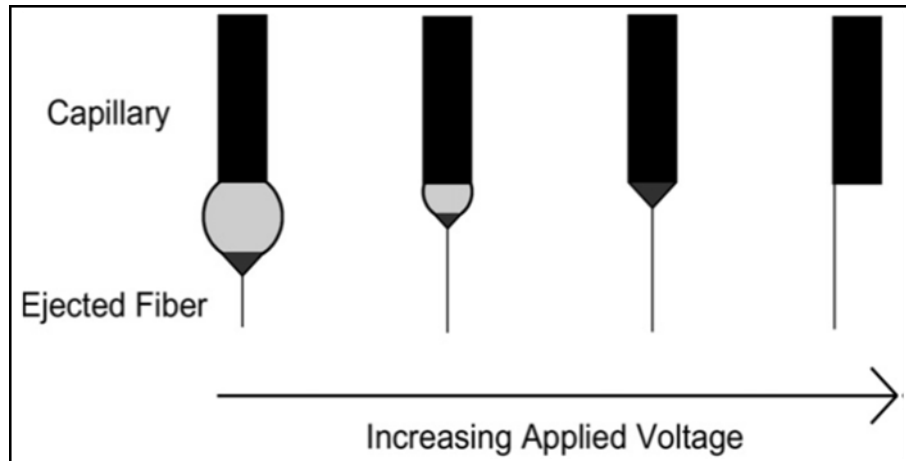
Figure 2.9 Changes in the Taylor cone at different applied voltages (Sill & von Recum, 2008)

Flow rate of the solution affects the fiber morphology and diameter. It has been stated that if the flow rate is not high enough to replace the solution fed as the fiber jet, Taylor cone at the tip of the needle is not maintained. In addition, using lower flow rates in the electrospinning process results in smaller diameters. Fiber diameter and pore sizes increase upon increasing flow rate. Besides, higher flow rates cause incomplete fiber drying during the spinning which leads to bead defects and formation of ribbon-like fibers (Pham, Sharma, & Mikos, 2006; Sill & von Recum, 2008).

The distance between needle tip and collector, working distance, has an effect on the morphology and diameter of the fiber even if it plays a smaller role than that of other parameters. In addition, the working distance designates whether the process ends with electrospinning or electro spraying. It has been stated that, the working distance should be high enough to allow the evaporation of the solvent before fibers are arrived the collector. Beaded fibrous structure is obtained at both too high and too low working distances (Pham, Sharma, & Mikos, 2006; Sill & von Recum, 2008).

2.4.5.1.3 Environmental Parameters. Temperature and humidity are environment parameters and they have significant importance for continuous spinning (Sill & von Recum, 2008; Zhu & Chen, 2013).

27

2.4.6 Wet-electrospinning Technique

Wet-electrospinning technique is one of the techniques developed to overcome the drawback of the electrospinning so that 3D nanofibrous structures can easily be produced in an effective way. Other developed techniques are multilayer electrospinning, post-processing of the 2D membranes and using a 3D template. It is important to have a 3D structure for tissue engineering scaffolds due to their advantages over 2D membranes in cell-cell interaction, cell migration and cell morphogenesis (Kim & G. Kim, 2014; Sun et al., 2014).

On the contrary of conventional electrospinning, in the wet-electrospinning technique, nanofibers are collected in a liquid bath, known as a coagulation bath, instead of a solid and metallic collector. The schematic illustration setup of this technique is seen in Figure 2.10. During the process, nanofibers are wet-electrospun into the coagulation bath which contains low surface tension non-solvents and then, the homogenously suspended nanofibers are collected from the bath, and freeze-dried to provide the cotton-wool-like 3D structures (Kostakova, Seps, Pokorny, & Lukas, 2014; Meli, Miao, Dordick, & Linhardt, 2010; Taskin et al., 2016).
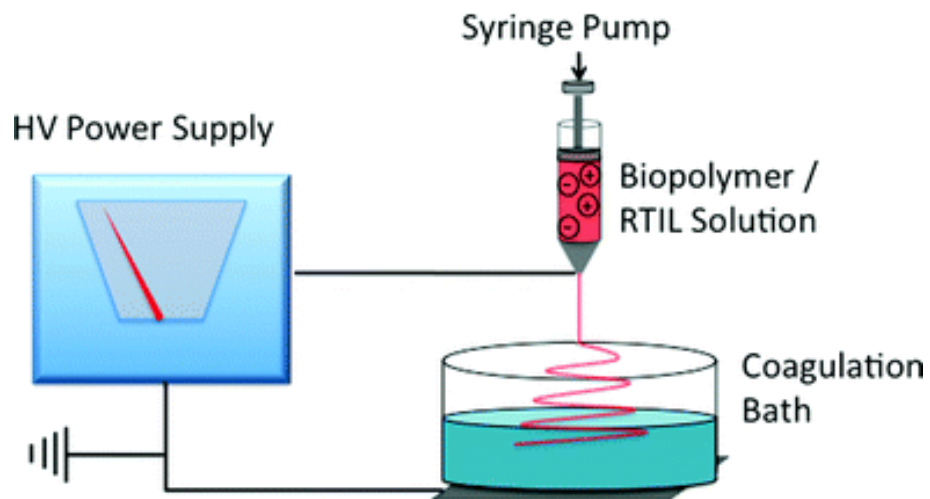
Figure 2.10 Schematic illustration of the wet-electrospinning technique (Meli, Miao, Dordick, & Linhardt, 2010)

2.4.7 Three-Dimensional Printing

Three-Dimensional Printing (3D-P) technique produces 3D structures by layering printing process with adhesive bonding, using powder as a base material. In this technique, firstly a layer of powder is spread over a building platform. Then, ink jet printing head scans the surface and eject binder from a jet head that moves in accordance to the CAD cross-sectional data. Here, the binder dissolves and joins adjacent powder particles to form a layer. Once the solvent has properly bonded the particles together, the build piston is lowered, another layer of powder is deposited and the process is repeated for each subsequent layer until the 3D structures obtained. After drying of the binder, the nonjoined powder is removed by an air jet flow. The resolution of 3D-P can be adjusted by the particle size of the powder, the nozzle size and degree of control over the position controller that defines print-head movement. The drawbacks of 3D-P include difficulties in removing the support powder from complex architectural features deep within the scaffold and the complete removal of the organic solvent (Liu, Xia, & Czernuszka, 2007; Weigel, Schinkel, & Lendlein, 2006).

CHAPTER THREE
BONE TISSUE ENGINEERING STUDY

3.1 Introduction

Bone tissue engineering aims to regenerate bone defects and induce the formation of new tissue by means of tissue engineering components (cells, biochemical factors, and a scaffold). In the tissue engineering strategies, it is important that the bone tissue engineering scaffold should mimic the bone ECM in composition, structure and function in order to modulate cell behavior (Puppi, Chiellini, Piras, & Chiellini, 2010; Stiers, van Gastel, & Carmeliet, 2016).

Bone ECM is a natural composite comprising well-arrayed HAP particles ($Ca_{10}(OH)_2(PO_4)_6$) embedded in collagen fibers. Synthetic HAP has been widely used in tissue engineering applications due to its similarity to the inorganic component of bone ECM as well as its good biocompatible and osteoconductive properties. However, its fragile character and low mechanical strength limit its further clinical application. Therefore, in order to meet all requirements of bone tissue engineering scaffold, composites of biodegradable polymers and HAP particles have attracted great attention (Hong et al., 2004; Zhou & Lee, 2011).

Scaffolds with nanofibrous structure have attracted great attention because they resemble structural similarity to the bone ECM (Jang, Castano, & Kim, 2009). Electrospinning is the simplest and widely applied technique with successful results for the production of nanofibers for tissue engineering applications (Vasita & Katti, 2006).

Song, Kim, & Kim, 2008 produced HAP incorporated collagen nanofibrous mats by electrospinning method for bone tissue engineering applications. First, they co-precipitated nanocomposite solution and freeze-dried. After dissolving the freeze-dried product, it was subjected to electrospinning process. They concluded that

produced nanofibrous mats with highly elongated HAP particles within the collagen fibers showed good biocompatibility on MC3T3-E1 osteoblastic cells.

In the study of Zhang et al., 2008, the *in-vitro* biological activities of human fetal osteoblast cells on HAP/chitosan nanofibers produced by electrospinning were reported in order to mimic the bone ECM structurally. Test results demonstrated that the incorporation of HAP nanoparticles significantly improved the bone formation compared to that of the pure chitosan nanofibrous structure.

Kim, Che, Ha, & Ryu, 2014 prepared electrospun silk fibroin mats which have a large surface area and high porosity. Besides, they added HAP nanoparticles in order to enhance the mechanical properties of the silk fibroin mats. Composite electrospun mat showed improved mechanical properties tested by a tensile test, and good biocompatibility results on the culture of human osteoblast cells.

In addition to the composites of natural biopolymers containing HAP, composites made from synthetic polymers and HAP have also attracted an enormous attention for bone tissue engineering. Kim, Lee, & Knowles, 2006 developed HAP/PLA nanocomposite fibers by electrospinning for bone regeneration. They introduced the use of HSA as a surfactant to uniformly disperse hydrophilic HAP nanopowders in a hydrophobic medium and maintain a stable solution. According to the good results of cell viability and proliferation, they concluded that developed HAP/PLA nanocomposite nanofibers may have the potential in tissue engineering applications.

Song, Ling, Ma, Yang, & Chen, 2013 prepared composite fibrous mats of HAP grafted PLLA particles (HAP-g-PLLA) and PLGA by electrospinning, and evaluated them in terms of mechanical properties, bioactivity, and biocompatibility. The highest strength of the fibrous mats was obtained for the composites consisting of 5 wt% HAP-g-PLLA nanoparticles. They concluded that the particle content affects the degradation and bioactivity of the composite fibrous mats directly. Besides, the highest particle content resulted in a more osteoblast cell adhesion and spread than that of other composites and pure PLGA fibrous mats.

Nanofibers produced by mixing of synthetic and natural biopolymers increase cell adhesion, spread, and proliferation. Paşcu, Stokes, & McGuinness, 2013 prepared HAP/PHBV/SF fibrous composites by electrospinning as bone regeneration scaffolds. Formation of bone-like apatite crystals was seen on the surface of the prepared composite fibrous mats as a result of the improved bioactivity. The mechanical properties also enhanced compared to that of the pure fibrous mat. *In-vitro* biological test results concluded that composite fibrous mats improved osteoblast cell attachment and proliferation.

Even though electrospinning has been a widely used technique for the production of fibrous structures for tissue engineering applications, the produced fibrous mats are two-dimensional. The third dimension in the tissue engineering scaffold gives better results in terms of cell adhesion, migration, and proliferation. Therefore, in order to produce three-dimensional fibrous structures by electrospinning, several modified techniques have been introduced such as multilayer electrospinning, post-processing of produced two-dimensional fibrous mats, use of a three-dimensional template or a liquid collector- coagulation bath (Sun et al., 2014). The wet-electrospinning technique is the modified electrospinning technique in which a coagulation bath is used instead of a metallic collector. It consists of spinning of a polymer solution into the coagulation bath, collecting the homogeneously suspended nanofibers and freeze-drying them to obtain a three-dimensional fibrous structure (Kostakova, Seps, Pokorny, & Lukas, 2014; Taskin et al., 2016).

Wet-electrospinning technique is a promising and newly developed technique for the production of three-dimensional fibrous structures. It was first introduced by Yokoyama et al., 2009 for the preparation of three-dimensional spongiform cotton-wool like PGA nanofibers.

Gang et al., 2012 used the wet-electrospinning technique for the fabrication of three-dimensional PLGA microfibrous scaffolds for skin tissue engineering applications. They showed that fabricated scaffolds improved normal human dermal fibroblast migration and proliferation compared to that of the electrospun mat.

Díez-Pascual & Díez-Vicente, 2016 prepared chitosan-grafted PCL/poly(3-hydroxybutyrate-co-3-hydroxyhexanoate) fiber blends by wet-electrospinning which did not show any toxic effect to human dermal fibroblasts.

Kasuga et al., 2012 produced composite fibers in micro scale consisting of siloxane-doped calcium carbonate and poly(L-lactic acid) using a wet-electrospinning technique. The prepared fibers showed enhanced MC3T3-E1 cell attachment and proliferation.

M. S. Kim & G. H. Kim, 2014 fabricated three-dimensional PCL/β-tricalcium phosphate micro/nanofibrous composite scaffolds by wet-electrospinning followed by freeze-drying. Homogeneous micropores were then produced by a femtosecond laser process. The scaffolds showed improved biocompatibility on MG-63 cells.

In another study of Kim's group (M. S. Kim & G. Kim, 2014), three-dimensional PCL/alginate composite scaffolds were prepared which comprised PCL/alginate microfibers obtained by wet-electrospinning and PCL struts produced by rapid-prototyping as a reinforcement. The scaffolds showed improved osteogenic differentiation on MC3T3-E1 cells and had enhanced mechanical strength.

In this part of the thesis, it was aimed to prepare three-dimensional, porous HAP incorporated and silk impregnated PHBV nanofibrous cotton wool-like scaffolds by wet-electrospinning followed by freeze-drying as a bone-filling material for tissue engineering applications. PHBV was chosen due to its non-toxic, biocompatible, biodegradable, and good electro-spinnability features. HAP nanopowders were used as the reinforcement for its superior osteoconductive properties as well as similarity to the inorganic part of the natural bone ECM. In order to improve the bioactivity and biocompatibility of the produced HAP/PHBV wet-electrospun fibers, they were immersed into silk solution, which is a promising biopolymer alternative to collagen because of its easier production and lower price. Scanning electron microscopy (SEM), Fourier Transform Infrared Spectroscopy (FTIR), X-Ray diffraction (XRD), and thermogravimetric differential thermal analysis (DTA/TGA) were used to characterize

the morphology, chemical and crystalline structures, and thermal behavior of the scaffolds, respectively. Biomineralization studies were performed in order to evaluate the CA-P mineralization tendency of the scaffolds in simulated body fluid (SBF). The *in-vitro* biocompatibility tests of the scaffolds were performed using MG-63 osteoblast-like cells and bioactivity of the scaffolds was evaluated by resazurin assay, alkaline phosphatase (ALP) activity, total protein assay (BCA), and histological and immunohistochemical analyses.

3.2 Experimental

3.2.1 Materials

A synthetic biopolymer PHBV (PHV content 3 wt%, $M_{n=}$80 kDa) was used as a matrix material and supplied from Helian Polymers, Netherlands. Benzyl triethylammonium chloride (BTEAC), chloroform, and HAP nanopowders (particle size <200 nm) were obtained from Sigma Aldrich, USA. 12-Hydroxystearic acid (HSA) was supplied from Alfa Aesar, USA. Cocoons of Bombyx mori silkworm silk were purchased from the Turkish Republic of Northern Cyprus. The required materials for the production of silk solution such as sodium carbonate (Na_2CO_3) and calcium chloride ($CaCl_2$) were obtained from Merck, Germany; dialysis tubing cellulose membrane was that of from Sigma Aldrich, USA.

The *in-vitro* biocompatibility tests were performed in the Department of Biomechanics, Dokuz Eylul University and the materials used for the test are given separately. MG-63 osteosarcoma human cell line was purchased from American Type Culture Collection, USA. MEM-Eagle with L-Glutamine (200 mM, G7513, Sigma Aldrich, USA), and Pen-Strep-Ampho (03-033-1B Biological Industries, USA) were used for cell culture study. The kits used for the biocompatibility assays are as follows: Resazurin assay (11884, Cell Signaling Technology, USA), Alkaline phosphatase (ALP) activity assay (Enzyline PAL Optimise, Biomerieux, France), Bicinchoninic acid (BCA) protein assay (39228.01, Serva, Germany). Materials used for histological studies are as follows: Hematoxylin (01562E, Surgipath Medical Industries, UK),

Eosin (01602E, Surgipath Medical Industries, UK), Masson Trichrome staining kit (Bio-Optica, Italia), type-I collagen antibody (C2456, Sigma-Aldrich, USA), 3,3'-diaminobenzidine chromogen (Roche, Germany), dakopen (Dako, Denmark), entellan (UN 1866, Merck, Germany).

3.2.2 Preparation of PHBV and HAP/PHBV Solutions

PHBV and HAP/PHBV solutions were prepared individually in chloroform. The concentration and conductivity of the polymer solution are important parameters that affect both spinnability of the solution and morphology of the obtained fibers. In order to optimize the concentration of PHBV solutions, different solutions were prepared with varying concentrations of PHBV (15, 10, 5, and 3 % (w/v)), and BTEAC (0.1, and 0.2 (w/v)). BTEAC was used as an organosoluble salt to increase the conductivity and spinnability of PHBV solution. As a result of electrospinning of these solutions at different process parameters (3 or 1 ml/h flow rate, 15 or 20 kV voltage and, 15 or 2 cm working distance), optimized concentrations were selected as 3% (w/v) for PHBV, and 0.2% (w/v) for BTEAC to produce wet-electrospun nanofibers in this part of the thesis (Unalan, Colpankan, Albayrak, Gorgun, & Urkmez, 2016; Ünalan, 2015). In order to obtain PHBV solution, PHBV and BTEAC were dissolved in chloroform at 50°C for 2 h and stirred at room temperature overnight.

For the preparation of HAP/PHBV solution, firstly, HSA was dissolved in chloroform at 0.1 or 0.2 % w/v with respect to chloroform. HSA was used as a surfactant to distribute the HAP nanopowders homogenously in the PHBV solution. In the incorporation step of HAP nanopowders, different concentrations (1.5, 1.0, 0.5, 0.3 (w/v)) were studied; however maximum 0.3% w/v concentration of HAP was homogeneously dispersed in chloroform without any agglomeration at 0.2 % w/v of HSA concentration. Therefore, it was chosen as an optimum HAP concentration. HAP nanopowders were added to the prepared HSA-chloroform solution, and then it was subjected to ultrasonic mixing for homogeneous dispersion. Finally, PHBV solution were mixed with the HAP suspension at an equal volume and it was left to stir at 50°C for 2 hours and at room temperature overnight.

3.2.3 Preparation of Silk Fibroin Solution

The preparation process of silk fibroin (SF) solution (~0.5% (w/v) includes three steps (Colpankan Gunes et al., 2019). In the first step, Bombyx mori cocoons of 1cm x 1cm were treated with 0.1 M Na_2CO_3 at 70ºC for 3 hours. This process, known as degumming, aimed to remove glue-like sericin protein from the outer shell of the cocoons. This degumming process was repeated three times and then degummed silk was rinsed with distilled water. In the second step, the degummed silk was dissolved in $CaCl_2/CH_3CH_2OH/H_2O$ (mole ratio: 1/2/8) at 70ºC for 6 hours and then filtered. The last step consists of dialysis of the filtrated solution using a tubing cellulose membrane in distilled water for 3 days.

3.2.4 Production of Nanofibrous Cotton Wool-Like Scaffolds

Wet-electrospinning together with freeze-drying were used to produce three-dimensional, porous and nanofibrous cotton wool-like scaffolds.

Initially, prepared PHBV or HAP/PHBV solution was subjected to wet-electrospinning process individually. The wet-electrospinning setup is seen in Figure 3.1. In this process, the prepared solution was filled into a plastic syringe (10 ml) containing blunt needle (22-gauge stainless). It was fed by a syringe pump (NE-1000, New ERA Pump System, Inc., USA) at different flow rates (1.0, 1.5, and 2.0 ml/h). The solution was electrospun towards a coagulation bath consist of ethyl alcohol-distilled water mixture at different volume ratios (10:0, 9:1, 8:2, and 7:3 v: v of ethyl alcohol: distilled water). Glass container (25 cm in diameter) was used as a coagulation bath, and a Cu plate was placed under it to provide electrical conductivity. In the wet-electrospinning process, a surface tension of the coagulation bath solution is very important because it is necessary to obtain homogenously suspended nanofibers within the coagulation bath. Therefore, the desired suspension of nanofibers was obtained by 9:1 v:v ratio of ethyl alcohol: distilled water. The coagulation bath was located at different distances of 10, 15 and 20 cm from the needle tip, and it was concluded that as the working distance increased the applied electric field decreases, and nanofibers

scattered much more. 20 and 25 kV of voltage was applied by a power supply (Gamma High Voltage ES30). As a conclusion, optimized electrospinning process parameters were selected as follows: 2.0 ml/h flow rate, 10 cm working distance, and 20 kV voltage. The fibers electrospun for 15 min were collected and rinsed with distilled water.
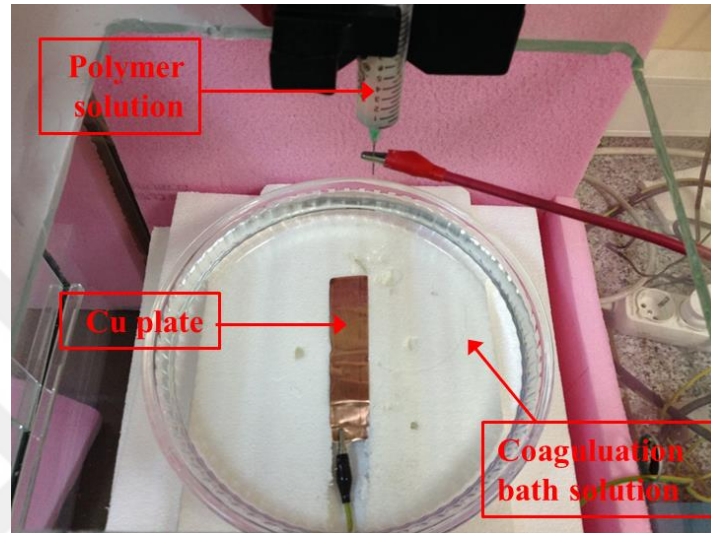
Figure 3.1 The wet-electrospinning setup used to produce PHBV and HAP/PHBV nanofibers (Personal archive, 2019)

In order to prepare the silk impregnated scaffolds, initially obtained wet-electrospun PHBV or HAP/PHBV nanofibers were immersed into the silk solution overnight. Then, methanol treatment was applied for an hour so that the silk could be immobilized. Lastly, the prepared nanofibers were subjected to freeze-drying (FreeZone Freeze Dry Systems) at -78°C for 24 hours and three-dimensional nanofibrous cotton wool-like scaffolds were obtained. The produced scaffolds without silk impregnation were coded as PHBV and HAP/PHBV, whereas for silk impregnated scaffolds PHBV-SF, and HAP/PHBV-SF were given that of the sample codes (Colpankan Gunes et al., 2019).

3.2.5 *Characterization of the Scaffolds*

3.2.5.1 SEM and EDX/Mapping Analyses

The morphologies of the produced three-dimensional nanofibrous cotton wool-like scaffolds were examined by SEM (JEOL, JSM-6060) at an accelerating voltage of 5 kV. All the scaffolds were coated with a thin layer of gold/palladium prior to analysis (Quorum Technologies, SC7620). Image J program was used to determine the average diameter of the fibers from their SEM images of 2500x by taking measurements from 25 different points for each sample.

EDX/mapping analysis was used to investigate the presence and dispersion of Ca-P minerals on the surface of the fiber of HAP incorporated scaffolds (HAP/PHBV and HAP/PHBV-SF).

3.2.5.2 Porosity Measurement

The percent porosity values of the produced scaffolds were obtained by a mercury porosimeter by low-pressure measurement (Quantachrome Corporation, Poremaster 60) in the Central Laboratory of Middle East Technical University.

3.2.5.3 ATR-FTIR Analysis

The characteristic chemical bonds of the scaffolds, the presence of HAP, and silk conformation were determined by ATR-FTIR (Perkin Elmer Spectrum BX). Each spectrum was obtained in the wavenumber range of 4000-500 cm^{-1} at a resolution of 4 cm^{-1}, and by scanning 25 times per sample.

3.2.5.4 XRD Analysis

The phase analysis of the scaffolds was determined by XRD (Rigaku, D/Max 2200) equipped with a Cu–Kα radiation (λ = 1.5406 Å). Diffraction patterns were recorded in the 2θ range 5-90° with a step size of 0.05°.

3.2.5.5 DTA/TGA

DTA/TGA (Shimadzu DTG-60H) was used to determine the thermal properties of the scaffolds. Analyses were performed under a nitrogen atmosphere at a heating rate of 10°C/min and in the temperature range of 25-700°C.

TGA curves showed the decomposition behavior of the scaffolds as well as the inorganic content percentages in the scaffolds, whereas, DTA curves demonstrated apparent melting peak (T_m) and maximum decomposition temperatures (T_p). Besides, the enthalpy of fusion (ΔH_f) was calculated from the area under the melting peak for each of the scaffolds, and then the relative degree of crystallinity (X_c) of the scaffolds was calculated by using equation 3.1.

$$X_c \ (\%) = \Delta H_f \ / \ (W_{PHBV} \ x \ \Delta H_{ref}) \ x \ 100 \tag{3.1}$$

In equation 3.1; ΔH_{ref} is the enthalpy of fusion of 100 % crystallized PHBV and it is 146 J/g (Cheng & Sun, 2009). The weight fraction of PHBV was abbreviated as W_{PHBV}. In order to determine W_{PHBV} in the silk impregnated scaffolds, PHBV-SF and HAP/PHBV-SF were assumed to have the same % crystallinities with that of PHBV and HAP/PHBV, respectively.

3.2.6 Biomineralization Studies of the Scaffolds

Biomineralization studies were performed in order to evaluate the mineralization tendency and bioactivity of the scaffolds in SBF which contains ion concentrations nearly equal to human blood plasma.

Studies were carried out considering the instructions of (Kokubo & Takadama, 2006). SBF was prepared as follows: 700 ml of ion-exchanged and distilled water was heated to 36.5 ± 1.5 °C in a plastic beaker. The first 8 chemicals given in Table 3.1 were added and dissolved one by one. Tris and HCl were added to this solution in a controlled manner, keeping pH in the range of 7.42-7.45. The final pH of the solution was adjusted to 7.40 and was poured into a 1000 ml volumetric flask. After that ion-exchanged and distilled water was added up to the marked line of the flask, and the solution was allowed to cool down to 20 °C.

Table 3.1 Order and amounts weights of reagents for preparing 1000 ml of SBF

Order	Reagent	Amount
1	NaCl	8.035 g
2	$NaHCO_3$	0.355 g
3	KCl	0.225 g
4	$K_2HPO_4.3H_2O$	0.231 g
5	$MgCl_2.6H_2O$	0.311 g
6	1.0 M-HCl	39 ml
7	$CaCl_2$	0.292 g
8	Na_2SO_4	0.072 g
9	Tris	6.118 g
10	1.0M-HCl	0-5 ml

20 ml of freshly prepared SBF was added to the scaffolds placed in falcon tubes, and incubation was held at 37ºC for 4 weeks. SBF solutions were changed twice a day. At the end of the incubation period, the biomineralized scaffolds were rinsed three times with deionized water so that the residual salts could be removed. Finally, for further analysis they were dried in a desiccator at ambient temperature. The mineral formation onto the scaffold was observed by SEM-EDX; the degradation behavior of the scaffolds after biomineralization was that of by DTA/TGA, and phase analysis of the formed minerals was that of by XRD.

3.2.7 In-Vitro Biocompatibility Studies of the Scaffolds

3.2.7.1 Cell Culture

MG-63 osteosarcoma human cells were cultured in MEM-Eagle medium containing 10% FCS, L-Glutamine, Pen-Strep-Ampho at 37°C in a 5% CO_2 humidified incubator in culture flasks, and the medium was changed once in three days. After a subconfluent monolayer was achieved, cells were trypsinized with Trypsin/EDTA buffer. Sterilization of the scaffolds were done by using ethylene oxide and after a week they were ready for the biocompatibility tests. The sterilized scaffolds were placed in 96-well culture plate and MG-63 cells were seeded at a density of $1x10^6$cells/μl onto the scaffolds with culture media, and cells were cultured for up to 10 days in a 5% humidified atmosphere at 37°C. by changing the media every other day. All experiments were performed in triplicate (n=3).

3.2.7.2 Cell Morphology

The morphology of the MG-63 cells, as well as the attachment on the surface of the scaffolds after cell culture period, was observed by SEM. Before the analysis, the fixation procedure of was carried out. Firstly, after aspirating the media was from the culture wells, scaffolds were rinsed with phosphate buffered saline (PBS) in triplicate. Then, they were incubated with 3.7% paraformaldehyde at room temperature for 20 minutes. Finally, they were washed with PBS three times and were dehydrated with ethanol series gradually (20%, 50%, 70%, 90%, and 100%) for 5 minutes each.

3.2.7.3 Cell Viability

Cell proliferation and viability of MG-63 cells on the scaffolds was determined by resazurin assay. After 3, 7 and 10 days of cell culture, the medium was removed, and replaced with phenol red-free medium. Incubation of the scaffolds was held for 3 hours at standard culture conditions. After incubation, 100 μl of the medium from each well was taken to a 96-well culture plate. Fluorescent signal of resorufin was monitored

using a fluorometer at 530-570 nm excitation wavelength, and 590-620 nm emission wavelength.

3.2.7.4 Alkaline Phosphatase Activity (ALP) Assay

ALP activity of the MG-63 cells on the scaffolds was assessed by a commercial assay by measuring the absorbance at 405 nm using a spectrophotometer (Thermolab Systems, Multiskan Spectrum) at 3, 7, and 10 days of culture.

3.2.7.5 Bicinchoninic Acid (BCA) Aassay

BCA protein kit was used for the measurement of the total protein content of the scaffolds. Initially, 25 µl of cell medium was added into a 96-well culture plate, and then 200 µl of the BCA working reagent was supplemented. After incubation for 30 minutes, absorbance at a wavelength of 562 nm by the spectrophotometer.

3.2.7.6 Histologic Analyses

The scaffolds after 10 days of cell culture were subjected to histological staining with hematoxylin and eosin (H&E), Masson trichrome (MT), and type-I collagen. The samples were fixed with 10% formalin solution for 3 days first, and then they were embedded in paraffin blocks, and finally, 5-µm thick cross-sections were retrieved from these blocks.

For H&E and MT staining, a similar procedure was performed until the staining. Firstly, the sections were deparaffinized by incubation at 60ºC and treated with xylene at room temperature. Then, they were rehydrated in ethyl alcohol series and rinsed with distilled water. Finally, for H&E staining, the sections were stained with Hematoxylin for 10 minutes and after washing step to remove the excess stain, the sections were stained with Eosin for 2 minutes. After that, stained sections were rinsed with absolute ethyl alcohol series of 70%, 80%, 96%, 100 %, and with Entellan. For MT staining, 6 drops of each Weigert's ferrous hematoxylin and ferric chloride

solutions were poured dropwise on the sections and left for 10 minutes. After that, sections were immersed into the picric acid, Ponceau acid fuchsine, and phosphomolybdic acid solutions respectively and washing in distilled water after 10 minutes waiting for each solution. Finally, Masson aniline blue solution was used for staining for 5 minutes, and the same washing steps as that of H&E were performed.

Immunohistochemical staining was performed by type I collagen antibody. First, the sections were subjected to deparaffinization and then, they were rehydrated in ethyl alcohol series. Dakopen was used to limit their surroundings. Samples were kept in trypsin for 15 minutes at 37ºC, and followed by in 3% H_2O_2 for 10 minutes. Then, the cross-sections were rinsed with PBS and incubated with a blocking solution for half an hour. After that, collagen type-I primary antibody was applied to the cross-sections. Stained cross-sections were kept at 4ºC overnight. Finally, they were incubated first with a biotinylated secondary antibody for half an hour, and then with an avidin-biotin complex (streptavidin) for another half an hour, and the same washing steps as that of H&E and MT were performed.

3.2.8 Statistical Analysis

Experiments were performed in triplicate and the statistical analysis of was performed using one-way analysis of variance (ANOVA) method.

3.3 Results and Discussion

3.3.1 Fabrication and SEM Analysis of the Scaffolds

For the preliminary studies of this part of the thesis, PHBV solutions with different concentrations were prepared with varying concentrations of PHBV (15, 10, 5, and 3 % (w/v)), and BTEAC (0.1, and 0.2 (w/v)), and all of them were subjected to electrospinning process. Based on the morphology and average diameter of the fibers, as optimum concentrations were selected as 3% (w/v) for PHBV, and 0.2% (w/v) for BTEAC. The SEM images of these produced PHBV nanofibers by conventional

electrospinning which used as an aluminum foil as a collector, and at 1 ml/h flow rate, 20 kV voltage, and 15 cm distance are seen in Figure 3.2. As seen from the images, continuous and bead-free nanofibers with 637±95 nm in size were obtained (Unalan, Colpankan, Albayrak, Gorgun, & Urkmez, 2016). Besides, PHBV electrospun nanofibrous mats had a porosity of 69.1% obtained by a mercury porosimeter.
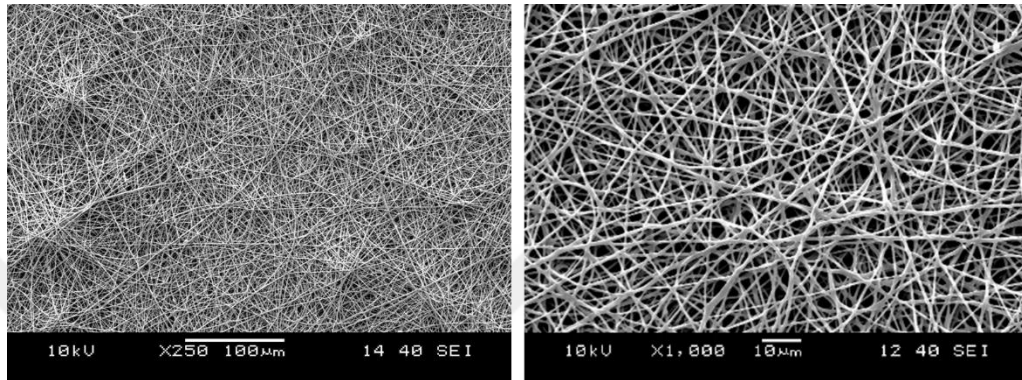
Figure 3.2 SEM images of the PHBV nanofibers by conventional electrospinning at 1 ml/h flow rate, 20 kV voltage, and 15 cm distance

For the preparation of HAP/PHBV solution, incorporated HAP nanopowder concentration was also optimized as 0.3% w/v which was the maximum concentration that can be dispersed without leading any agglomeration. This solution was also subjected to conventional electrospinning using the same process parameters that of PHBV, and uniform fibrous structure with 636±149 nm average fiber diameter was obtained as seen in Figure 3.3. Besides, HAP/PHBV electrospun nanofibrous mats had a porosity of 70.6% obtained by a mercury porosimeter.
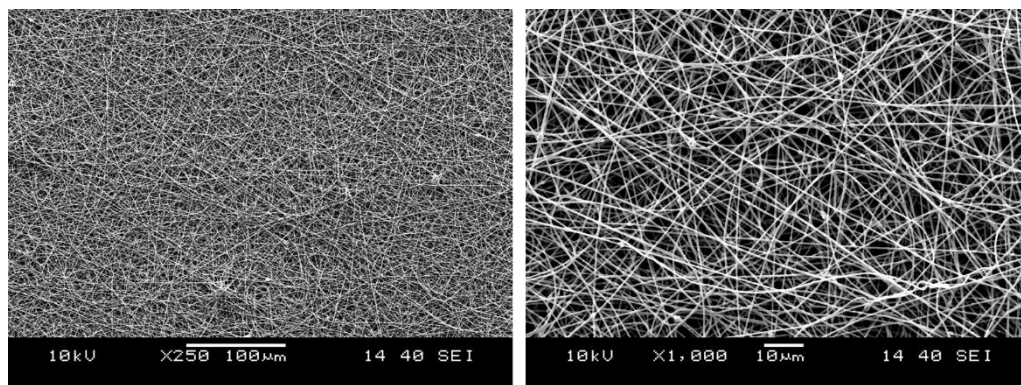
Figure 3.3 SEM images of the HAP/PHBV nanofibers by conventional electrospinning at 1 ml/h flow rate, 20 kV voltage, and 15 cm distance

Nanofibrous cotton wool-like scaffolds of PHBV and HAP/PHBV were produced by the wet-electrospinning of PHBV and HAP/PHBV solutions and followed by freeze-drying of these wet-electrospun nanofibers to obtain three-dimensional structures. Wet-electrospinning of the solutions were performed at 2 ml/h of flow rate, 20 kV of voltage, and 10 cm of distance using the coagulation bath comprising the mixture of ethyl alcohol and distilled water at a volume ratio of 9:1. Silk impregnated scaffolds (PHBV-SF and HAP/PHBV-SF) were produced by the immersion of the wet-electrospun nanofibers into the silk solution and then freeze-drying them.

Figure 3.4 and Figure 3.5 show the SEM images of the produced three-dimensional PHBV, HAP/PHBV, and silk impregnated PHBV-SF, HAP/PHBV-SF cotton-wool like scaffolds at different magnifications, respectively. At the end of the production process of the scaffolds, porous and three-dimensional structures were successfully obtained continuous and bead-free fibers. SEM images with 5000x of magnification demonstrated the surface of the HAP/PHBV nanofibers (Figure 3.4c), and also fibers of silk impregnated scaffolds with or without HAP-containing (Figure 3.5c, and f) was rougher than that of PHBV nanofibers (Figure 3.4c).

45
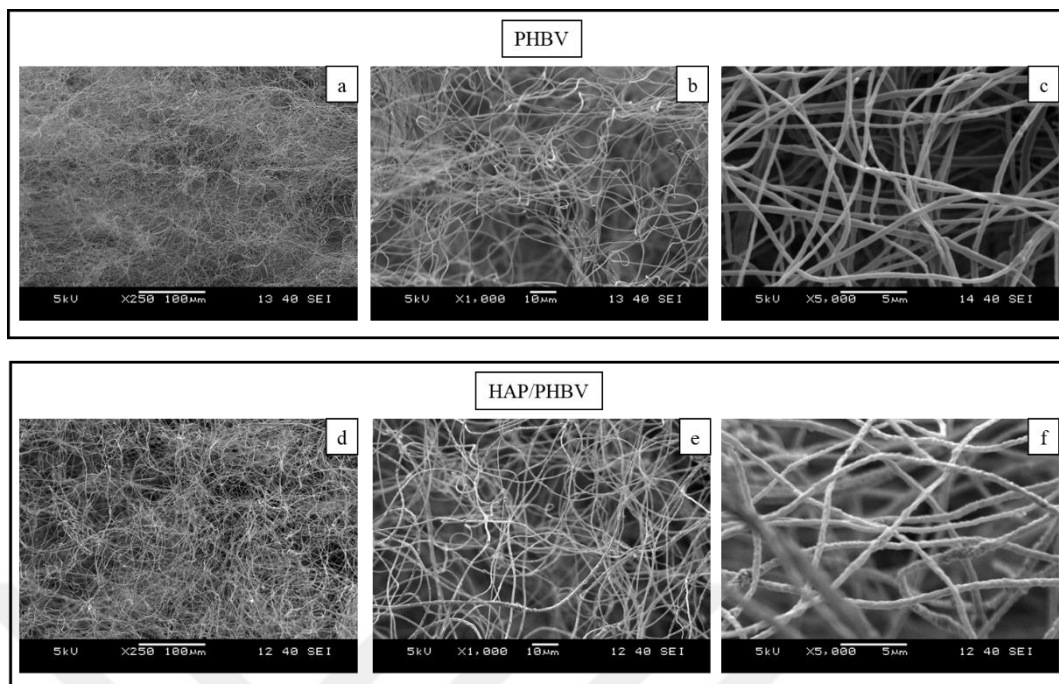
Figure 3.4 SEM images of PHBV and HAP/PHBV cotton wool-like scaffolds at different magnifications
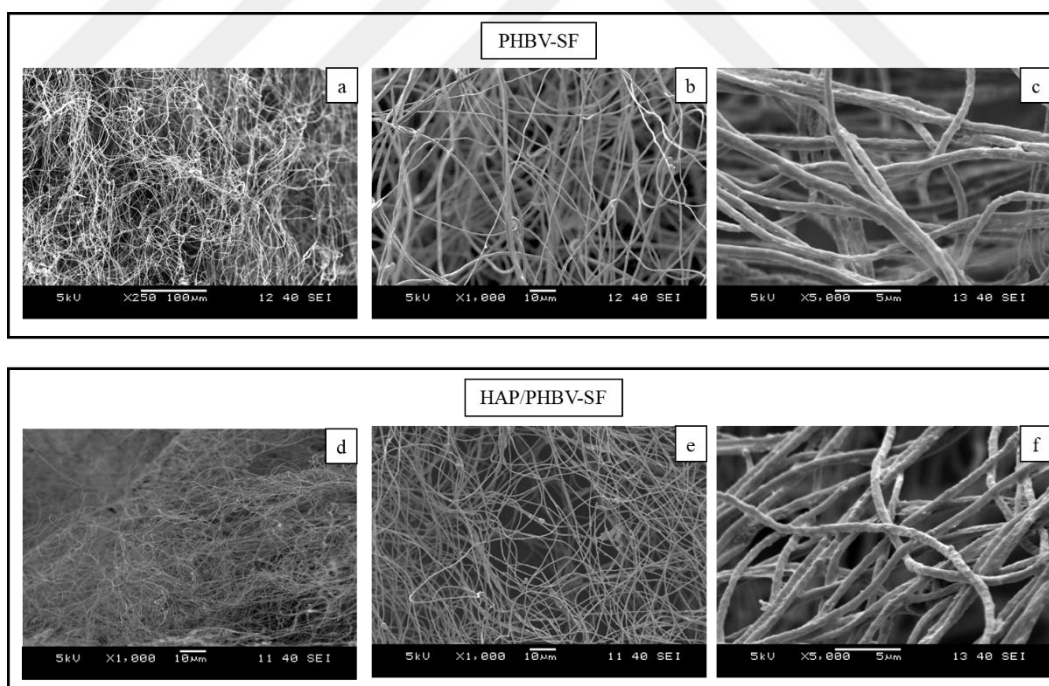
Figure 3.5 SEM images of the silk impregnated PHBV-SF and HAP/PHBV-SF cotton wool-like scaffolds

The fiber diameters and porosity values of the scaffolds are given in Table 3.2. The scaffolds had similar percent porosity values varying in the range of 80 to 85%. In terms of average fiber diameters; the diameter of the fibers increased after silk impregnation, while HAP incorporation did not have much effect.

Table 3.2 Average fiber diameters and percent porosity values of the produced scaffolds

Scaffold	Fiber Diameter (nm)	Porosity (%)
PHBV	552 ± 70	84.9
HAP/PHBV	590 ± 92	84.2
PHBV-SF	621 ± 95	81.3
HAP/PHBV-SF	664 ± 184	80.1

EDX/mapping analysis was performed to prove the presence and distribution of the HAP nanopowders within the scaffolds. As shown in the mapping images of the scaffolds in Figure 3.6, Ca-P minerals were present and homogeneously distributed throughout the scaffolds.
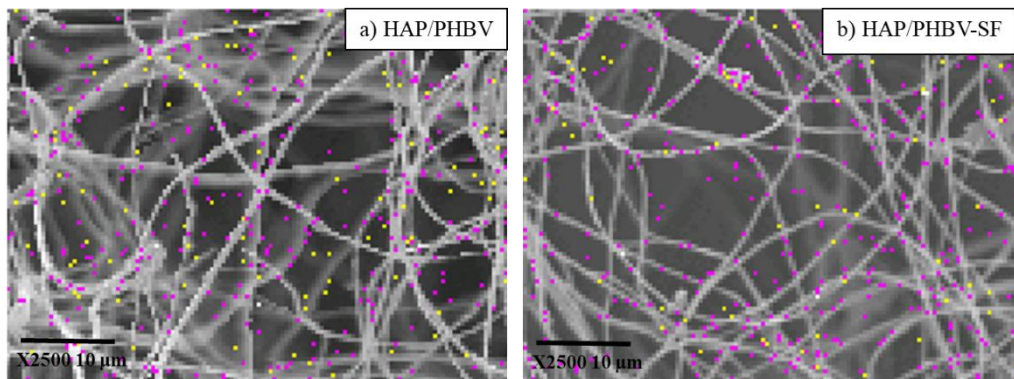
Figure 3.6 EDX/mapping images of the a) HAP/PHBV and b) HAP/PHBV-SF cotton wool-like scaffolds (pink spots: Ca; yellow spots: P; magnification: 2500x)

3.3.2 FTIR Analysis Results

FTIR spectra of the produced scaffolds are illustrated in Figure 3.7. Characteristic bands of PHBV appeared at 2978 cm^{-1} (C–H stretching), 1721 cm^{-1} (C=O stretching), 1453 and 1380 cm^{-1} (C–H bending), 1278 and 1055 cm^{-1} (C–O stretching). P–O stretching and bending vibrations of HAP were at around 1200–900 and 700–500 cm^{-1} regions, respectively. However, since C–O, and P–O stretching bands had similar wave numbers, only 602 and 570 cm^{-1} bands, assigned to bending modes of the phosphate groups of HAP, could be indicative the incorporation of HAP to the scaffolds (Colpankan Gunes et al., 2019). In addition, the conformational change of the silk could be analyzed from the FTIR spectrum. The amide I and amide II bands of water-soluble random coil structure of silk are at 1655±10 cm^{-1} and 1540±10 cm^{-1}, respectively. However, these amide bands shift to lower wavenumbers to 1625±10 cm^{-1} (amide I) and 1525±10 cm^{-1} (amide II) after methanol treatment of silk as indicative of insoluble β-sheet structure (Li, Vepari, Jin, Kim, & Kaplan, 2006). As seen from the FTIR spectra of the silk impregnated of the scaffolds, the bands at 1628 cm^{-1} and 1530 cm^{-1} proved the successful impregnation of silk and conformational change to the insoluble β-sheet structure of impregnated silk.
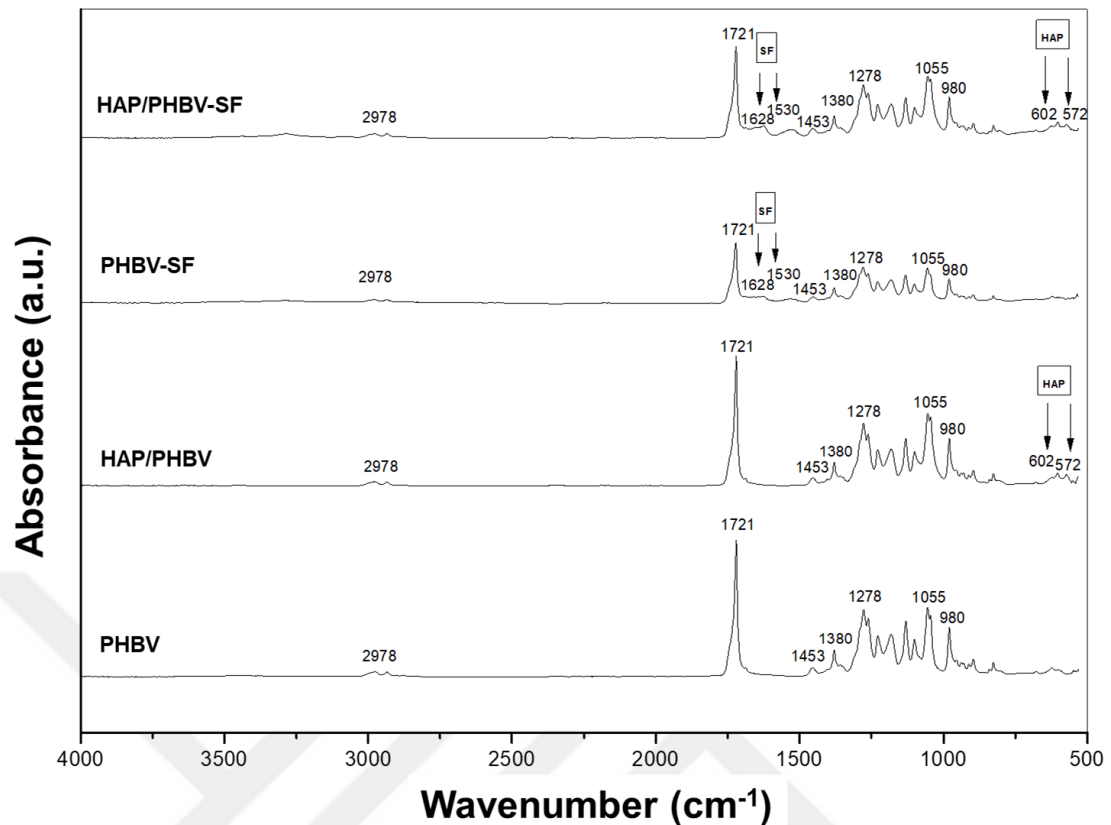
Figure 3.7 FTIR spectra of the cotton wool-like scaffolds

3.3.3 Thermal Analysis Results

Thermal analysis of the scaffolds was carried out by DTA/TGA. DTA curves of the scaffolds and obtained T_m, T_d, and ΔH_f values, and calculated X_c values of the scaffolds are shown in Figure 3.8 and Table 3.3, respectively. All of the scaffolds had similar T_m values of approximately 179°C. However, PHBV-SF and HAP/PHBV-SF scaffolds had higher T_d values (~256°C) than that of PHBV and HAP/PHBV scaffolds (~246°C) which indicated that silk impregnation enhanced the thermal stability of scaffolds, and this may be because of the maximum decomposition temperature of silk which was about 281°C (Barud et al., 2015). Besides, in the study of Moraes, Nogueira, Weska, & Beppu, 2010, it was stated that while increasing the silk content in the chitosan/silk fibroin films, the thermal stability of the films enhanced. It was also concluded that incorporation of HAP, as well as impregnation of silk, decreased the ΔH_f values of the scaffolds. Crystallinity values calculated by equation 1 were

49

found as 58.6 and 66.9 % for PHBV and HAP/PHBV scaffolds, respectively. X_c values of the silk impregnated scaffolds were taken as the same with that of their counterparts.
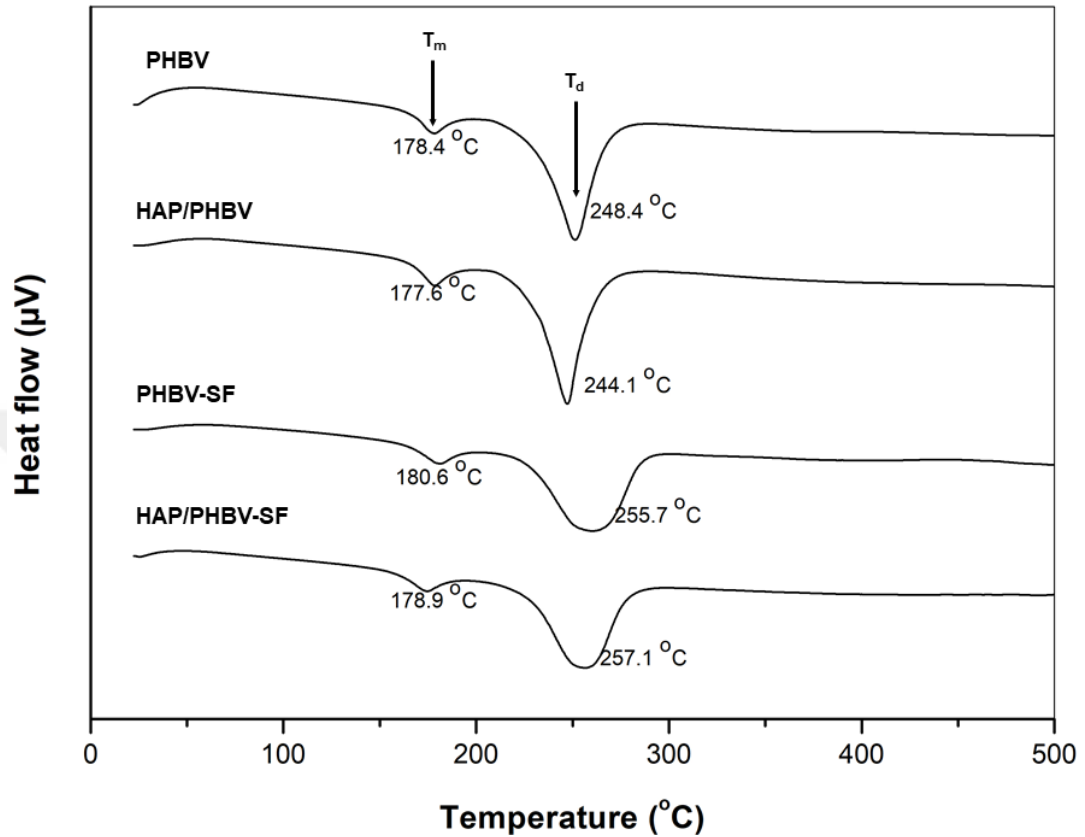
Figure 3.8 DTA curves of the cotton-wool like scaffolds

Table 3.3 Thermal properties of the cotton-wool like scaffolds

Scaffold	T_m (°C)	T_d (°C)	ΔH_f (J/g)	X_c (%)
PHBV	178.4	248.4	80.3	58.6
HAP/PHBV	177.6	244.1	79.2	66.9
PHBV-SF	180.6	255.7	70.8	58.6
HAP/PHBV-SF	178.9	257.1	67.8	66.9

Figure 3.9 shows the TGA curves of the produced scaffolds that decomposed in a single-stage. The incorporated HAP content of the HAP/PHBV and HAP/PHBV-SF scaffolds were calculated as 7.8 and 7.3 wt. %, respectively. The fact that these values

are similar to the HAP theoretical content (8 wt. %) was another proof that HAP nanopowders have been incorporated to the scaffold successfully and homogeneously.
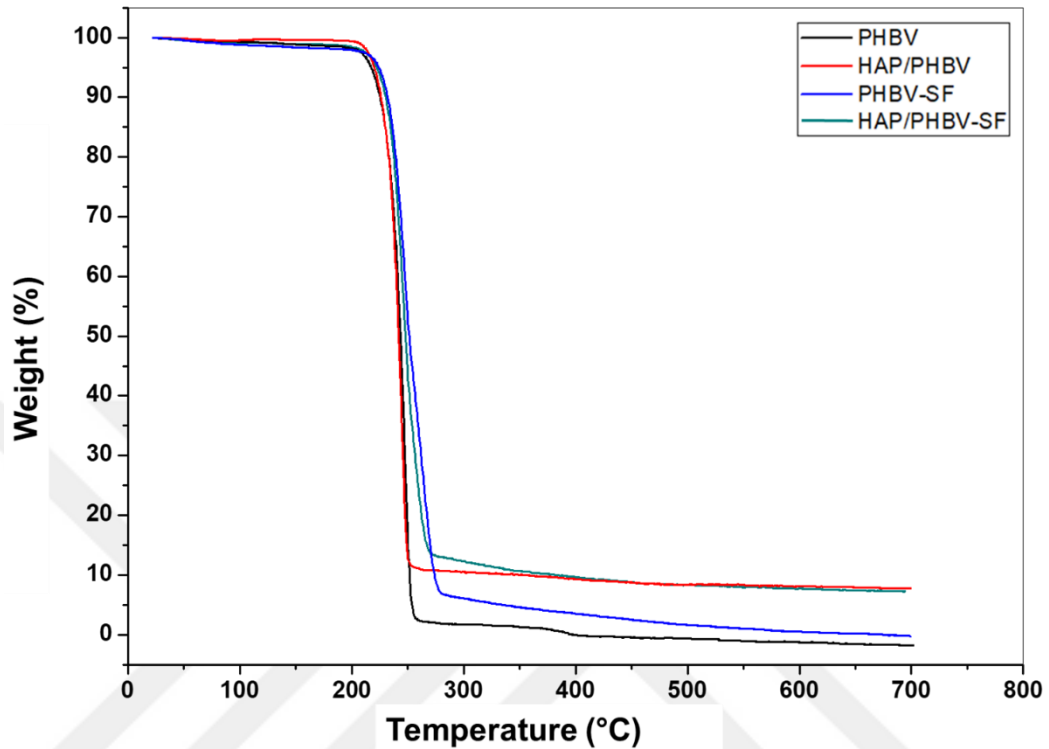
Figure 3.9 TGA curves of the cotton-wool like scaffolds

3.3.4 Biomineralization Studies

The biomineralization potential of the produced cotton-wool like scaffolds was investigated by incubating them in SBF solution at 37°C for 4 weeks. The biomineralization tendency of the scaffolds was investigated by SEM, EDX/mapping analysis, DTA/TGA and XRD.

3.3.4.1 SEM and EDX/Mapping Analyses

The formation of a bone-like apatite layer on the cotton-wool-like scaffolds was examined by SEM. Figure 3.10 and Figure 3.11 show the SEM images of the scaffolds after incubation in SBF 37°C for 2 and 4 weeks, respectively. After 2 weeks of biomineralization, an intense mineral formation was observed on the surface of the

HAP/PHBV (Figure 3.10b), PHBV-SF (Figure 3.10c) and HAP/PHBV-SF (Figure 3.10d) scaffolds, whereas less amount of non-homogeneously nucleated minerals on the surface of the PHBV scaffold were seen (Figure 3.10a). Besides, by increasing the incubation time, the mineral density was enhanced on the surface of HAP-containing (Figure 3.11b) as well as silk impregnated scaffolds (Figure 3.11c) or both HAP-containing and silk impregnated one (Figure 3.11d).
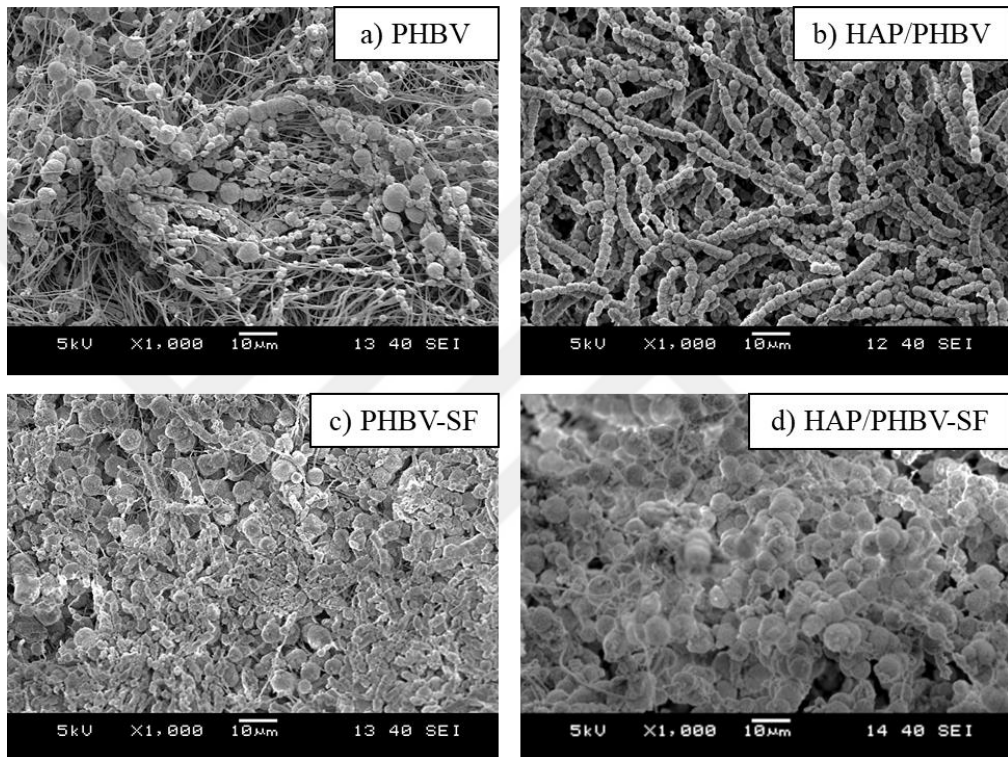
Figure 3.10 SEM images of the a) PHBV, b) HAP/PHBV, c) PHBV-SF and d) HAP/PHBV-SF cotton-wool like scaffolds after 2 weeks of biomineralization
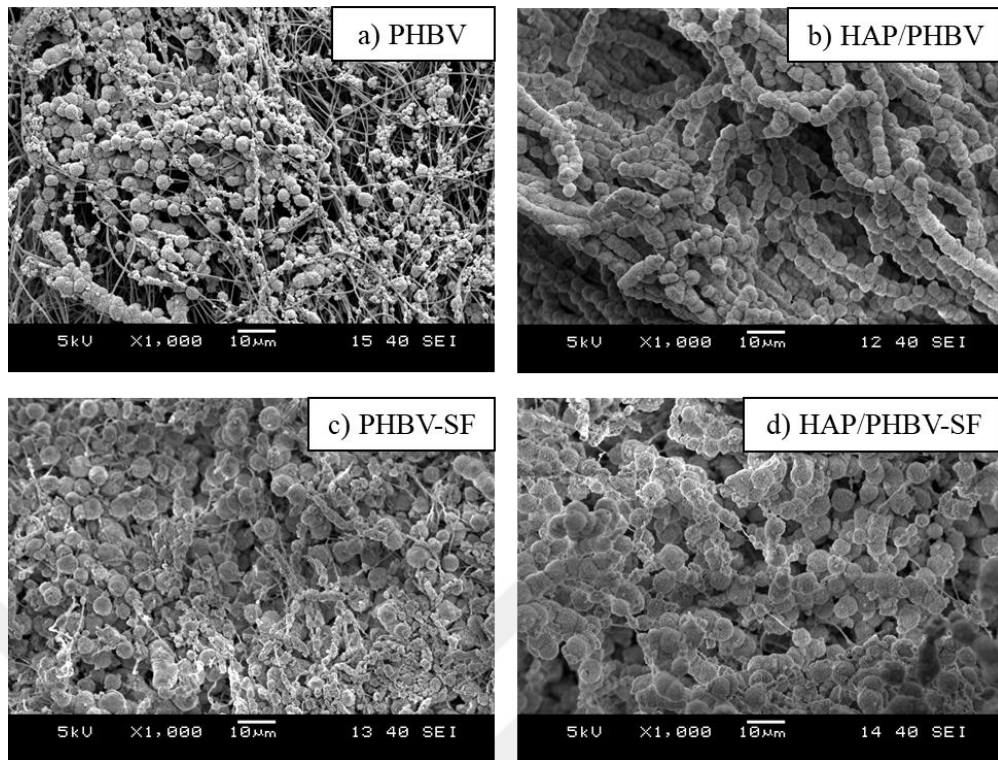
Figure 3.11 SEM images of the a) PHBV, b) HAP/PHBV, c) PHBV-SF and d) HAP/PHBV-SF cotton-wool like scaffolds after 4 weeks of biomineralization

EDX/mapping analysis was carried out in order to analyze the presence and distribution of formed Ca-P minerals on the scaffolds after incubation in SBF. It is seen from the EDX/mapping images of the scaffolds after 4 weeks of biomineralization (Figure 3.12), Ca and P minerals were distributed uniformly on the surface of all the scaffolds.

As a result, it can be concluded from SEM and EDX/mapping results that HAP incorporation is highly effective on bone-like mineral growth. HAP particles act as nucleation points and Ca-P minerals grow on the surface from these points. Silk impregnation also promoted the nucleation and adhesion of Ca-P minerals on the surface of the scaffolds. Andiappan et al., 2013 produced a composite scaffold comprising electrospun eri silk fibroin (ESF) and HAP, and evaluated the mineralization tendency of the scaffolds in SBF. Similar to our results, they also observed that ESF-HAP scaffold promotes the nucleation and growth of hydroxyapatite crystals.
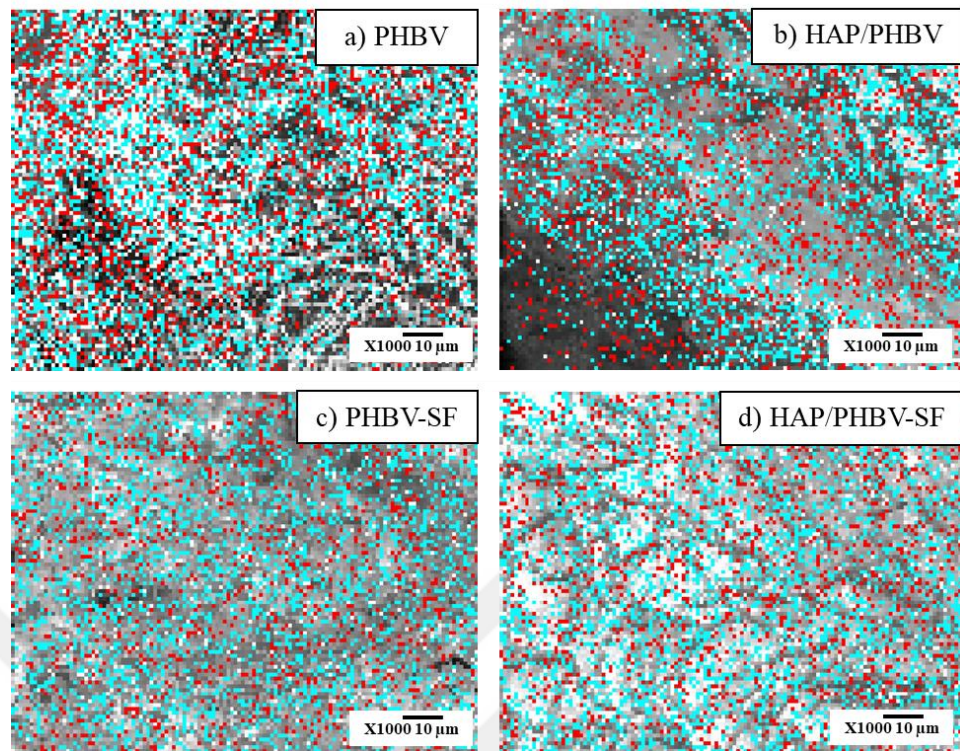
Figure 3.12 EDX/mapping spectra of the cotton-wool like scaffolds after 4 weeks of biomineralization (red spots: Ca; blue spots: P; magnification: 1000x)

3.3.4.2 DTA/TGA

TGA curves of the mineralized scaffolds are given in Figure 3.13 with the comparison with that of scaffolds before biomineralization. While scaffolds before mineralization exhibited single-stage decomposition, mineralized scaffolds showed two-stage decomposition. The initial weight loss (~5 wt. %) of the mineralized scaffolds between temperatures of 25 and 200 °C was because of the loss of adsorbed water. After 2 weeks of biomineralization, the mineral content of the PHBV and PHBV-SF scaffolds were found to be 21.4 and 28.5 wt. %, respectively. Besides, the mineral content of the HAP/PHBV and HAP/PHBV-SF scaffolds increased from theoretical 8 wt. % HAP to 37.6 and 58.1 wt. %, respectively. After 4 weeks of incubation, while the mineral content of PHBV scaffold did not change, a remarkable increase was obtained for the HAP/PHBV, PHBV-SF and HAP/PHBV-SF scaffolds with the mineral content of 44.5, 49.6 and 67.4 wt. %, respectively. Therefore, it can be concluded that incorporation of HAP and impregnation of silk affected the

nucleation and growth of mineral phase and clearly increased the amount of the Ca-P minerals on the scaffold surface.
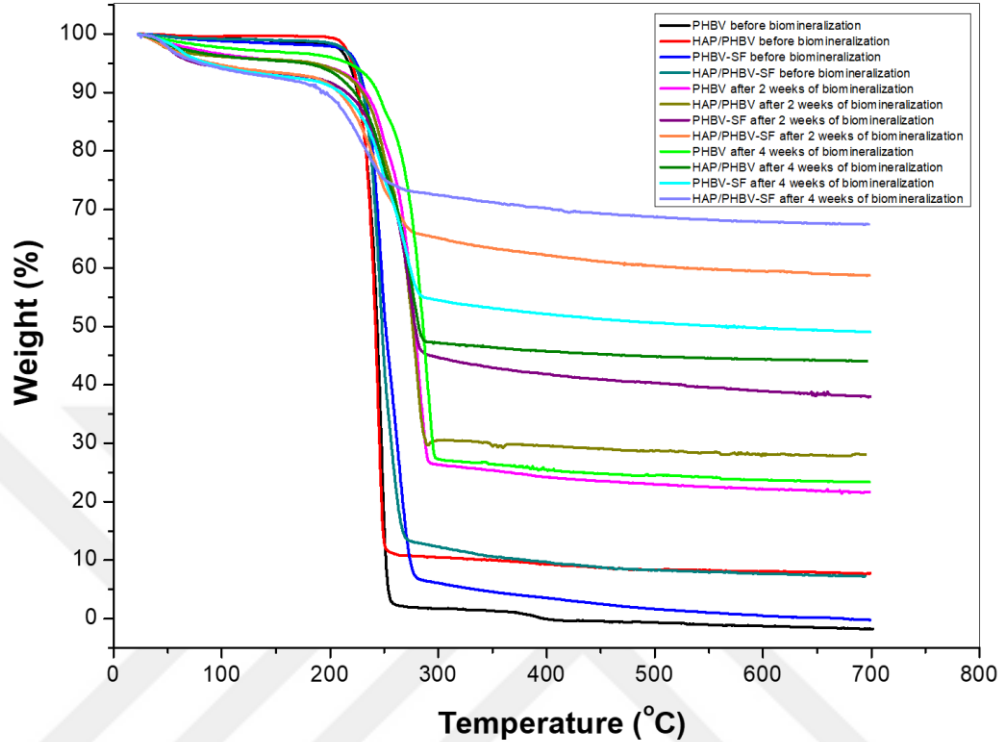
Figure 3.13 TGA curves of the scaffolds before and after 2 and 4 weeks of biomineralization

DTA curves of the scaffolds after 2 and 4 weeks of biomineralization are seen in Figure 3.14 and Figure 3.15, respectively. Besides, obtained thermal properties are listed in Table 3.4. All the scaffolds had higher T_d values after biomineralization compared to that of before biomineralization (Table 3.3) due to the accumulation of minerals. Even though on the PHBV-SF and HAP/PHBV-SF scaffolds much more mineral formation was observed after biomineralization, the increment of T_d was more pronounced for the PHBV and HAP/PHBV scaffolds which might be due to their higher percent crystallinity values after the incubation period. In addition, as seen from the comparison of data before and after biomineralization (Table 3.3 and Table 3.4), X_c values of all the scaffolds decreased significantly after biomineralization which may cause the degradation of polymer chains as chain scission can occur in the amorphous part of the scaffold matrix. Also, by increasing time of incubation and hydrophilicity of the scaffold, this difference in crystallinity became clearer.
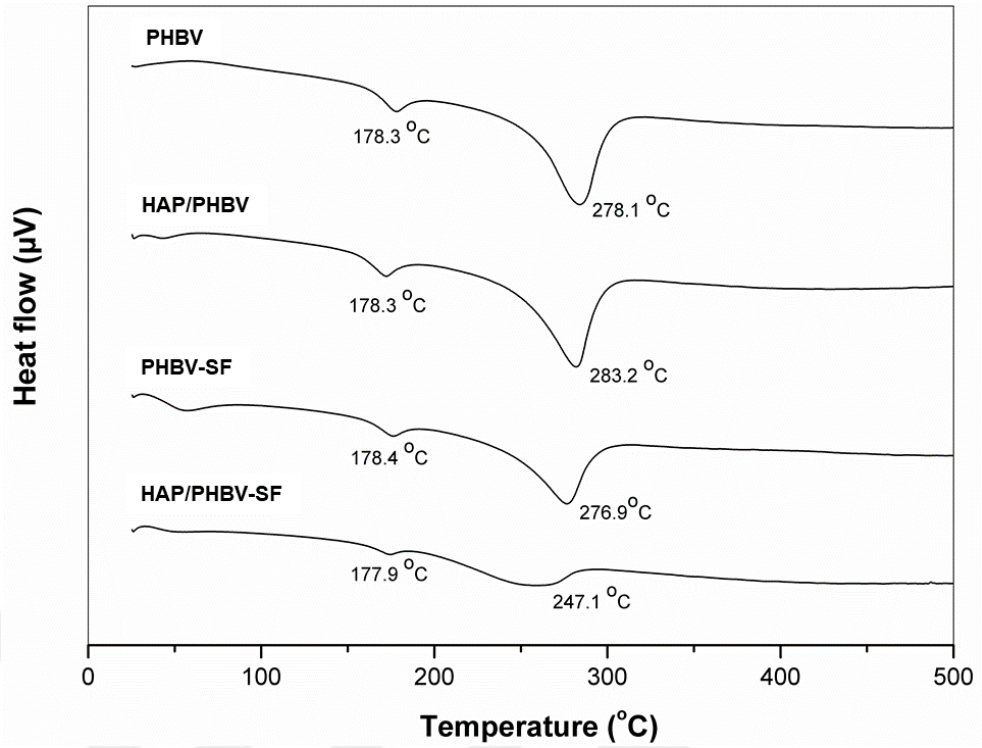
Figure 3.14 DTA curves of the scaffolds after 2 weeks of biomineralization
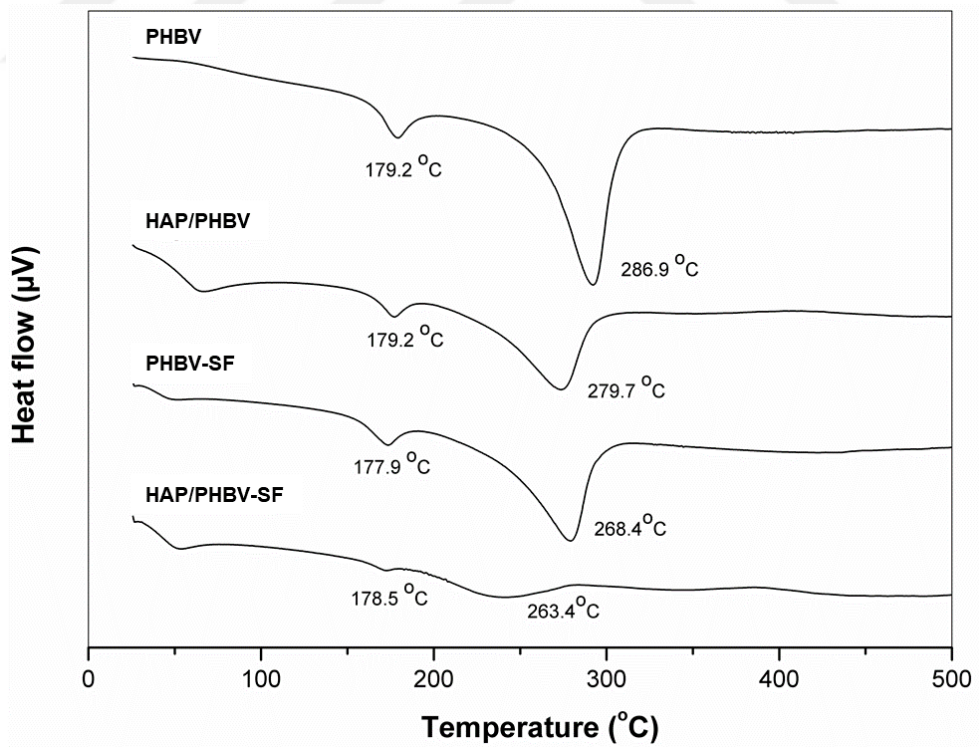
Figure 3.15 DTA curves of the scaffolds after 4 weeks of biomineralization

Table 3.4 Thermal properties of the scaffolds before and after biomineralization

Scaffold	After 2 weeks of biomineralization				After 4 weeks of biomineralization			
	T_m (°C)	T_d (°C)	ΔH_f (J/g)	X_c (%)	T_m (°C)	T_d (°C)	ΔH_f (J/g)	X_c (%)
PHBV	178.3	278.1	53.4	50.0	179.2	286.9	52.6	50.1
HAP/PHBV	178.3	283.2	50.5	59.3	179.2	279.7	28.5	43.0
PHBV-SF	178.4	276.9	32.0	42.7	177.9	268.4	24.1	39.2
HAP/PHBV-SF	177.9	247.1	14.4	34.4	178.5	263.4	6.6	20.0

3.3.4.3 XRD Analysis

XRD analysis was carried out in order to analyze the phases of the Ca-P minerals on the surface of the scaffold after biomineralization. In Figure 3.16 XRD patterns of the HAP/PHBV-SF scaffold after 4 weeks of biomineralization is given with the comparison of the pattern that of before biomineralization. The scaffold before biomineralization showed two intense and sharp peaks at $2\theta = 13.6°$ (020), 17.1° (110), and one broad peak at $2\theta = 22.9°$ (111) ascribable to PHBV (Thiré, Arruda, & Barreto, 2011). In the diffraction pattern HAP peaks at $2\theta = 25.8°$ (002), 31.9° (211) and 32.9° (300) were also seen clearly. Besides, it was stated in the literature that freeze-dried silk fibroin scaffold had the most intense peak at 22.6° (Barud et al., 2015), but this peak was overlapped with the plane of (111) of PHBV at $2\theta = 22.9°$. After 4 weeks of biomineralization, while decreasing the intensities of the diffraction peaks of PHBV especially at 13.6° and 17.1°, the intensities of that of HAP highly increased. In addition, some additional peaks of HAP appeared at $2\theta = 34.1°$, 39.8°, 46.7°, 49.6°, and 53.1° which corresponded to (202), (310), (222), (213), (004) planes, respectively. Based on the fact that the obtained XRD pattern and HAP literature data (JCPDS no: 00-009-0432) are quite compatible, it can be concluded that the Ca-P minerals formed on the surface of the scaffold after 4 weeks of incubation on the scaffold are crystalline HAP minerals.
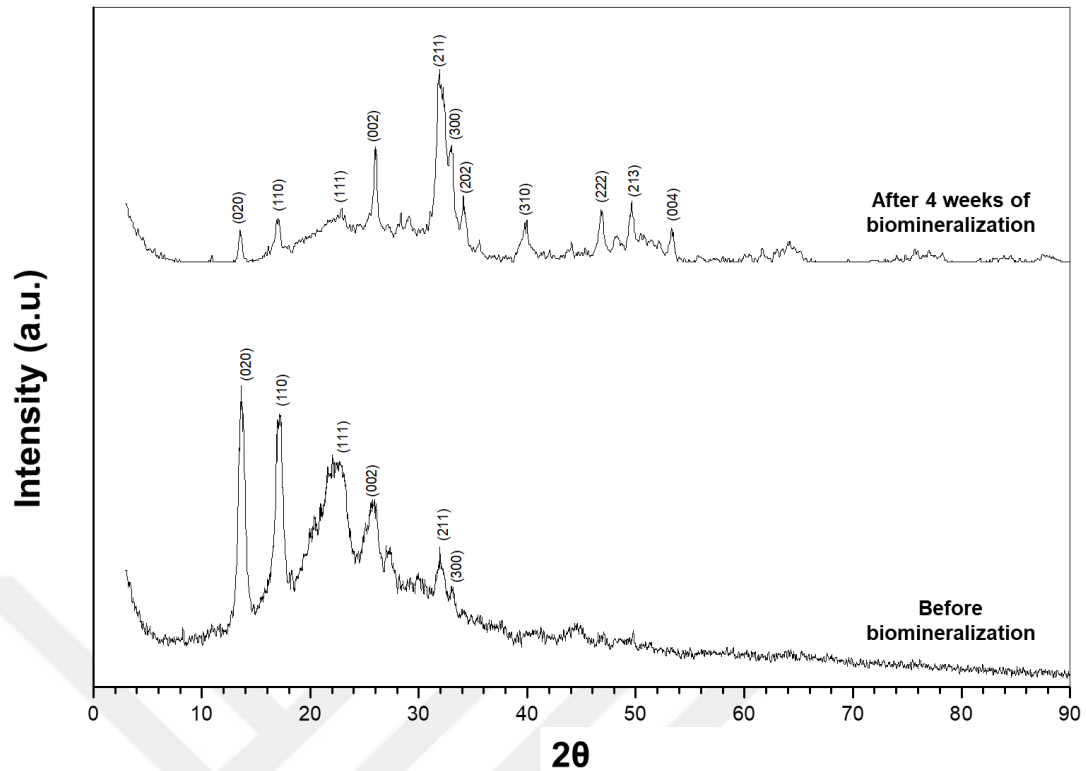
Figure 3.16 XRD patterns of the HAP/PHBV-SF scaffold before and after 4 weeks of biomineralization

3.3.5 In-vitro Cellular Activities

3.3.5.1 Cell Morphology

Figure 3.17 shows the SEM images of the MG-63 osteosarcoma human cell adhesion and spreading on the scaffolds after 10 days of cell culture. Cells had a flattened morphology on all the scaffolds and firmly attached to the nanofibers. In addition, on the surface of the HAP/PHBV, PHBV-SF and HAP/PHBV-SF scaffolds more dispersed cells were seen, whereas there was a smaller number of cells on the PHBV scaffold.
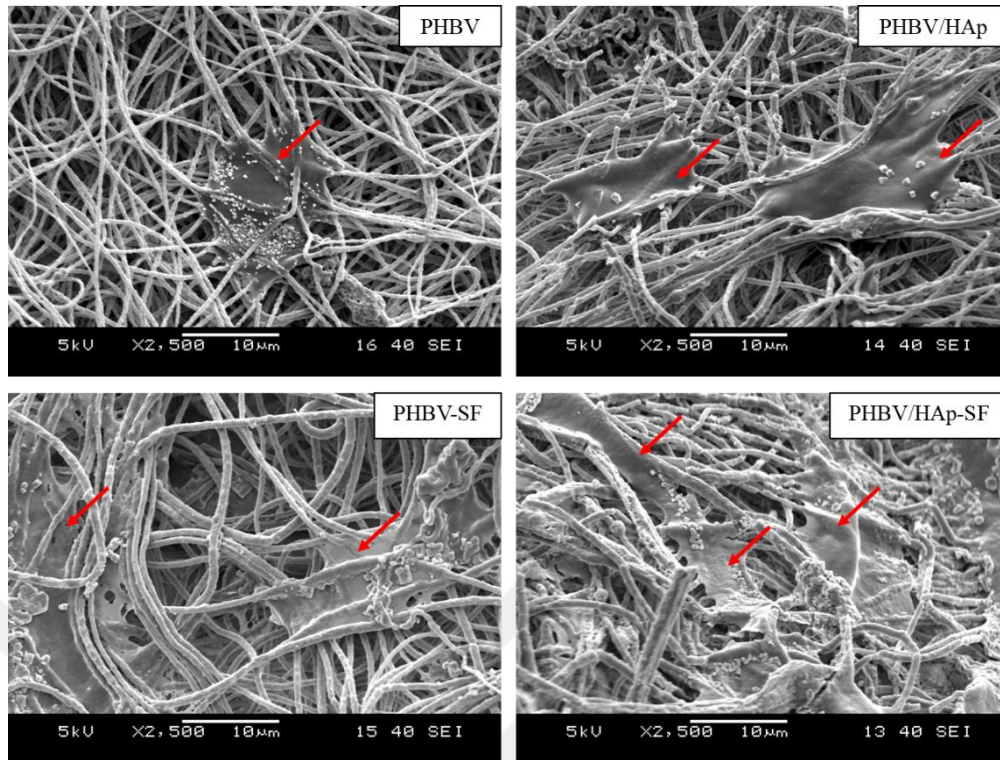
Figure 3.17 SEM images of MG-63 cells on the scaffolds after 10 days of cell culture. Red arrows represent the MG-63 cells

3.3.5.2 Cell Viability

The viability and proliferation of MG-63 cells cultured on the cotton-wool like scaffolds were evaluated by resazurin assay at different culture times (3, 7 and 10 days). Resazurin is a blue and non-fluorescent dye, and it is irreversibly reduced by mitochondrial dehydrogenase enzyme of viable cells to the pink and red fluorescent resorufin. The amount of resorufin, which can be monitored by a spectrophotometer, is proportional to the number of viable cells (McGaw, Elgorashi, & Eloff, 2014). Figure 3.18 shows the cell viability levels of the cells cultured on the scaffold in terms of cell number. It was clearly seen that MG-63 cells proliferated gradually during the culture period on all the scaffolds. After 3 days of cell culture, there was not any significant difference in the viability levels of the cells on the scaffolds. However, with increasing incubation time MG-63 cell seeded PHBV-SF and HAP/PHBV-SF scaffolds had better cell viability compared to that of PHBV scaffold with statistically significant differences. The results suggested that impregnation of silk played a major

59

role in MG-63 cell viability and proliferation, while HAP incorporation alone did not show any significant effect. Yang et. al., 2015 stated that silk fibroin scaffolds with the incorporation of HAP enhance the proliferation of osteoblasts compared to collagen scaffold.
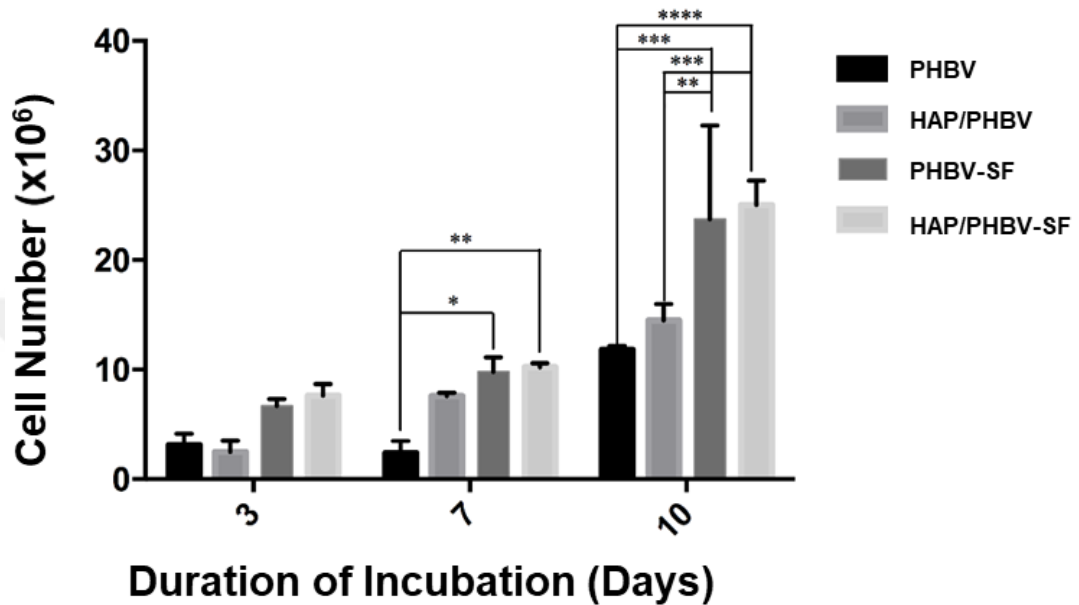
Figure 3.18 Cell viability levels of the cells cultured on the scaffolds after 3, 7 and 10 days of culture. The experiment was repeated in triplicate (n=3) for each sample. Data are shown as averages with the error bars indicating the standard deviation, *p = 0.0142, **p = 0.0092 for 7 day; **p = 0.0023, ***p= 0.0002, ***p=0.0006, ****p <0.0001 for 10 days of culture

3.3.5.3 ALP Assay

ALP is an important enzyme used as an early marker of osteoblastic phenotype, and associated with the synthesis and deposition of type-I collagen and non-collagenous bone matrix proteins (Li et al., 2018). ALP assay uses p-nitrophenyl phosphate as a phosphatase substrate that turns yellow (λmax = 405 nm) when dephosphorylated by ALP. Figure 3.19 illustrates the ALP activity of the MG-63 cells cultured on the scaffolds for 3, 7 and 10 days. An increment in the ALP activity was obtained on the 10th day of cell culture compared to that of other incubation days. However, there was not any statistically significant difference in ALP activity of cells on the scaffolds during the culture period may be due to shortened incubation time. Because it was

stated in the literature that, ALP activity of the osteoblasts cultured on HAP incorporated scaffolds especially at prolonged cell culture times (Kim, Lee, & Knowles, 2006; Tuzlakoglu et al., 2005).
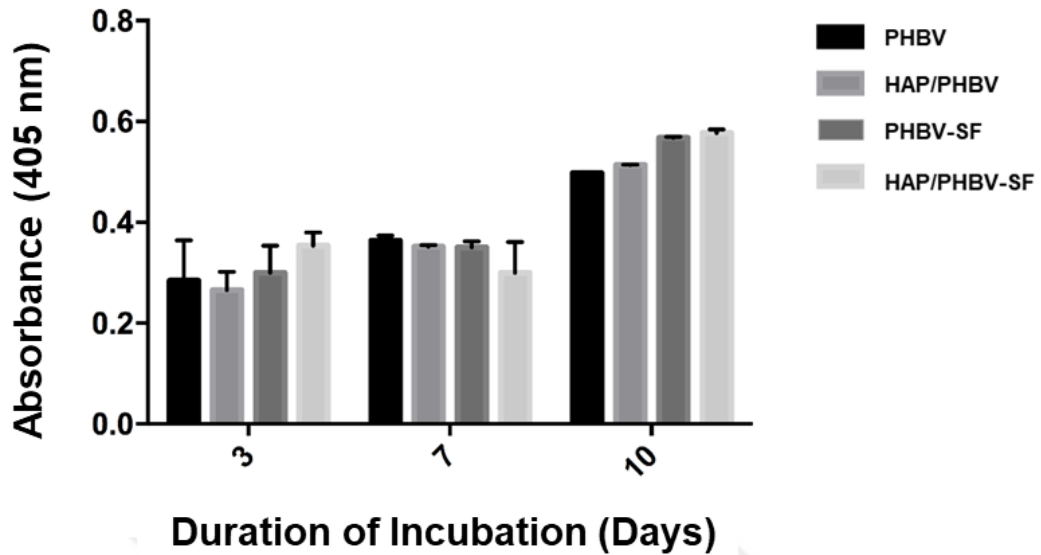
Figure 3.19 ALP activity of the cells cultured on the scaffolds after 3, 7 and 10 days of culture. The experiment was repeated in triplicate (n=3) for each sample. Data are shown as averages with the error bars indicating the standard deviation

3.3.5.4 BCA Assay

BCA protein assay was used to detect and quantify the total protein in the scaffolds. The principle of this assay is the formation of light blue Cu^{2+} and protein complex under alkaline condition first, and then the reduction of Cu^{+2} to Cu^{+1}. Eventually, a purple-colored complex is formed by reacting BCA with Cu^{+1}. Figure 3.20 shows the total cellular protein amounts of the scaffolds determined by micro-BCA assay. The total protein content of the scaffolds was not significantly different within 7 days of culture. However, a significant increase in the protein expression was observed after 10 days of culture between the silk impregnated scaffolds (PHBV-SF and HAP/PHBV-SF) and PHBV indicating that cells started to produce an extracellular matrix containing collagen protein. In the study of Sangkert, et. al., 2016 silk scaffold

with collagen had the highest protein content and they stated that osteoblasts start synthesizing protein after 7 days of cell culture.
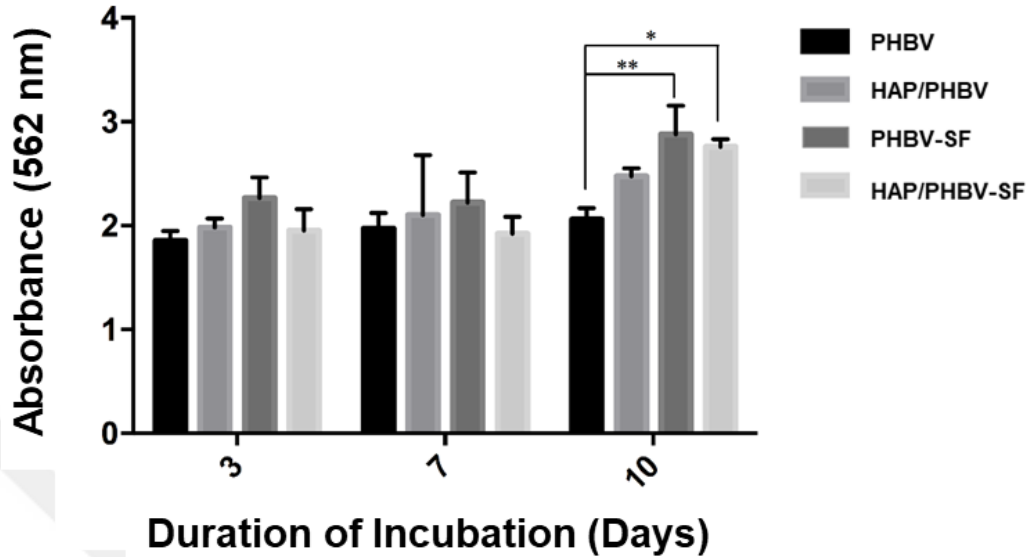
Figure 3.20 Total protein concentration on the scaffolds. The experiment was repeated in triplicate (n=3) for each sample. Data are shown as averages with the error bars indicating the standard deviation, *p =0.0106, **p =0.0028 for 10 days of culture

3.3.6 Histological and Immunohistochemical Analyses

MG-63 cell proliferation and colonization on the PHBV-SF and HAP/PHBV-SF scaffolds after 10 days of cell culture were evaluated by histological analysis in terms of H&E and MT staining (Figure 3.21). As seen from the histological images, even though cells attached and proliferated well on both of the scaffolds, cell migration and accumulation into the inner layer was clearer for HAP/PHBV-SF scaffold than that of PHBV-SF scaffold. In addition, while on PHBV-SF scaffold, cells tend to be aligned in a single row, cells formed clusters on HAP/PHBV-SF scaffold.
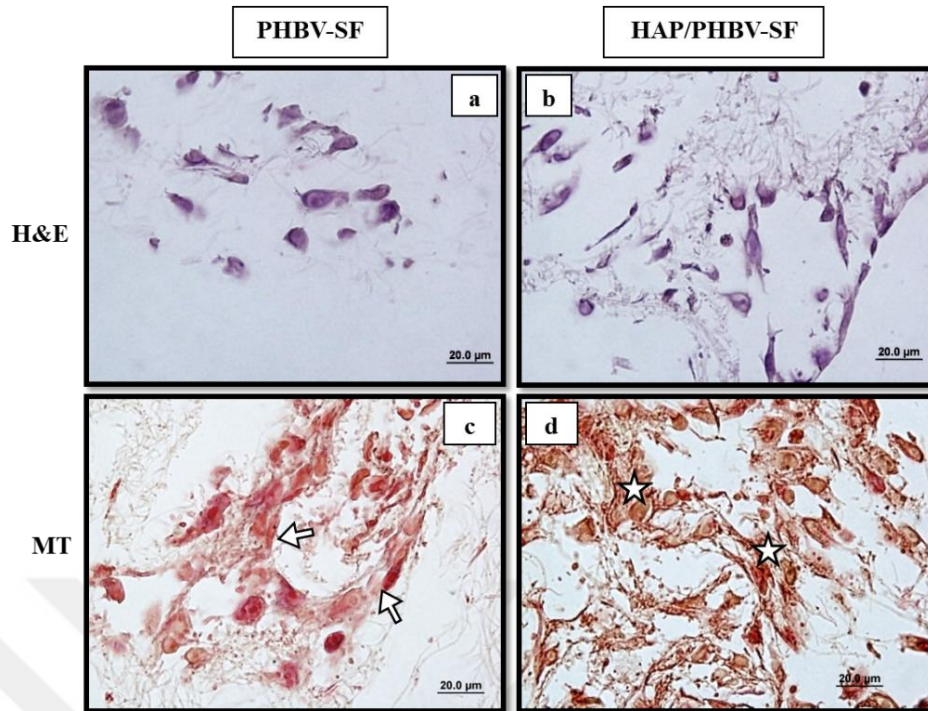
Figure 3.21 Histological images of the PHBV-SF and HAP/PHBV–SF scaffolds by H&E and MT staining after 10 days of cell culture. White arrows represent the aligned MG-63 cells in a single row and stars represent clusters of the MG-63 cells

Figure 3.22 shows the images of immunohistochemical staining by type-I collagen of the HAP/PHBV-SF and PHBV-SF scaffolds after 10 days of cell culture. Both of the scaffolds exhibited immunopositivity. Cells seemed to be lined up on the PHBV-SF scaffold (Figure 3.22 a-c-e). However, on the HAP/PHBV-SF scaffold cells penetrated into the inner layers and they had the tendency to form clusters (Figure 3.22 b-d-f) indicating that cells are ready to produce minerals (Chen et al., 2015). In addition, expression of type-I collagen was more pronounced on the HAP/PHBV-SF scaffold in line with the BCA assay results (Figure 3.20). These results proved that silk together with HAP improved the MG-63 cell adhesion, spreading, proliferation, and osteoblastic activity.
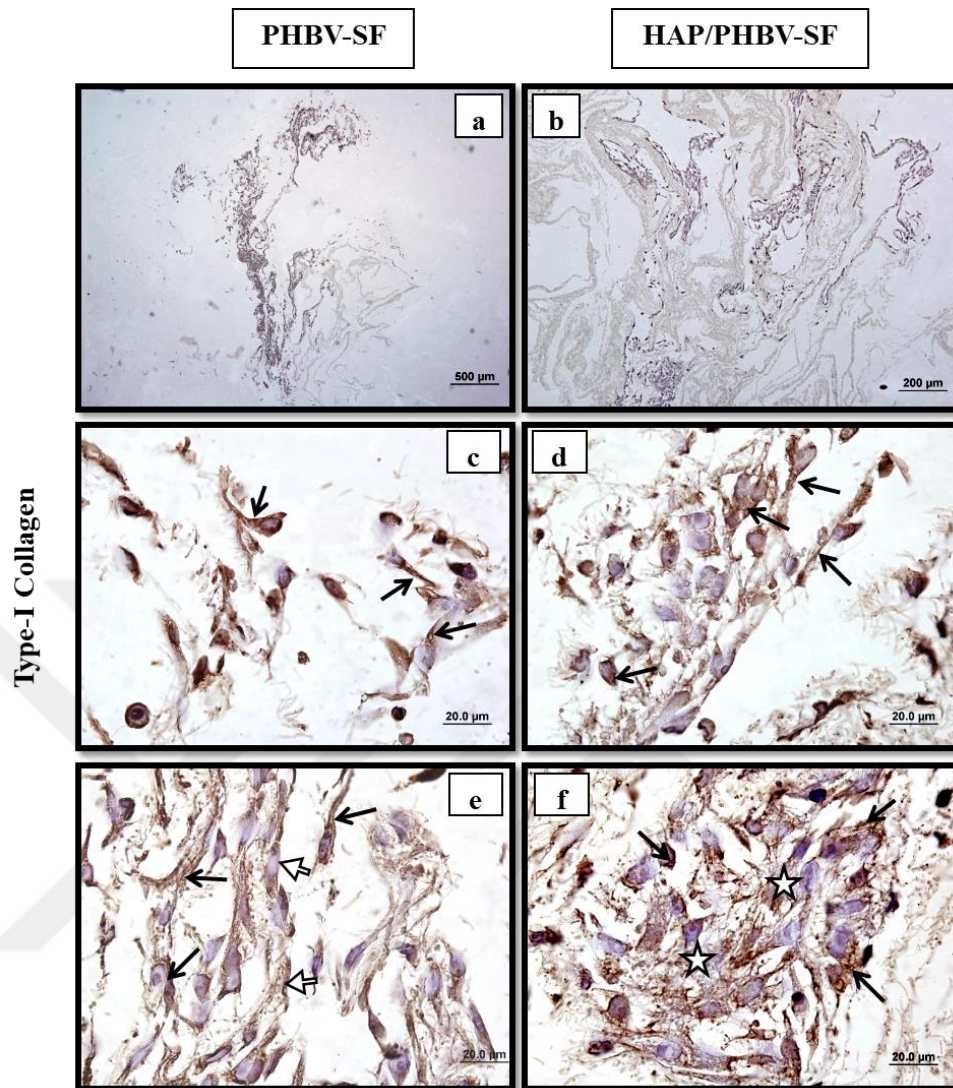
Figure 3.22 Immunohistochemical images of the PHBV-SF and HAP/PHBV–SF scaffolds by type-I collagen staining after 10 days of cell culture. Black arrows represent the immunopositively staining, white arrows represent the aligned MG-63 cells in a single row and stars represent clusters of the MG-63 cells

3.4 Conclusion

In this study, three dimensional and porous PHBV based nanofibrous cotton wool-like scaffolds with the average fiber diameter of 450-850 nm and an average porosity of 80-85% were produced by wet-electrospinning and freeze-drying techniques. Morphology of the scaffolds, which was suitable for tissue engineering applications favored osteoblast cell ingrowth and distribution within the scaffold. According to the

biomineralization and *in-vitro* biocompatibility test results, HAP/PHBV-SF scaffold could be considered as a promising filling material for bone regeneration.

CHAPTER FOUR
CARTILAGE TISSUE ENGINEERING STUDY

4.1 Introduction

Cartilage is an avascular, flexible connective tissue. It is composed of a cartilaginous matrix consisting of collagen fibers, proteoglycans and water, and chondrocytes cells distributed within the matrix (Eslahi, Simchi, Mehrjoo, Shokrgozar, & Bonakdar, 2016; Sharma, Gautam, Dinda, & Mishra, 2011).

There are three types of cartilage in the body with different cartilaginous matrix composition, structure, and function; hyaline, elastic and fibrocartilage. Hyaline cartilage (e.g., tracheal and articular cartilages) is the most abundant type of cartilage in the body. It is rich in type II collagen fibers. Elastic cartilage such as cartilage in the outer part of ear has more elastin fibers and therefore, it is the most flexible one among the cartilages. Fibrocartilages, for example, meniscus and intervertebral disc, are the strongest and the most rigid one since they contain type-I collagen more which is tougher than type-II collagen (Ahmadi, Giti, Mohammadi-Samani, & Mohammadi, 2017; Sharma, Gautam, Dinda, & Mishra, 2011).

Articular cartilage is a hyaline cartilage and it covers the articular-epiphyseal surface of the articulating bones. It keeps the bones together, withstands repetitive loadings, provides a low-friction interface, and makes the joint part shockproof (Ahmadi, Giti, Mohammadi-Samani, & Mohammadi, 2017; Armiento, Stoddart, Alini, & Eglin, 2017).

In the articular cartilage, three zones (superficial, middle, and deep zone) with a different cellular organization and collagen fiber architecture are described. The cross-sectional image of the articular cartilage is seen in Figure 4.1. The superficial zone (STZ) is in contact with a synovial fluid and has the protection function of the deeper zones from shear stress. It constitutes nearly 10% to 20% of articular cartilage thickness. This zone contains tightly packed collagen fibers that are aligned parallel to

the articular surface and more flattened chondrocytes. The middle zone acts as a bridge between superficial and deep zones. It is a thicker zone, representing approximately 40% to 60% of the total cartilage volume. This zone is also the first zone that resists to compressive forces. The proteoglycan content, as well as the diameter of the collagen fibers, are more than that of superficial zone. Besides, it contains randomly oriented collagen fibers, less and spherical chondrocytes. The deep zone has an important function as it provides the greatest compressive resistance due to the perpendicular arrangement of the collagen fibers to the articular surface. The largest diameter of the collagen fibers along the articular cartilage is present at this zone. Besides, this zone contains the highest proteoglycan and the lowest water content. The chondrocytes locate parallel to the collagen fibers that are vertically oriented to the articular surface. The zone right after the deep zone is known as a calcified zone due to the presence of minerals inside. It locates between articular cartilage and subchondral bone and it is not among the main zones of the articular cartilage. This calcified zone has an integral role in securing the cartilage to bone (Armiento, Stoddart, Alini, & Eglin, 2017; Fox, Bedi, & Rodeo, 2009).
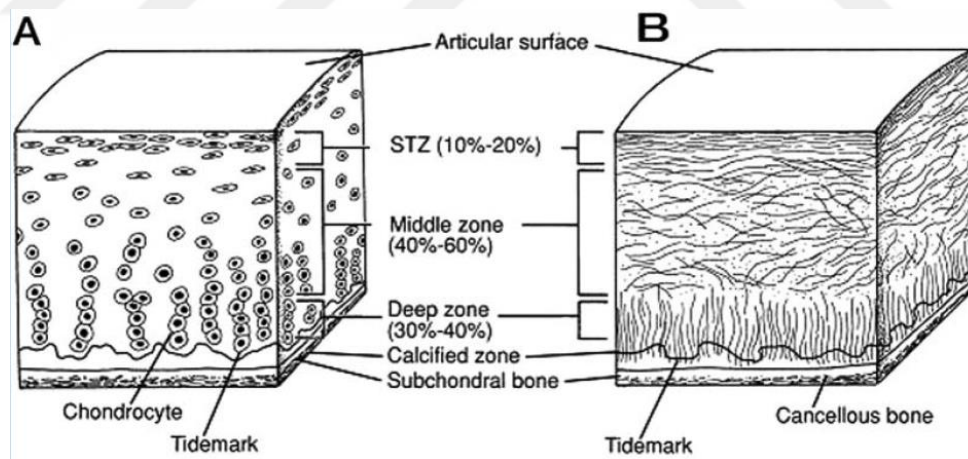
Figure 4.1 A) Cellular organization and B) Collagen fiber architecture of the cross-section of the articular cartilage (Fox, Bedi, & Rodeo, 2009)

Articular cartilage damage arising from trauma, osteoarthritis, excessive wear or low mitotic activity of the cells causes serious cartilage lesions which can induce pain, immobility and joint degeneration. In recent years the number of people suffering from

these lesions has increased considerably as the population aging which demonstrates the importance of the treatment strategies (De Mori, Peña Fernández, Blunn, Tozzi, & Roldo, 2018; Liu et al., 2017; Saladino et al., 2014). However, articular cartilage has limited ability to self-repair due to the absence of direct blood or nerve supply (Ainola et al., 2016; Gugjoo, Amarpal, Aithal, & Kinjavdekar, 2016) Therefore, in order to repair articular cartilage defects traditional techniques such as joint surgery, subchondral bone drilling and microfracture, osteochondral autograft transfer, and osteochondral allograft transplantation have been widely used. However, these techniques are not very successful in repairing defects and forming long-lasting cartilage tissue with a similar natural structure, composition and mechanical behavior. In addition, they have side effects such as pain, donor site morbidity, and risk of infection. Therefore, there is an enormous need for developing new cartilage regeneration approaches in order to overcome the drawbacks of the traditional techniques (Coburn, Gibson, Monagle, Patterson, & Elisseeff, 2012; Seol et al., 2015).

Cartilage tissue engineering is a promising therapeutic strategy for cartilage repair and regeneration by the help of tissue engineering components- cells, growth-stimulating signals and a scaffold (Iwasaki et al., 2010). In this regard, for the scaffold design, the model is the natural ECM and it is important to create the ideal structure that can mimic the structure, composition, morphology, and bioactivity of the natural ECM until the new tissue is formed (Holzwarth & Ma, 2011a; Li, Laurencin, Caterson, Tuan, & Ko, 2002).

Hydrogels have attracted great attention as the scaffolds for cartilage tissue engineering due to the similarity between their hydrated structures and hydrophilic environment of cartilaginous ECM. Hydrogels are lightly cross-linked structures with a swelling ability and high-water uptake capacity (Varaprasad, Raghavendra, Jayaramudu, Yallapu, & Sadiku, 2017; Yodmuang et al., 2015) They can be classified according to source (natural and synthetic origin), polymeric composition (homopolymer, copolymer, interpenetrating polymer hydrogels), configuration (amorphous, semi-crystalline, crystalline), type of cross-linking (physical and

chemical), electrical charge (nonionic, ionic, amphoteric, zwitterionic) and physical appearance (Ahmed, 2015).

For the development of functional cartilage tissue, various synthetic and natural hydrogel materials have been used. Chitosan, a natural polysaccharide, has attracted great attention due to its structural similarity to glycosaminoglycans (GAGs) in the cartilage ECM as well as its nontoxic, biodegradable and biocompatible properties (Dimida et al., 2017; Yang, Zhang, Yue, & Khademhosseini, 2017) Due to the fact that chitosan is insoluble in water, carboxymethyl chitosan (CMCht) has been recently used in biological applications due to its desired water solubility and biological properties. For the chemical cross-linking of chitosan and CMCht, instead of toxic formaldehyde and glutaraldehyde cross-linking agents, recently non-toxic genipin and poly (ethylene glycol) diglycidyl ether (PEGDE) cross-linkers were introduced (Cao et al., 2018; Gonçalves, da Silva, Signini, & Naves, 2017).

Genipin is a natural, colorless and non-toxic cross-linking agent obtained by the extraction of fruits of Gardenia jasminoides ellis. It forms stable hydrogels by the reaction of amino groups and genipin (Kanoujia, Singh, Singh, & Saraf, 2016; Neri-Numa, Pessoa, Paulino, & Pastore, 2017).

PEGDE or with another common name, diepoxy PEG, is a cheaper cross-linking agent used in recent years as an alternative to genipin. It is a water-soluble epoxy resin and has two epoxide functional groups (cyclical ether with a three-membered ring) located at both ends of each molecule. It has been used as a cross-linking agent for polysaccharides and proteins *via* ring opening of the epoxide group by the chemical reaction with the amino, carboxyl and hydroxyl functional groups (Gámiz-González, Edlund, Vidaurre, & Gomez Ribelles, 2017; Lu, Xu, Zheng, Zhang, & Su, 2006; Vargas, Acevedo, López, & Romero, 2008).

Yan et al., 2010 prepared biodegradable and porous genipin-cross-linked collagen/chitosan scaffolds for articular cartilage regeneration. The *in-vitro* cell

culture study results showed that the prepared scaffolds demonstrated good cell adhesion, spread, and viability.

Saladino et al., 2014 produced chitosan hydrogel scaffolds cross-linked with PEGDE. *In-vitro* test results have shown that hydrogels are non-toxic and induce chondrocyte differentiation.

CMCht is a prominent polymer in recent years, therefore; in the literature, there are not many studies comprising CMCht for tissue engineering applications. Gámiz-González, Edlund, Vidaurre, & Gomez Ribelles, 2017 produced highly swellable CMCht hydrogels cross-linked with PEGDE. The indirect cytotoxicity assay, porosity analyses, swelling and degradation tests showed that the produced hydrogels have the potential to apply in soft tissue regeneration.

Although natural biopolymers are often preferred due to their improved biocompatibility; their mechanical properties are not high enough. Therefore, composite scaffolds have become important to provide desired mechanical properties while maintaining high biocompatibility (Mirahmadi, Tafazzoli-Shadpour, Shokrgozar, & Bonakdar, 2013). The composite structure of the cartilaginous ECM plays a critical role in the load-bearing joints during dynamic loading. Besides, it provides complex mechanical properties such as viscoelasticity and stress relaxation. Therefore, the development of fiber-reinforced hydrogel scaffolds in cartilage tissue engineering is of great importance. The fibers as a reinforcement agent within the hydrogels significantly improve the mechanical properties of the structure due to stress transfer between the matrix and the reinforcement (Bas et al., 2017; Butcher, Offeddu, & Oyen, 2014). In the literature, there are only a few studies about fiber-reinforced composite scaffolds for tissue engineering applications. Bas et al., 2017 produced melt spun polycaprolactone fiber reinforced poly(ethylene glycol)/heparin hydrogel scaffolds that can mimic the complex mechanical behavior of articular cartilage. These produced scaffolds showed viscoelastic and anisotropic properties as well as high biocompatibility.

In this part of the thesis, it was aimed to produce PHBV nanofiber reinforced CMCht-SF hydrogel composite scaffolds that can mimic the structure and mechanical properties of the cartilaginous ECM for cartilage tissue engineering. Considering that the macromolecules in the ECM are fibrous structures, wet-electrospun PHBV nanofibers were added to CMCht-silk solution and they were allowed to cross-link by PEGDE. CMCht was chosen since it is structurally similar to various GAGs that are present in cartilage tissue. Besides, in the production of the scaffolds silk was used as a natural protein because of its similarity to collagen and lower cost. Scanning electron microscopy and Fourier Transform Infrared Spectroscopy were used for the characterization of the morphology and chemical structure of the scaffolds, respectively. Swelling ratios and thermal behavior of the scaffolds were also evaluated. Dynamic mechanical analysis (DMA) was used to examine the viscoelastic properties of the scaffolds. Compression test together with texture profile analysis were applied to determine the mechanical properties of the scaffolds. The attachment, viability and proliferation, and chondrogenic differentiation of rat bone marrow-derived mesenchymal stem cells on the scaffolds were investigated by SEM, alamar blue assay, and histological analysis by of alcian blue staining, respectively.

4.2 Experimental

4.2.1 Materials

O-carboxymethylated CMCht with a deacetylation degree around 91% was obtained from Santa Cruz Biotechnology, USA. Cocoons of Bombyx mori silkworm silk were supplied from the Turkish Republic of Northern Cyprus. The required materials for the production of silk solution; Na_2CO_3 and $CaCl_2$ were obtained from Merck, Germany; dialysis tubing cellulose membrane was purchased from Sigma Aldrich, USA. PHBV (PHV content 3 wt%, $M_n=80$ kDa) was supplied from Helian Polymers, Netherlands. BTEAC, chloroform and PEGDE ($M_n=500$) were obtained from Sigma-Aldrich, USA.

The *in-vitro* cell growth and differentiation tests were performed in the Biomaterials and 3D Biointerphases Laboratory at Department of Bioengineering, Ege University. Alpha-MEM (Alpha modified Dulbecco's Eagle's medium, F0915, Biochrom), PBS (14190-144, Gibco, USA), trypsin-EDTA (T3924, Sigma), alamar blue dye (30025-1, Biotium), gluteraldehyde (8.20603.1000, Merck), sucrose (A2211, Applichem), osmium tetraoxide (201030-16, Sigma), hexamethyldisilazane (HMDS) (804324, Sigma), fetal bovine serum (FBS) (A0500-3010, Cegrogen), L-glutamine (K0283, Merck), gentamicin (A2712, Merck), DMEM-LG (F0415, Merck), alcian blue dye (A5268, Sigma), dexamethasone (D2915, Sigma-Aldrich, USA), ascorbic acid (A8960, Sigma-Aldrich, USA), TGF-β1 (H8541, Sigma-Aldrich, USA), ITS premix (I3146-5ML, Sigma-Aldrich, USA), paraformaldehyde (PFA) (100496, Merck), HCl (07102, Riedel-de Haen) were used.

4.2.2 Production of Wet-Electrospun PHBV Nanofibers

PHBV nanofibers were produced by wet-electrospinning technique as described in the previous chapter: Initially, PHBV solution was prepared by dissolving PHBV (3% (w/v)) and BTEAC (0.2% (w/v)) in chloroform at 50°C for 2 h and at room temperature overnight by means of stirring. Then, prepared PHBV solution was subjected to the wet-electrospinning process for 15 min at optimized spinning parameters (working distance: 10 cm, flow rate: 2.0 ml/h and voltage: 20 kV). As the coagulation bath solution ethanol-distilled water mixture at 9:1 volume ratio was used. Finally, homogeneously suspended nanofibers were collected and washed thoroughly in distilled water.

4.2.3 Preparation of CMCht and Silk Solutions

CMCht solutions at different concentrations (1 and 5% (w/v)) were prepared by dissolving CMCht in distilled water and stirring at room temperature overnight.

Silk solution was prepared by following the steps described in the previous chapter: Bombyx mori cocoons were firstly degummed with 0.1 M Na_2CO_3 solution at 70ºC

for 3 hours in order to remove sericin. After three times of degumming cocoons were rinsed thoroughly with distilled water. Then, the degummed silk was dissolved in a ternary solvent system of $CaCl_2/CH_3CH_2OH/H_2O$ in a molar ratio of 1/2/8 at 70ºC for 6 hours and filtrated. Next, the filtrated solution was subjected to dialysis in distilled water. After 3 days, silk aqueous solution with the concentration of 2% (w/v) was obtained.

4.2.4 Production of Hydrogel Composite Scaffolds

PHBV nanofiber reinforced CMCht-SF hydrogel composite scaffolds were produced by freeze-drying of the chemically cross-linked hydrogels in order to obtain the three-dimensional and porous structure.

Before the production of hydrogel composite scaffolds, CMCht and SF solutions consisting of various PEGDE concentration were prepared separately and allowed to cross-link at different temperatures to determine the optimum cross-linking parameters. CMCht hydrogels were prepared by adding 2.5 and 5% (w/v) PEGDE to the CMCht solution (1 and 5% (w/v)), and cross-linking behavior of these solutions was observed at 25ºC and 40ºC. For the preparation of SF hydrogels, various PEGDE concentrations (2.5, 5, 50 and 100% (w/v)) were mixed with 2 ml SF solution (2% (w/v)) and the hydrogel formation was observed at the same temperatures as that of CMCht gelation.

In order to obtain hydrogel composite scaffolds, initially CMCht (5% (w/v)) and silk solutions (2% (w/v)) were mixed at an equal volume, and PEGDE was added to the polymer mixture at different weight ratios (polymer: PEGDE; 2:1, 1:1, 1:2 (w:w)). The resultant mixtures were stirred at room temperature for 1 h to yield homogeneous solutions. Then, suspended wet-electrospun PHBV nanofibers were incorporated to these solutions and allow to disperse for an hour. After cross-linking at 40°C overnight, the produced hydrogels were freeze-dried (TELSTAR – LyoQuest -85) at -25°C under 0.1mbar pressure for 2 days. Then, they were treated with methanol for an hour to immobilize the silk and washed with distilled water to remove methanol and excess

PEGDE. Finally, they were freeze-dried. CMCht-SF hydrogel scaffolds were also produced without PHBV nanofiber reinforcement. The codes of the scaffolds were given in Table 4.1.

Table 4.1 The codes of the produced hydrogel scaffolds

Scaffold code	CMCht-SF:PEGDE (w/w)	PHBV nanofiber addition
CMCht-SF2:PEGDE1	2:1	-
CMCht-SF1:PEGDE1	1:1	-
CMCht-SF1:PEGDE2	1:2	-
PNFs/CMCht-SF2:PEGDE1	2:1	✓
PNFs/CMCht-SF1:PEGDE1	1:1	✓
PNFs/CMCht-SF1:PEGDE2	1:2	✓

4.2.5 Characterization of the Hydrogel Scaffolds

4.2.5.1 SEM Analysis

The cross-section morphological analyses of the scaffolds were performed by SEM (JEOL JSM-6060) at an accelerating voltage of 5 kV. All the scaffolds were coated with a thin layer of gold/palladium prior to analysis. The average diameter of the PHBV fibers was estimated from the SEM images of 2500x *via* Image J program by taking measurements from 25 different points for each of the sample.

4.2.5.2 ATR-FTIR Analysis

The chemical structures of the scaffolds were determined by ATR-FTIR (Perkin Elmer Spectrum BX). Each spectrum was obtained in the wavenumber range of 4000-650 cm^{-1} at a resolution of 4 cm^{-1}, and by scanning 25 times per sample.

4.2.5.3 DTA/TGA

DTA/TGA (Shimadzu DTG-60H) was used to determine the thermal properties of the scaffolds. Analyses were performed under a nitrogen atmosphere at a heating rate of 10°C/min and in the temperature range of 25-700°C, and the decomposition behavior, T_m and T_p values of the scaffolds were estimated.

4.2.5.4 Swelling Ratio Test

The swelling test of the scaffolds was performed in phosphate buffered saline (PBS) solution. First, the dried scaffolds (n=3) were weighed (w_0), and then immersed in PBS at 37°C for 24 hours. After excess water was removed with a filter paper, scaffolds were weighed (w_s) again. Swelling ratio and water content values of the hydrogel scaffolds were calculated according to the following equations (4.1) and (4.2), respectively.

$$Swelling\ ratio\ (\%) = \left(\frac{w_s - w_0}{w_0}\right) x\ 100 \qquad (4.1)$$

$$Water\ content\ (\%) = \left(\frac{w_s - w_0}{w_s}\right) x\ 100 \qquad (4.2)$$

4.2.5.5 Viscoelastic Property Characterization

The viscoelastic measurements were performed using a dynamic mechanical analyzer, DMA (TA, Q800) equipped with the compression mode. The measurements were carried out using dynamic frequency sweep with frequencies ranging from 100 Hz to 0.1 Hz at 37°C under a constant strain amplitude (1%). The storage (E') and loss modulus (E") of the samples were measured, and the tan delta (tan δ) values were calculated from the moduli.

4.2.5.6 Mechanical Test

Mechanical properties of the prepared scaffolds were determined by TA XT Plus Texture Analyzer with a 5 kgf load cell. The cylindrical samples with a dimension of 7 mm diameter and a thickness of 10 mm were compressed at a constant deformation rate of 0.5 mm/sec up to a strain of 80%. All the experiments were performed at room temperature in triplicates. Stress values at a strain of 80% were recorded as the compressive strength. Compressive moduli of the scaffolds were determined by slope fitting the initial linear region of stress-strain curves.

4.2.5.7 Texture Profile Analysis (TPA)

In order to evaluate the mechanical behavior of the scaffolds in a wet environment, swollen scaffolds were subjected to two-cycle compression test by texture profile analysis (TA XT Plus Texture Analyzer with a 5 kgf load cell). The scaffolds were immersed in PBS at physiological pH (~7.4) and temperature (~37ºC) overnight prior to the tests. The swollen scaffolds with a dimension of 14 mm diameter and a thickness of 7 mm were compressed twice with a probe (25 mm diameter) at a test rate of 0.5 mm/sec up to 40% deformation. All the experiments were conducted at room temperature in triplicates. Parameters such as hardness, cohesiveness, springiness and resilience were determined from the obtained force-time plot.

4.2.6 In-vitro Biological Assays

4.2.6.1 Culture of Bone Marrow Mesenchymal Stem Cells (BMSCs)

The bone marrow mesenchymal stem cells (BMSCs) which were isolated from the rats in accordance with the 2015-020 numbered and 26.08.2015 dated permission of Ege University Animal Experiments Local Ethics Committee (EUHADYEK) were cultured in Alpha MEM medium supplemented with 10% (v/v) FBS, 1% (v/v) L-glutamine and 0.1% gentamicin at 37°C in a 95% humidified incubator of 5% CO_2 in 75 cm^2 cell culture flasks. The medium was changed once in three days. Cells were

76

passaged after 70-80% confluency was achieved. The cells were trypsinized with trypsin-EDTA (2.5g/L trypsin, 0.5 mM EDTA) and suspended in fresh media. The prepared hydrogel scaffolds were put in a petri plate and sterilized with ethylene oxide. The sterilized materials were left for a week prior to using in cell culture studies. The scaffolds were conditioned with Alpha MEM medium containing 10% FBS and 1% L-glutamine overnight. After the conditioning, the nutrient medium was taken and cells were seeded dropwise at a density of 4.6×10^5 cells/ml (0.132 cm^3 one scaffold volume and 10^6 cells/cm^3 cell seeding density with 0.3 ml medium) onto the scaffolds. After cell attachment, the culture media was added and the cells on the scaffolds were cultured for up to 10 days in a 95% humidified and 5% CO_2 atmosphere at 37°C. The media were changed every other day. All experiments were performed in triplicate (n=3).

4.2.6.2 Alamar Blue Assay

The proliferation analysis of BMSC-seeded scaffolds was done using Alamar Blue assay for a period of 10 days. After 1, 4, 7, and 10 days of cell culture, the medium was removed, and 500 µl of a medium containing 10% Alamar blue (resazurin) dye was added to each well. The cells were incubated for 3 hours at 37°C. After incubation 100 µl of the medium was transferred to the 96-well plate in triplicate (n=3) and absorbance was measured at 570 and 600 nm wavelengths. In this assay, resazurin reduced by mitochondrial dehydrogenase enzyme of viable cells to the pink and red fluorescent resorufin. Therefore, to evaluate the cell viability, the absorbance value of background at 600 nm was subtracted from the absorbance value of 570 nm which is the absorbance value of the resorufin.

4.2.6.3 Cell Morphology

The cell morphology of the bone marrow mesenchymal stem cells on the scaffolds after cell culture was observed by SEM after the fixation process. Firstly, the medium was aspirated from the wells and samples were washed with PBS for 30 seconds. Then, they were fixed in buffer A (5% glutaraldehyde in 0.1M sodium cacodylate),

buffer B (7% sucrose in 0.1M sodium cacodylate), and buffer C (2% osmium tetroxide in 0.1 M sodium cacodylate), respectively for 30 min each. Following a buffer rinse, the samples were washed with distilled water twice for 5 minutes and they were dehydrated in gradual ethanol series (35%, 50%, 70%, 85%, 95%, and 100%). Finally, samples were treated with HMDS solution for 5 min. After the withdrawal of HMDS solution from samples, samples were left to dry overnight, and stored in a desicator. Samples were sputter-coated with thin layer gold/palladium prior to imaging by SEM.

4.2.6.4 Chondrogenic Differentiation

The chondrogenic differentiation protocol was performed to examine the differentiation ability of the bone marrow stem cells to the cartilage tissue on the scaffolds. Initially, the cells covering 80% of the culture plate surface were removed by trypsinization and they were seeded on the scaffolds in a 48-well plate at a concentration of 4.6×10^5 cells/ml with α-MEM, 10% FBS and 0.1% gentamicin-containing culture medium. After 48 hours, the cells were placed in differentiation medium, which contains DMEM-LG, 10% FBS, 0.1% gentamicin (50 mg/ml), 100 nM dexamethasone, 50 µg/ml ascorbic acid, 10ng/ml TGF-β1, ITS premix (1%). It was changed three times a week for 21 days.

In order to determine the chondrogenic differentiation of the cells on the scaffolds, alcian blue staining was performed. Initially, the media was removed and scaffolds were washed with PBS without Ca^{+2} and Mg^{+2} twice. Then, they were fixed with 4% PFA by shaking for 30 minutes. The washing step with PBS was repeated and samples were left in distilled water containing sucrose (3%) for cryosectioning. Micronized sections (5 µm) were taken from the scaffolds by a cryostat. After that, 1% alcian blue solution was added onto the samples and they were incubated for 30 minutes in a dark place. After incubation, they were washed with 0.1N HCl three times. Finally, a reverse phase light microscope was used to observe the differentiation.

4.3 Results and Discussion

4.3.1 Preparation of the Hydrogels

In the preparation step of pure CMCht hydrogels 5% (w/v) CMCht solution was selected as the optimum concentration as gelation was not observed in the 1% (w/v) CMCht solution at any cross-linker concentration or temperature. Besides, due to the fact that gelation at 25ºC lasted more than a day, the optimum cross-linking temperature was chosen as 40ºC. On the other hand, pure SF hydrogels could not be obtained at neither 25ºC nor 40ºC at any PEGDE concentration. Even though, in the literature insoluble SF films were prepared with the addition of PEGDE followed by drying at 60°C (Moonsri, Watanesk, Watanesk, Niamsup, & Deming, 2008; Wang et al., 2013; Wei, Sun, Yi, Zhao, & Wang, 2014). Higher cross-linking temperatures were not tried due to the potential risk of protein denaturation.

CMCht-SF hydrogels were prepared by mixing of CMCht (5% (w/v) and SF (2% w/v) solutions at a 1:1 volume ratio and subsequently adding PEGDE to the polymer mixture at different weight ratios related to the total weight of the polymers in the solution (Table 1). After homogenization under constant stirring for 1 hour at room temperature, they were left to cross-link at 40°C overnight.

Figure 4.2 and Figure 4.3 shows the photos obtained from the inverted eppendorf testing for gel formation of three kinds of solutions with or without PHBV nanofiber integration, respectively. It was seen that after cross-linking at 40°C overnight, liquid CMCht-SF solutions converted to gel state through the ring-opening reaction of the epoxy groups between in PEGDE with the amine and hydroxyl groups in carboxymethyl chitosan (Cao et al., 2018; Gámiz-González, Edlund, Vidaurre, & Gomez Ribelles, 2017).
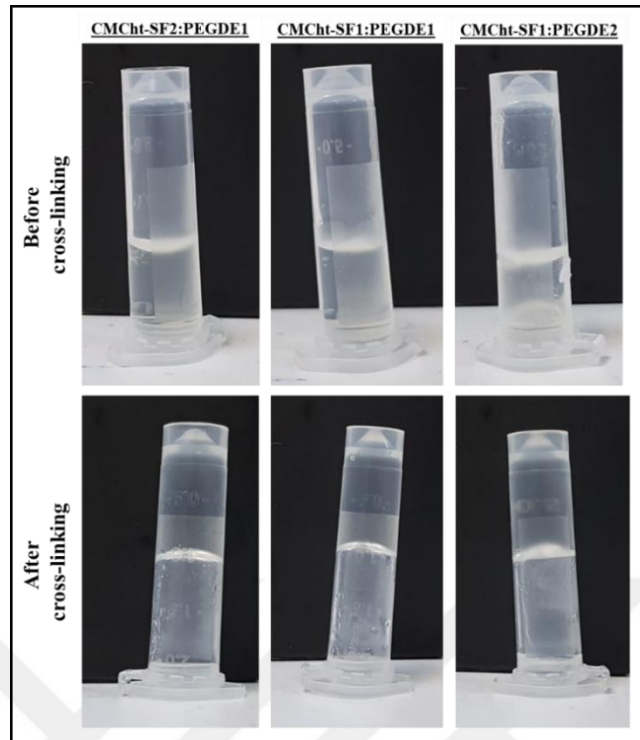
Figure 4.2 CMCht-SF hydrogels before and after cross-linking reaction (Personal archive, 2019)
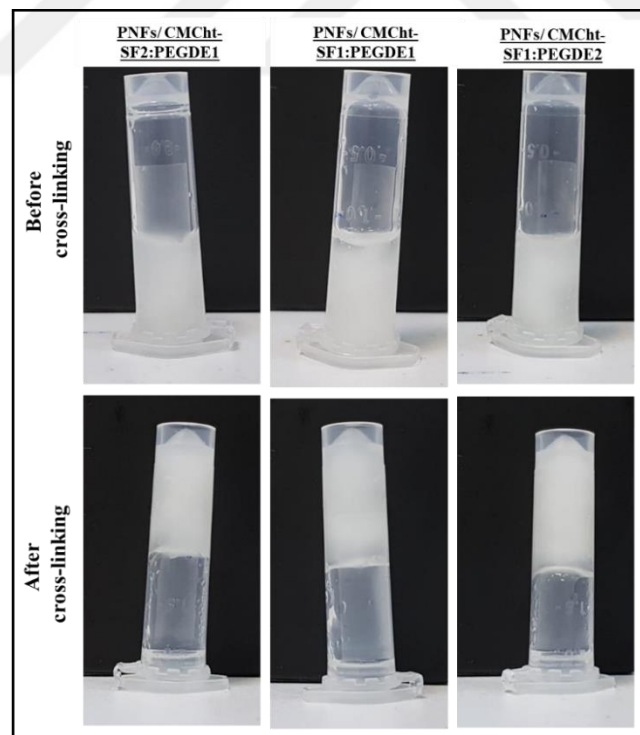
Figure 4.3 PHBV nanofiber reinforced CMCht-SF hydrogels before and after cross-linking reaction (Personal archive, 2019)

4.3.2 Production and SEM analysis of the Hydrogel Scaffolds

The scaffolds were obtained by freeze-drying the hydrogels followed by methanol treatment for the immobilization of the silk. The images of the produced CMCht-SF and PHBV nanofiber reinforced CMCht-SF hydrogel scaffolds are seen in Figure 4.4. At the highest PEGDE concentration, the CMCht-SF1:PEGDE2 and PNFs/CMCht-SF1:PEGDE2 scaffolds collapsed due to increased cross-linking.
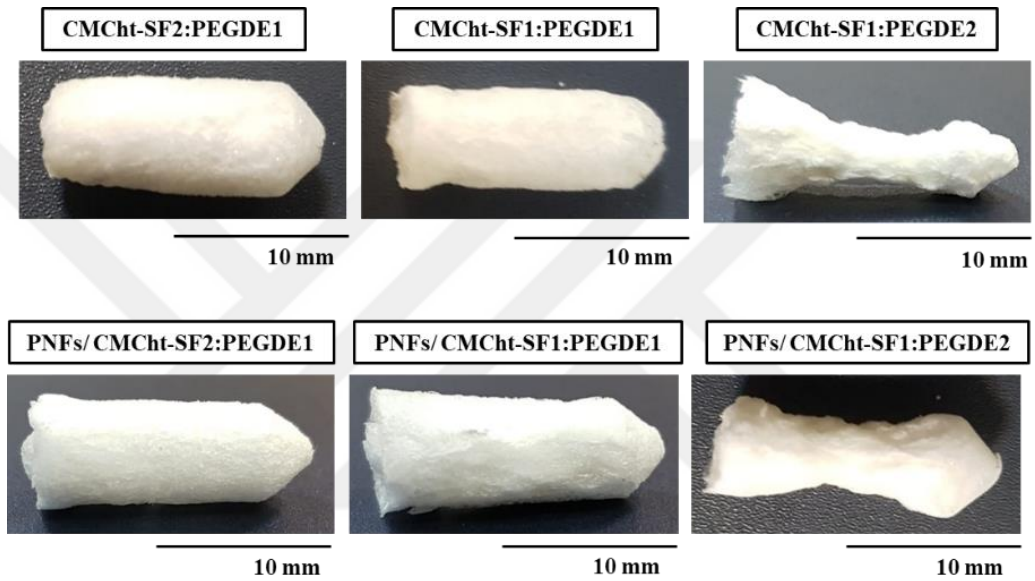
Figure 4.4 Images of the freeze-dried hydrogel scaffolds (Personal archive, 2019)

Figure 4.5 shows the cross-sectional SEM images of the CMCht hydrogel scaffolds that were obtained by chemically cross-linking of CMCht (5% (w/v)) with PEGDE (2.5 and 5% (w/v)) at 40°C for 3 hours followed by freeze-drying. A well-documented fact is that for cartilage regeneration, a three-dimensional interconnected porous structure of the scaffold is a requisite in order to assure cell attachment, growth and migration within the scaffolds (Raghunath, Rollo, Sales, Butler, & Seifalian, 2007; Weigel, Schinkel, & Lendlein, 2006).
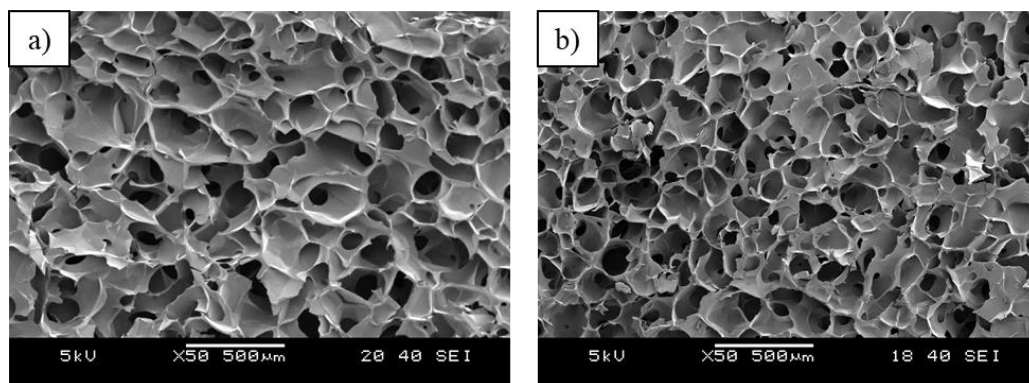
Figure 4.5 Cross-sectional SEM images of the CMCht hydrogel scaffolds cross-linked with a) 2.5% and b) 5% (w/v)) of PEGDE

The cross-sectional morphologies of the PEGDE cross-linked CMCht-SF and PHBV nanofiber reinforced CMCht-SF hydrogel scaffolds were also examined by SEM. The SEM images at 50x magnification were seen in Figure 4.6. All the scaffolds displayed a three-dimensional interconnected microporous structure formed by virtue of the freeze-drying, with the pores being the result of ice crystal formation (Yan et al., 2016). On the other hand, nanofiber reinforced hydrogel scaffolds showed more uniform microporous structure with smaller pores (Figure 4.6d, e and f). Regardless of whether PHBV nanofiber incorporation, the scaffolds containing doubled cross-linker concentration with respect to polymer (Figure 4.6 c and f) showed non-homogeneous structure due to the collapse of the scaffolds.
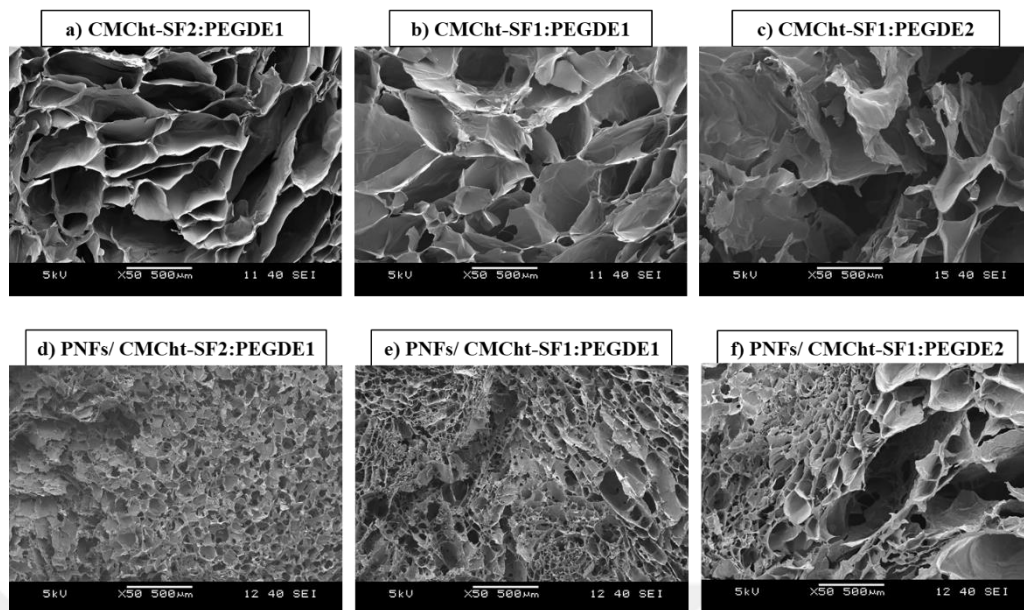
Figure 4.6 Cross-sectional SEM images of the prepared hydrogel scaffolds

Figure 4.7 shows the cross-sectional SEM images of the PHBV nanofiber reinforced CMCht-SF hydrogel composite scaffolds with higher magnification images. An ideal cell-carrier substance should be one that closely mimics the natural environment in the cartilaginous ECM which is a composite structure consisting of collagen fibers and proteoglycans. Therefore, a fibrous structure in the scaffold is also important due to their structural similarity with the native cartilage ECM (Xu, Cai, Xu, & Yang, 2014). As seen from Figure 4.7, PHBV nanofibers were well incorporated into the pore walls of the scaffolds. The average diameter of the nanofibers was obtained as 728 ± 64, 735 ± 70, and 731 ± 81 nm for PNFs/ CMCht-SF2:PEGDE1, PNFs/ CMCht-SF2:PEGDE1, and PNFs/ CMCht-SF2:PEGDE1 scaffolds, respectively.

PNFs/ CMCht-SF2:PEGDE1
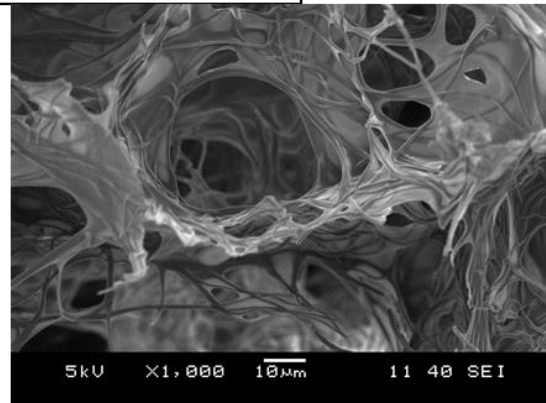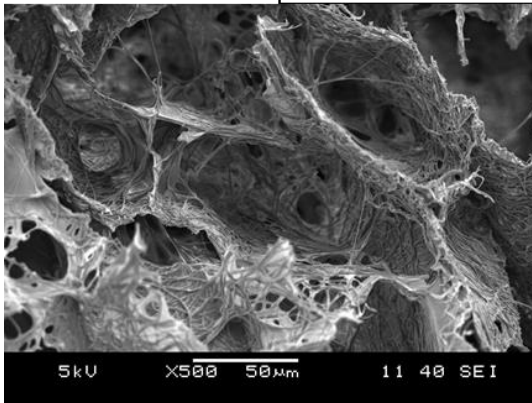
PNFs/ CMCht-SF1:PEGDE1
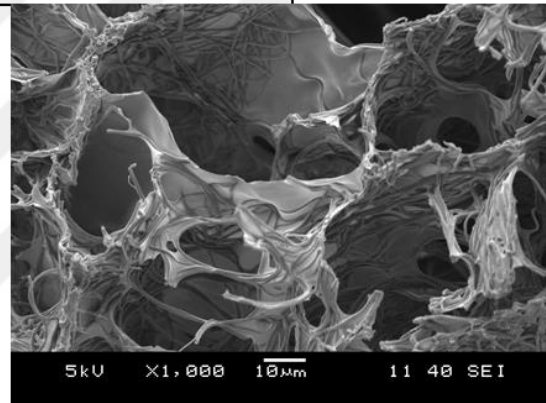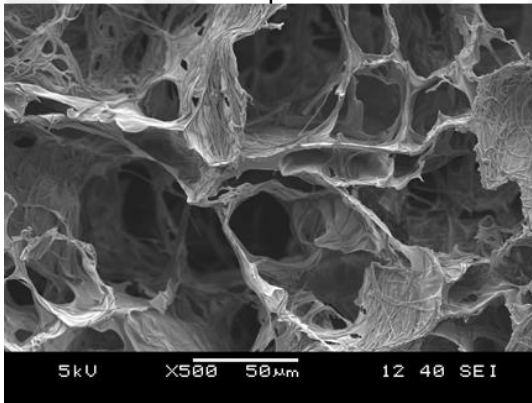
PNFs/ CMCht-SF1:PEGDE2
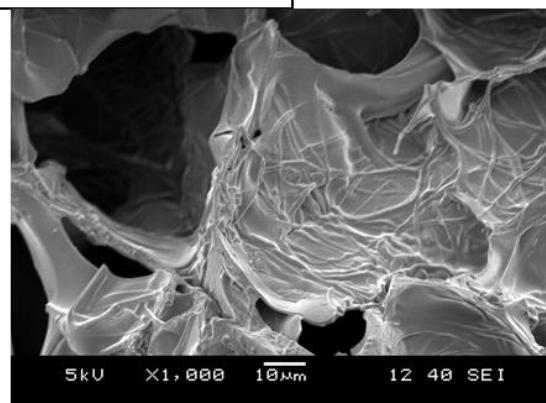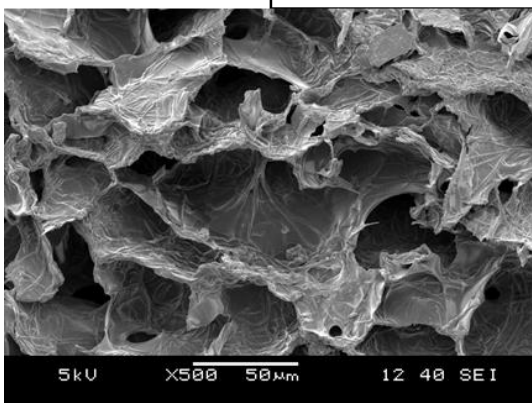
Figure 4.7 Higher magnification SEM images of the cross-sections of PHBV nanofiber reinforced CMCht-SF hydrogel scaffolds

4.3.3 ATR-FTIR Analysis

FTIR analysis was carried out to investigate the cross-linking behavior of the hydrogel scaffolds as well as the presence of PHBV nanofiber into the composite hydrogel scaffolds by comparing with the spectra of pristine CMCht, PEGDE, and uncross-linked CMCht-SF scaffolds.

The FTIR spectra of the CMCht and PEGDE are seen in Figure 4.8. In the FTIR spectrum of CMCht, the broad peak appeared at 3400–3200 cm^{-1} referred to both the O–H and N–H stretching vibrations. C–H stretching vibration was at ~2900 cm^{-1}. The peaks at 1587 and 1410 cm^{-1} were assigned to the asymmetric and symmetric stretching vibrations of the carboxy group, respectively. Besides, N-H bending vibration of the amine group overlapped with the asymmetric vibration of the carboxy group. Also, the absorption peak of the secondary hydroxyl group appeared at 1053 cm^{-1} (Chen et al., 2017; Chen et al., 2015; Kumar Singh Yadav & Shivakumar, 2012). FTIR spectrum of PEGDE showed the small absorption band of O-H group at 3517 cm^{-1}. C-H stretching, C-H bending and C-O stretching were at 2866 cm^{-1}, 1456 cm^{-1} and 1096 cm^{-1}, respectively. Epoxy group vibration of PEGDE appeared at 911 and 854 cm^{-1}. It is known that the weak band located at 3050 cm^{-1} is attributed to the C-H vibration of the methylene group of the epoxy ring (Achilias, Karabela, Varkopoulou, & Sideridou, 2012; Badr, Amer, & Shehat, 2010; Fouchal, Knight, & Dickens, 2004; González, Cabanelas, & Baselga, 2012).
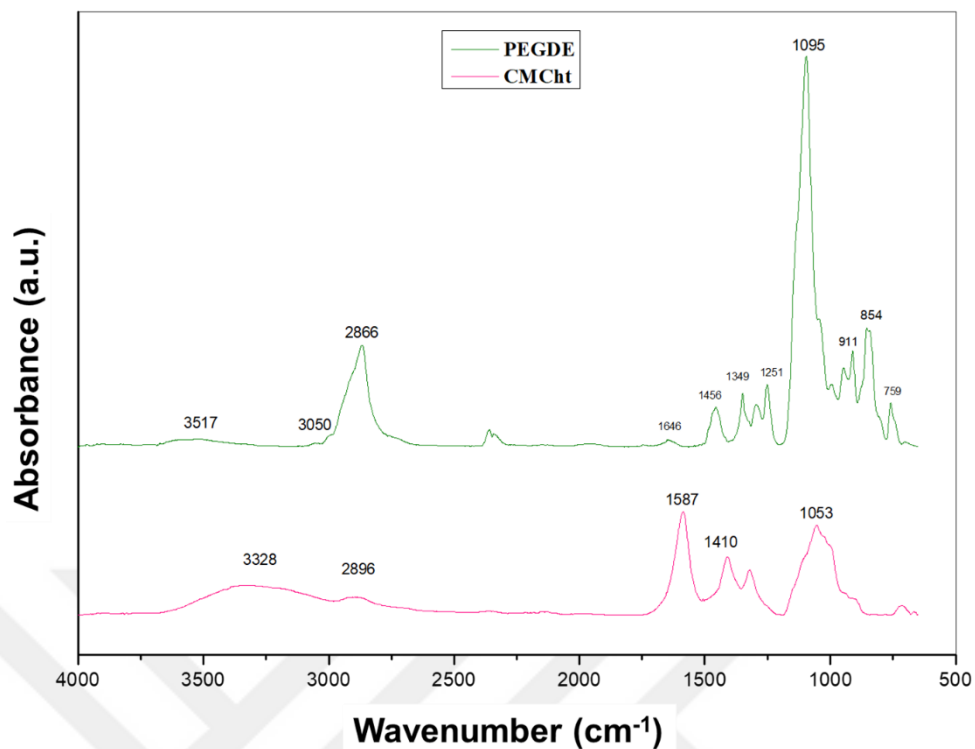
Figure 4.8 FTIR spectra of pristine CMCht and PEGDE

Figure 4.9 shows the spectra of the uncross-linked CMC-SF-PEGDE porous scaffolds, prepared by mixing CMCht and SF with PEGDE at different weight ratios. In the spectra, characteristic bands of both CMCht and PEGDE are clearly seen. The amide I (1655 ± 10 cm^{-1}) and amide II (1540 ± 10 cm^{-1}) bands of water-soluble random coil structure of SF could not be distinguished as they overlapped with the band of CMCht at 1587 cm^{-1}. In the uncross-linked scaffolds, these bands merged and appeared at 1597 cm^{-1}. Furthermore, as the PEGDE concentration increased, the ratio of the intensities of the peaks at 1095 and 1597 cm^{-1} increased, as expected.
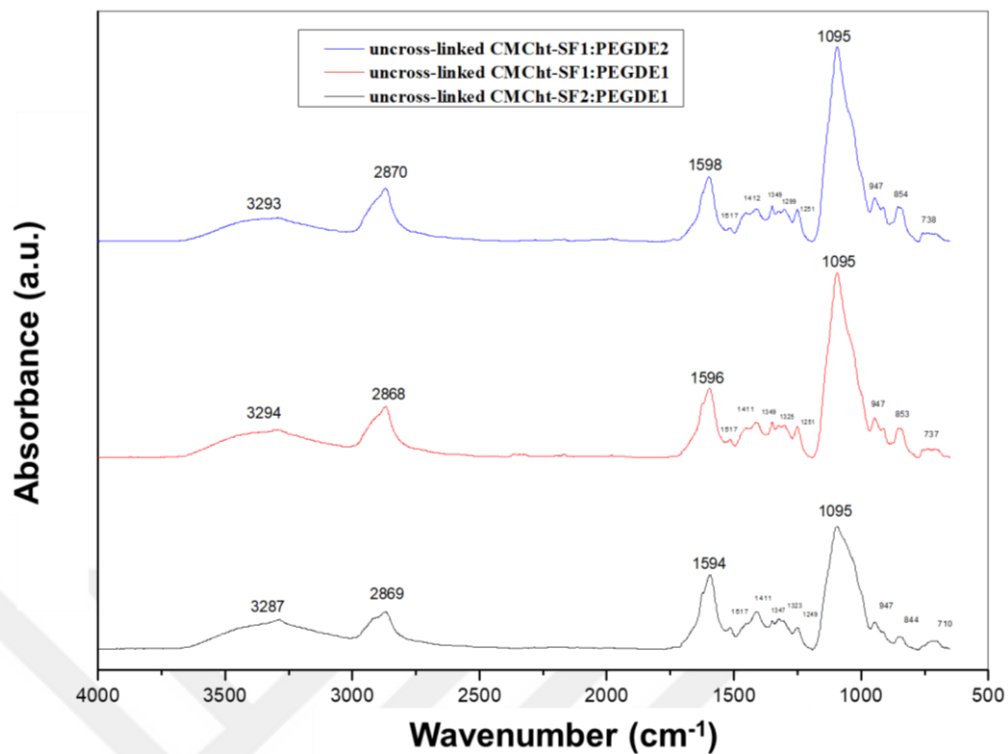
Figure 4.9 FTIR spectra of CMCht-SF scaffolds at different PEGDE concentrations before cross-linking reaction

FTIR spectra of the cross-linked CMCht-SF hydrogel scaffolds are seen in Figure 4.10. In the spectra, intensities of the epoxy group vibrations at 911 and 854 cm^{-1} decreased *via* the ring opening reaction of the epoxide. Besides, formation of new O-H bonds slightly increased the intensity of the broad band at 3400–3200 cm^{-1} with respect to the band at 1595 cm^{-1} (Gámiz-González, Edlund, Vidaurre, & Gomez Ribelles, 2017). As SF could not be cross-linked with PEGDE, methanol treatment was applied in order to immobilize the SF in the hydrogel. The methanol treatment resulted in the formation of insoluble β-sheet structure with bands at 1625±10 cm^{-1} (amide I) and 1525±10 cm^{-1} (amide II) (Li, Vepari, Jin, Kim, & Kaplan, 2006). However, these bands could not be seen as they overlapped with the CMCht bands.
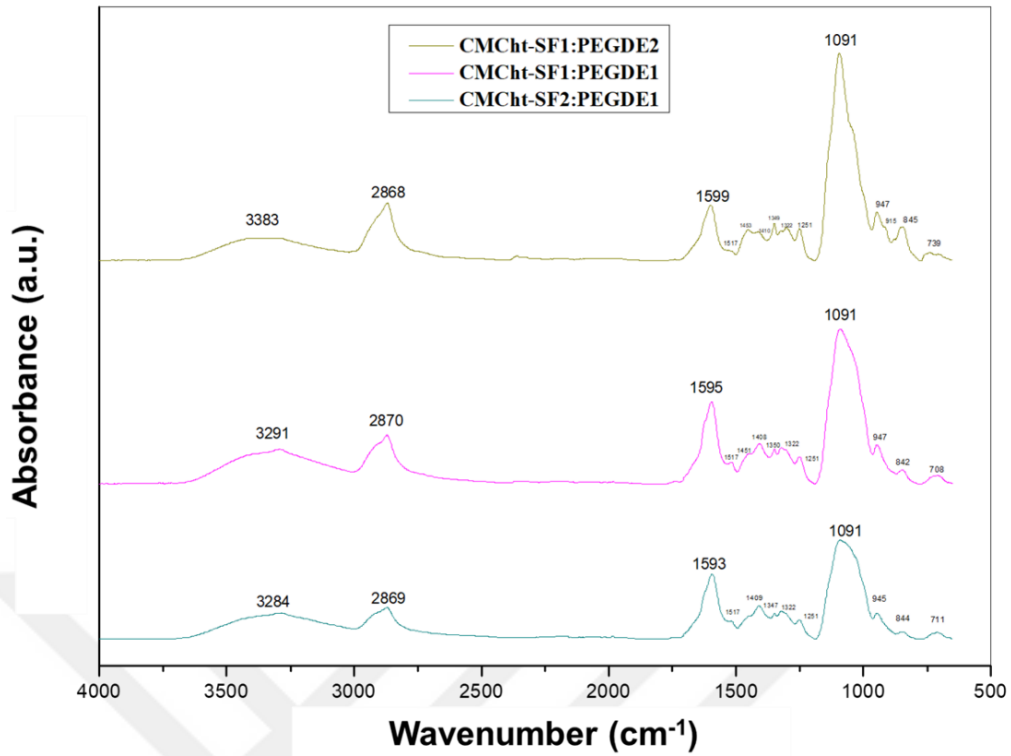
Figure 4.10 FTIR spectra of produced CMCht-SF hydrogel scaffolds

In the FTIR spectra of PHBV nanofiber reinforced hydrogel composite scaffolds (Figure 4.11), besides the absorption peaks of the hydrogels, the FTIR peaks of the PHBV nanofibers were clearly seen. C=O stretching vibration of PHBV appeared at 1723 cm^{-1} and C–O stretching bands were at 1281 and 1056 cm^{-1}. C–H stretching (~ 2900 cm^{-1}) and bending vibrations (1453 and 1380 cm^{-1}) overlapped with the hydrogel bands (Unalan, Colpankan, Albayrak, Gorgun, & Urkmez, 2016).
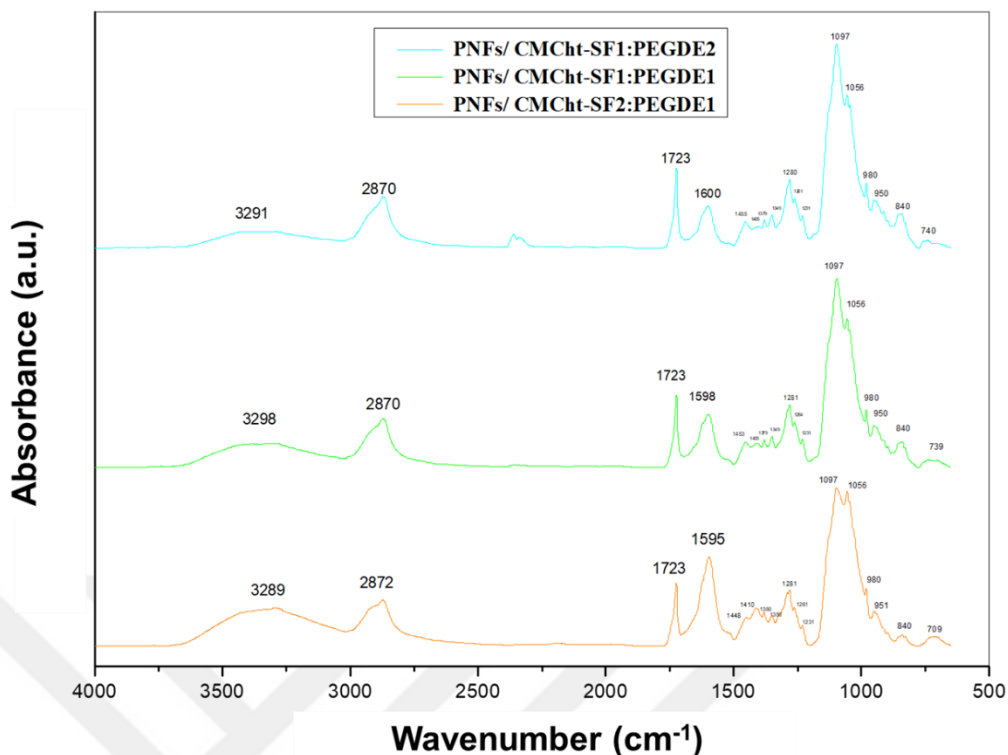
Figure 4.11 FTIR spectra of PHBV nanofiber reinforced CMCht-SF hydrogel composite scaffolds

4.3.4 DTA/TGA

Thermal properties of the hydrogel scaffolds were examined by DTA/TGA. TGA curves of the produced hydrogel scaffolds are given in Figure 4.12. All of the scaffolds exhibited two-stage decomposition assigned to loss of adsorbed water between 75-100°C followed by thermal decomposition of the hydrogel between 250-400°C. Onset decomposition temperatures of the hydrogel scaffolds were 251, 280 and 298°C for CMCht-SF2:PEGDE1, CMCht-SF1:PEGDE1 and CMCht-SF1:PEGDE2, respectively. With the addition of PHBV nanofibers, onset decomposition temperatures of the PNFs/CMCht-SF2:PEGDE1, PNFs/CMCht-SF1:PEGDE1 and PNFs/CMCht-SF1:PEGDE2 hydrogel scaffolds were obtained as 257, 280 and 293 °C, respectively. It can be concluded that PHBV nanofiber reinforcement did not affect the thermal property of the hydrogel scaffolds. However, the main thermal decay temperatures of the hydrogel scaffolds shifted to a higher temperature as the concentration of PEGDE increased which resulted in enhancement of the thermal stability.
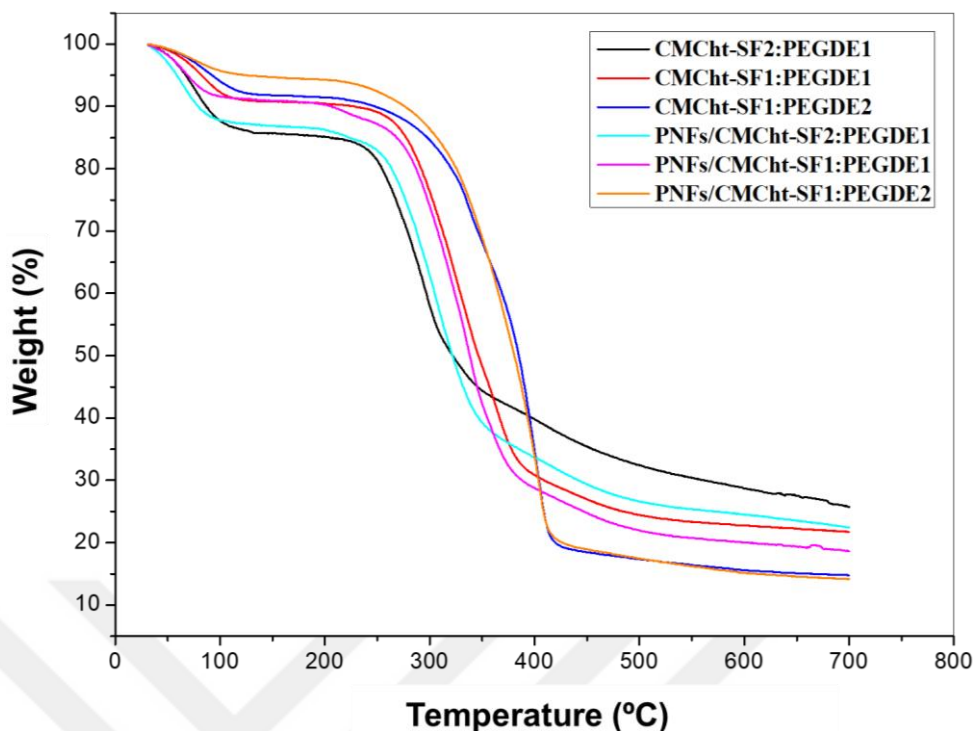
Figure 4.12 TGA curves of the produced hydrogel scaffolds

The DTA curves of the CMCht-SF hydrogel and PHBV nanofiber reinforced hydrogel scaffolds are shown in Figure 4.13 and Figure 4.14, respectively. The samples presented an endothermic peak in the 75–100°C range, which was attributed to water loss. The second decomposition stage of the hydrogel scaffolds consisted of two exothermic steps. In the literature, the main degradation step of CMCht and PEGDE took place between 210-310°C and 325-425°C, respectively (Gámiz-González, Edlund, Vidaurre, & Gomez Ribelles, 2017). Besides, the onset decomposition temperature of the SF was given as 281°C (Barud et al., 2015). Accordingly, the first exothermic peak should be ascribed to the breakdown of the main polysaccharide chain of CMCht and the cleavage of the peptide bonds of SF. The second exothermic peak could be associated with the decomposition of the PEG moiety. This argument was supported by the shift of the peak temperatures of the second stage to higher temperatures as well as the increment of the peak intensity of the second step in the hydrogel scaffolds with higher PEGDE concentration.

90
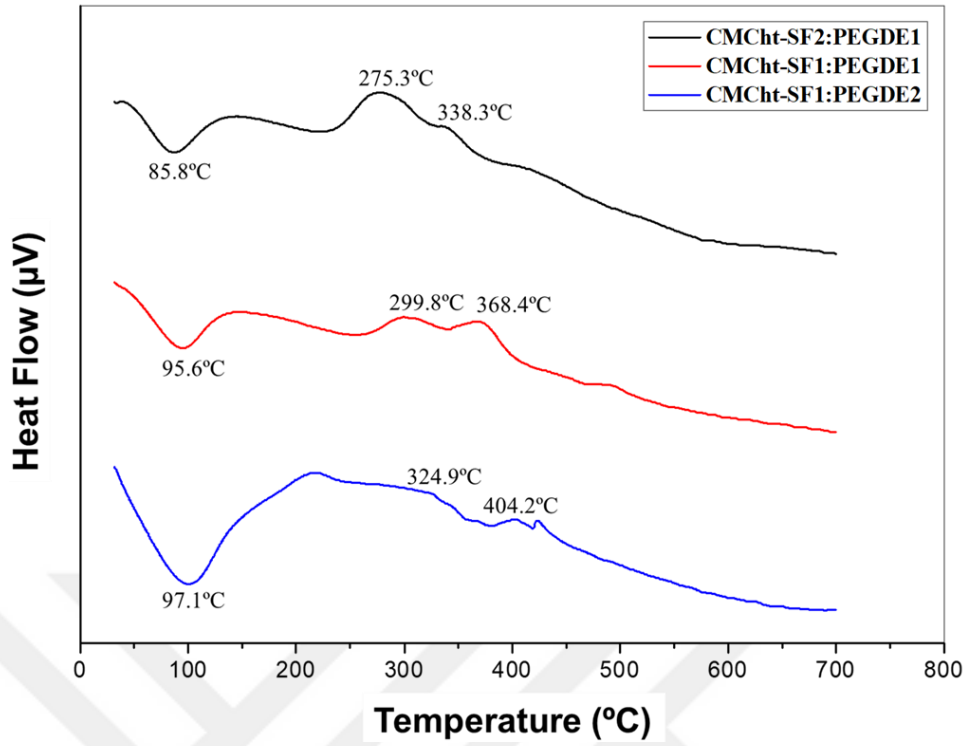
Figure 4.13 DTA curves of the CMCht-SF hydrogel scaffolds
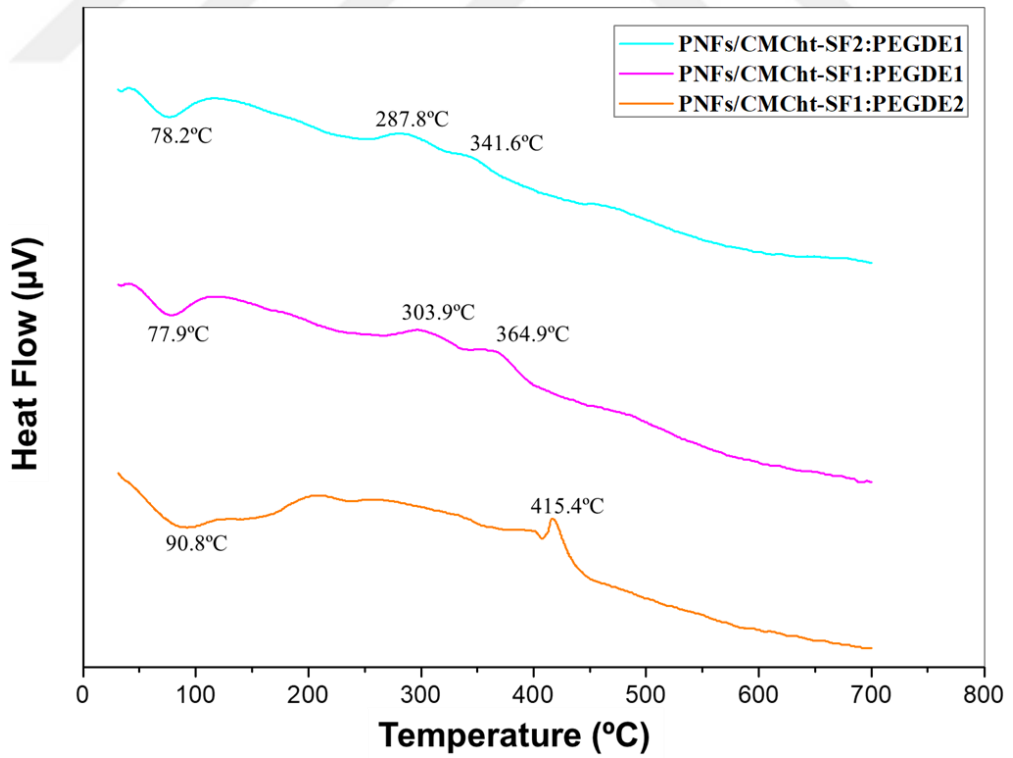
Figure 4.14 DTA curves of the PHBV nanofiber reinforced CMCht-SF hydrogel scaffolds

4.3.5 Swelling Behavior

The hydrophilic environment of the cartilaginous ECM enables the cartilage tissue to experience a swelling pressure and therefore, swelling behavior of the scaffold is an essential aspect to be evaluated. Articular cartilage contains up to 80% water of its wet weight (Fox, Bedi, & Rodeo, 2009). Hydrogel scaffolds with high-water content provide good permeability toward nutrients, easy growth of cells, swelling kinetics and a hydrated environment that is similar to native ECM (Lee, Kung, & Lee, 2005; Yodmuang et al., 2015). The swelling behavior of the developed hydrogel scaffolds was evaluated by immersing the scaffolds in PBS at 37°C overnight. The swelling ratio (eq. 4.1) and water content (eq. 4.2) of the hydrogel scaffolds were calculated from the formulas given in the experimental section (Zhao, Gwon, Lim, Nho, & Kim, 2014).

Figure 4.15 shows the swelling ratio values of the hydrogel scaffolds. Swelling ratios of the hydrogel scaffolds both with and without PHBV nanofiber reinforcement significantly decreased upon increasing PEGDE content. Among the hydrogel scaffolds without PHBV nanofiber reinforcement CMCht-SF2:PEGDE1 showed the highest swelling ratio of 1382±54%, whereas the lowest ratio of 624±14% was obtained for the CMCht-SF1:PEGDE2 scaffold. After PHBV nanofiber addition, their swelling ratios slightly decreased to 1303±63% and 463±39%, respectively (Table 4.2). Gámiz-González, Edlund, Vidaurre, & Gomez Ribelles, 2017 also reported that the swelling ratio of the CMCht hydrogel scaffolds decrease as the PEGDE concentration increased. As seen from the Table 4.2, all the hydrogel scaffolds had water content between 82-93%. The lowest water content value was obtained for the scaffolds with highest PEGDE concentration, as expected.
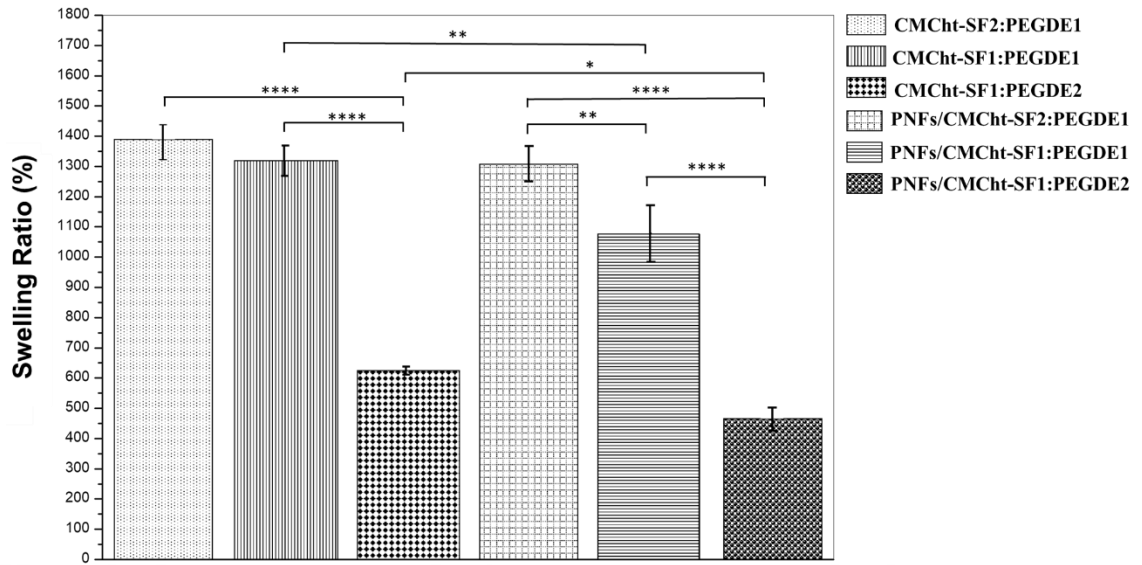
Figure 4.15 Swelling ratios of the hydrogel scaffolds after immersion in PBS at 37°C overnight (*p≤0.05, **p≤0.01, ****p≤0.0001)

Table 4.2 Swelling ratio and water content values of the hydrogel scaffolds

	Swelling ratio (%)	Water content (%)
CMChtSF2:PEGDE1	1382.5±54.5	93.2±0.2
CMChtSF1:PEGDE1	1316.1±52.2	92.9±0.3
CMChtSF1:PEGDE2	624.5±14.1	86.2±0.3
PNFs/CMCht-SF2:PEGDE1	1303.8±62.5	92.9±0.3
PNFs/CMCht-SF1:PEGDE1	1074.6±96.6	91.4±0.7
PNFs/CMCht-SF1:PEGDE2	463.4±39.1	82.2±1.3

4.3.6 Viscoelastic Properties

The articular cartilage is a load-bearing tissue with good viscoelasticity that endows cartilage the capability to withstand continuous complex mechanical loading. Therefore, it is very important that the scaffold to be used in cartilage regeneration has a viscoelastic structure (Chen, Zhang, Yang, Zhang, & Wang, 2016; Yang et al., 2011) The viscoelastic properties of cartilage has been characterized over frequencies ranging from typical gait frequencies (≥1 Hz) and up to frequencies representative of

rapid heel-strike rise times (90 Hz). Therefore, in order to obtain physiologically relevant results frequency sweep method are recommended to use for viscoelastic property measurements (Byju & Kulkarni, 2013; Lawless et al., 2017).

Viscoelastic measurements of the hydrogel scaffolds were performed using DMA at 37°C which is an appropriate tool to characterize the viscoelastic properties of the polymeric materials (Yan et al., 2010). The measurements were carried by using compression clamp and dynamic frequency sweep mode with frequencies ranging from 0.1 Hz up to 100 Hz. The viscoelastic measurements were carried out for the CMCht-SF2:PEGDE1, CMCht-SF1:PEGDE1 scaffolds and their composites. CMCht-SF1:PEGDE2 and PNFs/CMCht-SF1:PEGDE2 were not used due to their collapsed structures.

Figure 4.16 and Figure 4.17 show the storage and loss modul values of the CMCht-SF and PHBV nanofiber reinforced CMCht-SF hydrogel scaffolds, respectively. Storage modulus (E') is linked to the elastic response and proportional to the recoverable or stored energy; whereas loss modulus (E'') is linked to the viscous response and proportional to the irrecoverable or dissipated energy (Placet & Foltête, 2010). All the hydrogel samples have E' >E'' over the entire frequency range indicating an elastic solid behavior. Also, due to the relaxations in the hydrogels, the E' and E'' slightly increased as frequency increased (Liu & Chan-Park, 2009; Reis & Cohn, 2012). The storage moduli value highly enhanced upon addition of PHBV nanofiber with increasing the density of polymer chains. The PHBV nanofiber reinforced CMCht-SF hydrogel scaffolds had higher E' and E'' values that of CMCht-SF hydrogel scaffolds. Besides, a sharp decrease in the E' values of the hydrogels at higher frequencies can be ascribed to possible resonance and cavitation occurring in the hydrogels that result in micro-damage of the samples (Byju & Kulkarni, 2013).
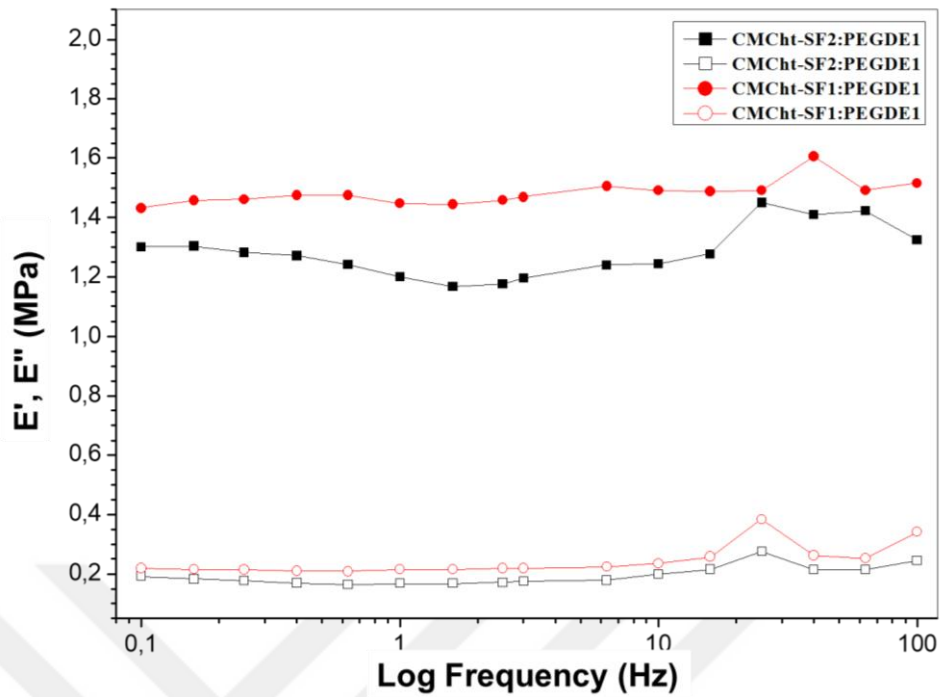
Figure 4.16 Storage (E', solid symbols) and loss modulus (E", hollow symbols) of CMCht-SF hydrogel scaffolds
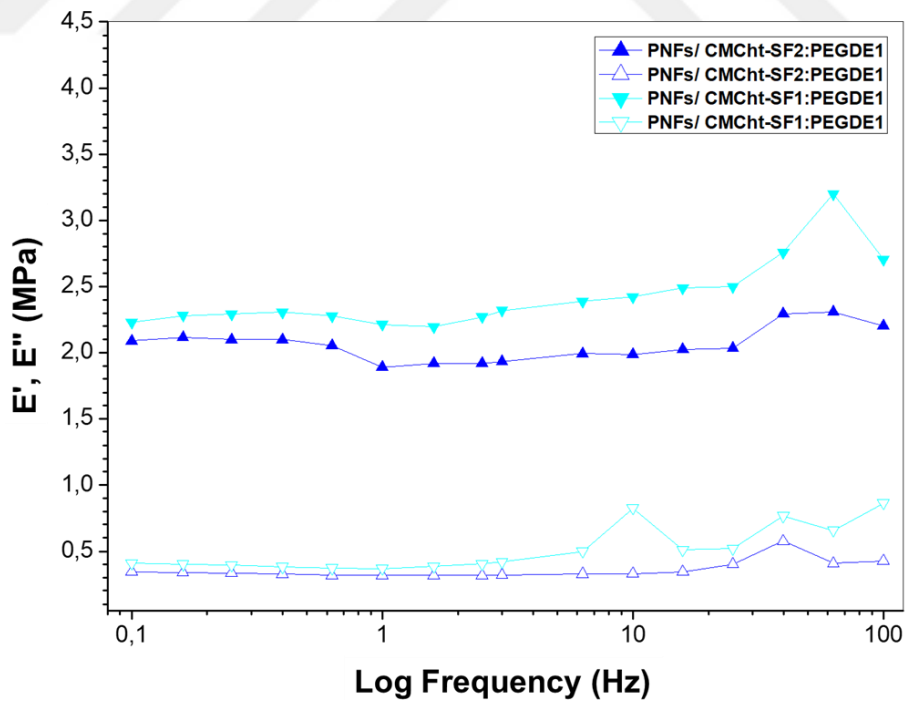
Figure 4.17 Storage (E', solid symbols) and loss modulus (E", hollow symbols) of PHBV nanofiber reinforced CMCht-SF hydrogel scaffolds

Tan δ is determined by the ratio of loss modulus and storage modulus which provides information about the damping capability of the hydrogel scaffolds. Tan δ values of the hydrogel scaffolds are shown in Figure 4.18. As frequency increased, tan δ also increased slightly, but at some critical frequencies where relaxational process appears tan δ pass through a maximum. The PNFs/CMCht-SF1:PEGDE1 scaffold showed the best viscoelastic nature due to its higher tan δ values (tan δ value of 0.183 at 1 Hz) as well as the presence of two maxima which were probably related to the α and β relaxations resulting in enhanced damping capability (Reis & Cohn, 2012). On the other hand, tan δ value of the human articular cartilage was given as 0.266 (Temple, Cederlund, Lawless, Aspden, & Espino, 2016).
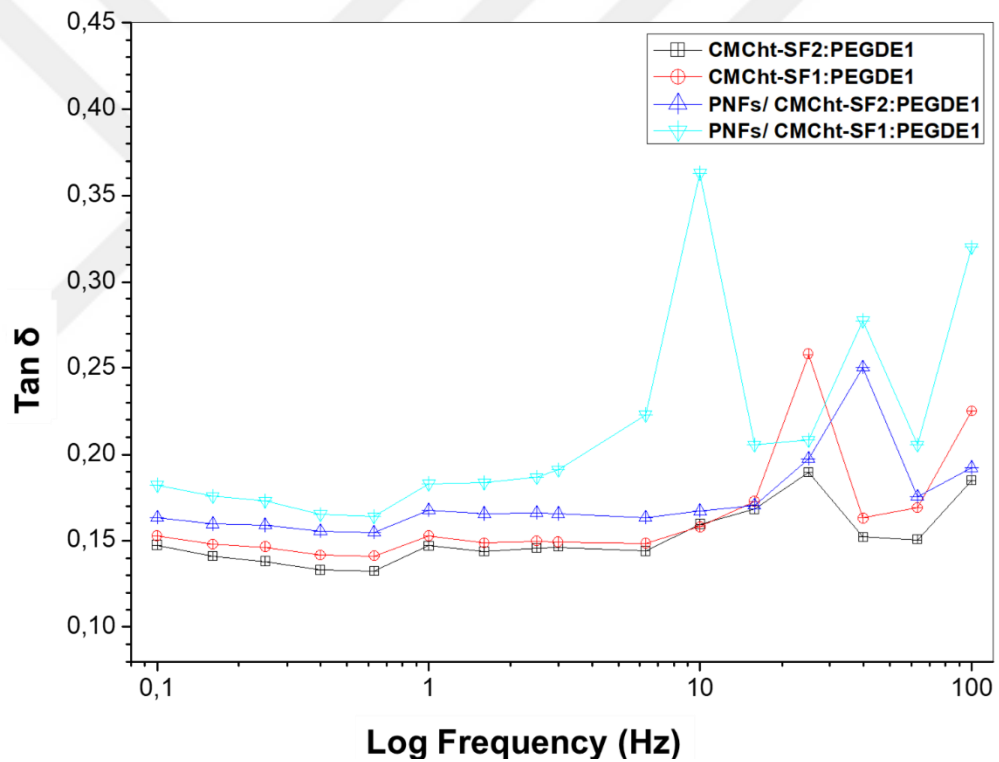
Figure 4.18 Tan δ values of the hydrogel scaffolds

4.3.7 Mechanical Properties

Mechanical properties of the scaffolds were determined by compression test by compressing the scaffolds at a constant deformation rate of 0.5 mm/sec up to a strain of 80%. Representative stress-strain curves for the compressive behavior of each of

the scaffolds are presented in Figure 4.19. All the scaffolds had S-shaped curves typical of lightly cross-linked polymers. Curves can be defined by three regions; linear elastic (I), plateau (II) and densification (III). In the linear elastic region, cell walls bent and then, cell walls buckled, yielded or fractured in the plateau region. Finally, with the clustering of the crushed cell walls, stress sharply increased. The area under the stress-stain curve until the densification region corresponded to the dissipated energy (Avalle, Belingardi, & Montanini, 2001). The hydrogel composite scaffolds with the plateau region at higher compressive stress values dissipated the same amount of energy at lower deformations compared to the scaffolds without PHBV nanofiber reinforcement.
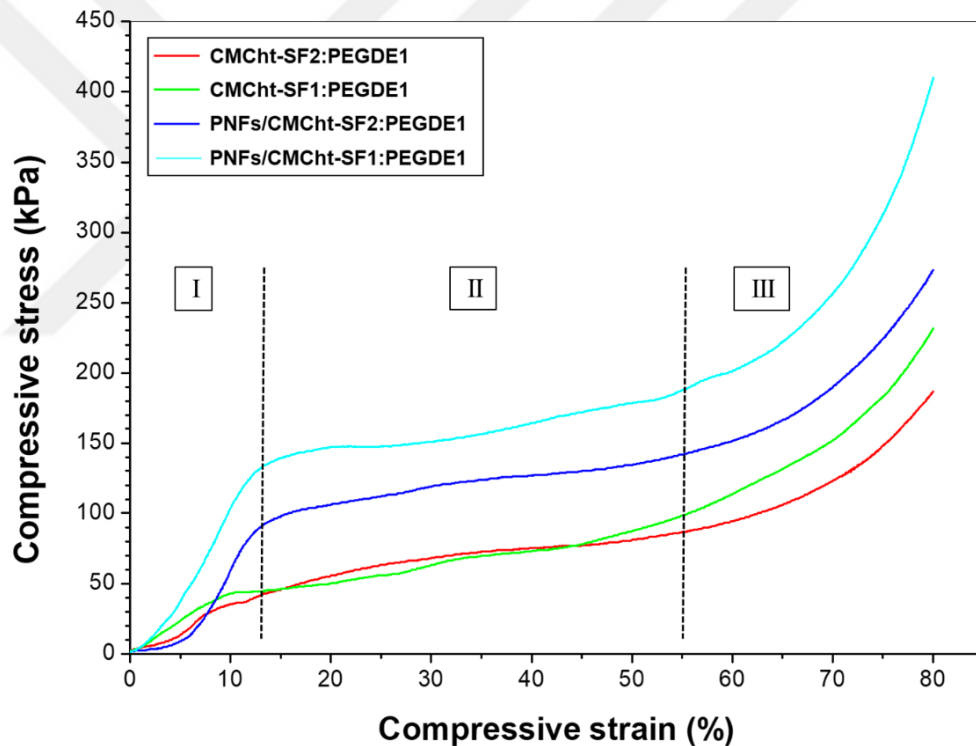
Figure 4.19 Representative strain–stress curves of the prepared hydrogel

Figure 4.20 and Figure 4.21 show the compressive strength and calculated compressive modulus values of the scaffolds. CMChtSF2:PEGDE1 and CMChtSF1:PEGDE1 scaffolds had a compressive strength of 177±32 kPa and 207±45 kPa, and compressive modulus of 2.5±1 and 5.5±0.8 kPa, respectively. As is seen, with increasing the cross-linker concentration in the hydrogels, compressive modulus slightly improved, whereas there was no significant difference in the compressive strength values. The PHBV nanofiber containing scaffolds, PNFs/CMCht-SF2:PEGDE1 and PNFs/CMCht-SF2:PEGDE1, had considerably higher modulus (9.5±1 kPa and 11.5±1.5 kPa) and strength (299±62 kPa and 457±85 kPa) values as compared to the scaffolds without PHBV nanofiber, CMChtSF2:PEGDE1 and CMChtSF1:PEGDE1, confirming that PHBV nanofibers acted as a reinforcement in the hydrogels. Vishwanath, Pramanik, & Biswas, 2016 prepared silk fibroin-chitosan freeze-dried porous scaffolds and the compressive strength of the scaffold was measured as 190 ± 0.2 kPa. As a conclusion, even though human articular cartilage is stiffer than the developed composite scaffolds with a higher compressive modulus value (~1750 kPa) (Bartnikowski, Wellard, Woodruff, & Klein, 2015), composite scaffolds had compressive strengths within the desired range of 0.01–3 MPa for cartilage tissue engineering application.
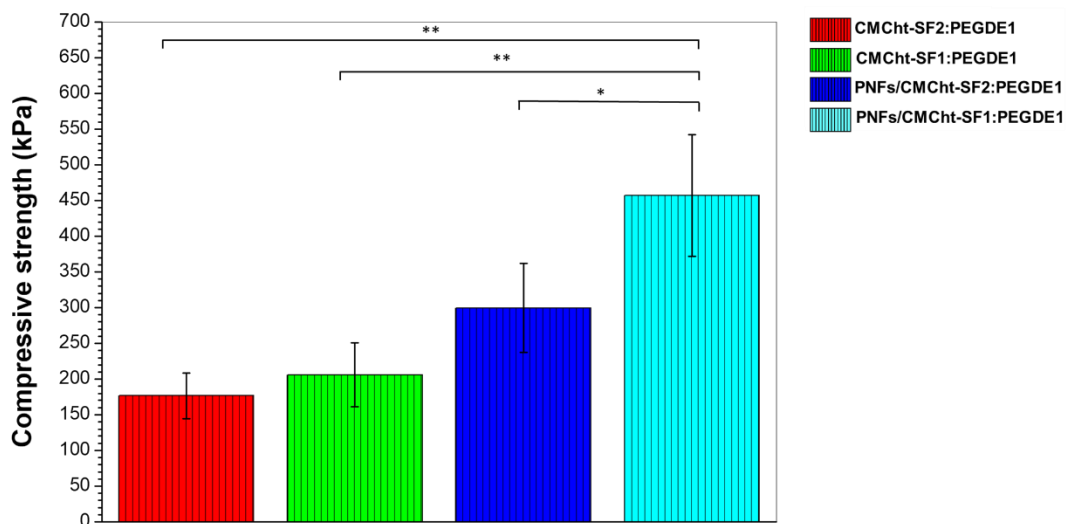
Figure 4.20 Compressive strength values of the prepared hydrogel scaffolds (*p≤0.05, **p≤0.01)
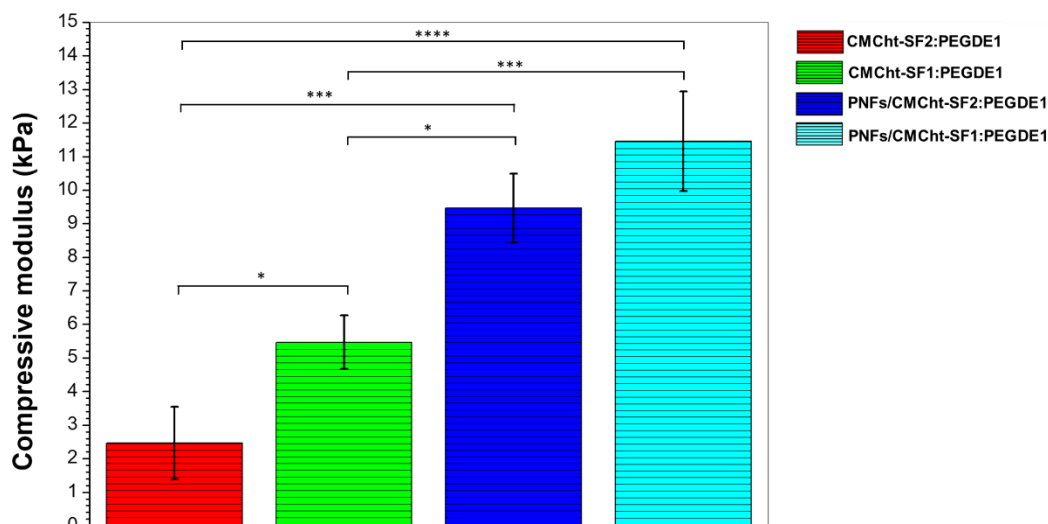
Figure 4.21 Compressive modulus values of the prepared hydrogel scaffolds (*p≤0.05, ***p≤0.001, ****p≤0.0001)

4.3.8 Texture Profile Analysis

Texture profile analysis (TPA) was originally proposed by Jones, Woolfson, & Djokic, 1996 as an appropriate method for the characterization of semisolid drug dosage forms. Even though TPA has been widely used for solid and semisolid food, recently it has attracted great attention in the characterization of pharmaceutical and polymeric systems (Ferreira, Calvinho, Cabrita, Schacht, & Gil, 2006). Several mechanical parameters such as hardness, cohesiveness, springiness, adhesiveness, and compressibility can be determined through TPA (Hurler, Engesland, Poorahmary Kermany, & Škalko-Basnet, 2012).

The representative force-time graphs of the produced hydrogel scaffolds are shown in Figure 4.22. From the graphs in order to obtain the mechanical parameters some points (numbered from 1 to 6), areas between these points (A_{1-2}, A_{2-3}, A_{1-3}, A_{4-6}), and time intervals (T_{1-2}, T_{4-5}) were determined first and as an example they were illustrated in the force-time graph of CMCht-SF2:PEGDE1 scaffold (Figure 4.23).
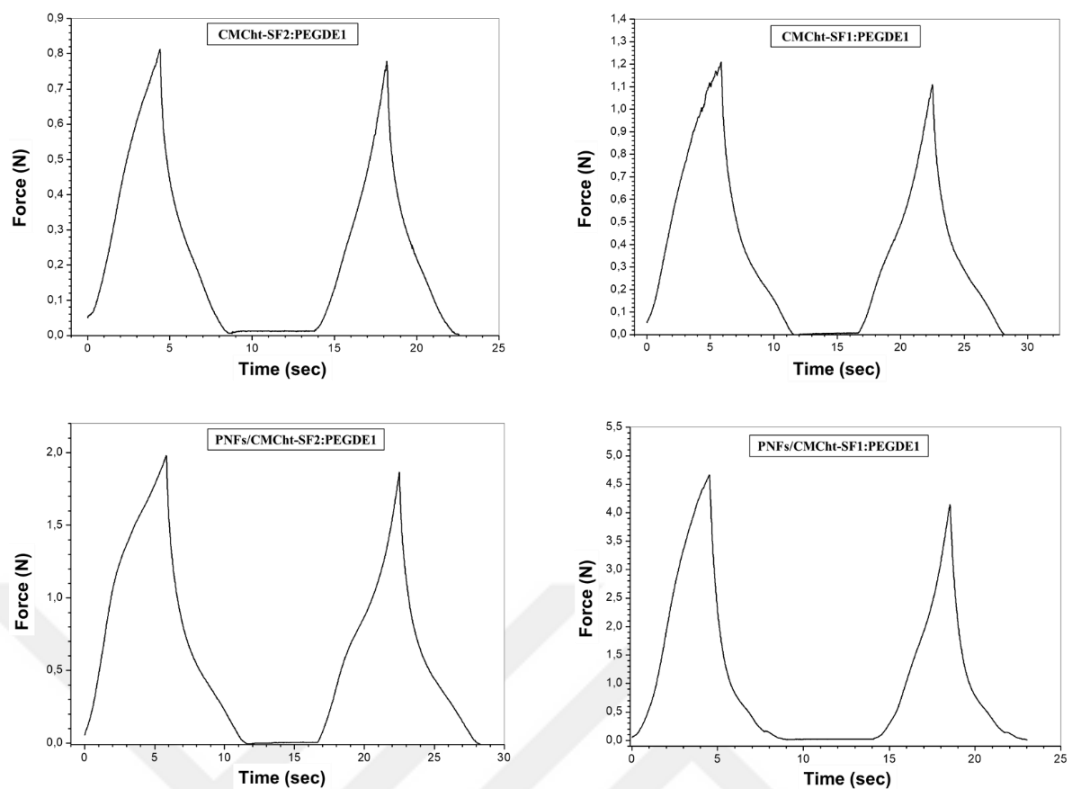
Figure 4.22 Representative force-time graphs of the hydrogel scaffolds
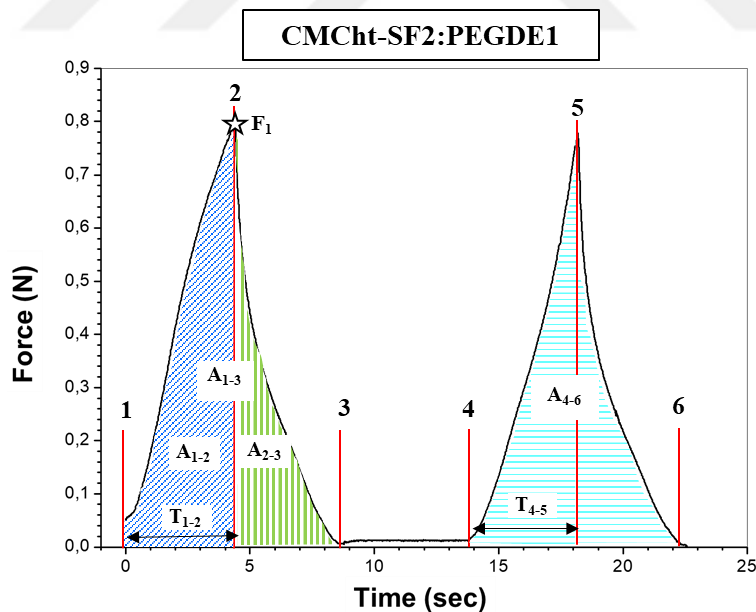
Figure 4.23 Labelled force-time graph of the CMCht-SF2:PEGDE1 hydrogel scaffold

Hardness was defined as a force required for a pre-determined deformation of 40%, and it was given as F_1 value, the maximum force of the first compression of the

scaffolds (Figure 4.23). Cohesiveness is related with how well the sample resists a second deformation relative to how it behaves under the first deformation. It was calculated as (A_{4-6}/A_{1-3}), the ratio of the energies expanded in the first and second compression. Springiness or elasticity gives the information about the sample's capability of physically springs back after it has been deformed, it was calculated as (T_{4-5}/T_{1-2}). Resilience is known as instant springiness, and it is the measure of how well a sample "fights to regain its original height". It was measured by the ratio of the upstroke energy and downstroke energy of the first compression (A_{2-3}/A_{1-2}). (Ferreira, Calvinho, Cabrita, Schacht, & Gil, 2006; Hurler, Engesland, Poorahmary Kermany, & Škalko-Basnet, 2012; Król, Malik, Marycz, & Jarmoluk, 2016; Rosenthal, 2010). The obtained mechanical parameters of the produced hydrogel scaffolds from TPA are given in Table 4.3. The hardness values of the samples increased with the cross-linker ratio as well as fiber incorporation. The cohesiveness and springiness values were similar to each other as there was no significant difference between the samples. However, the resilience of the hydrogel scaffolds was found to be higher than that of composite scaffolds. On the other hand, scaffolds did not fracture during the compression, as there was no shoulder in the first cycle. In terms of adhesiveness, defined as the required energy used to overcome the sticky forces between the sample and the probe, and calculated from the area between the points 3 and 4, none of the hydrogel scaffolds showed any negative force meaning that they did not present an adhesive profile.

Table 4.3 TPA parameters for hydrogel scaffolds

Scaffold	Hardness (N)	Cohesiveness	Springiness	Resilience
CMChtSF2:PEGDE1	0.81±0.03	0.81±0.02	1.01±0.01	0.60±0.06
CMChtSF1:PEGDE1	1.22±0.22	0.77±0.09	1.02±0.03	0.60±0.11
PNFs/CMCht-SF2:PEGDE1	2.40±1.41	0.77±0.05	0.98±0.05	0.49±0.09
PNFs/CMCht-SF1:PEGDE1	4.61±1.70	0.73±0.05	0.99±0.02	0.47±0.04

4.3.9 In-vitro Biological Assays

4.3.9.1 Alamar Assay

The growth and proliferation of the cells cultured on the scaffolds were evaluated at different culture times (1, 4, 7 and 10 days) by Alamar assay and the results are given in Figure 4.24. Resazurin is an active ingredient in Alamar blue solution and by viable cells it is converted to its reduced state (resorufin) which is indirectly reveal the viability and proliferative state of the cells (Maji, Agarwal, Das, & Maiti, 2018). The amount of resorufin, which can be monitored by a spectrophotometer, is proportional to the number of viable cells (McGaw, Elgorashi, & Eloff, 2014). According to Figure 4.24, there is an increment in cell proliferation up to day 4 whereas the mitochondrial activity remained constant after 4 days of culture in all the scaffolds. The CMCht-SF1:PEGDE1 scaffolds showed more significant proliferation compared to other scaffolds during the culture period.
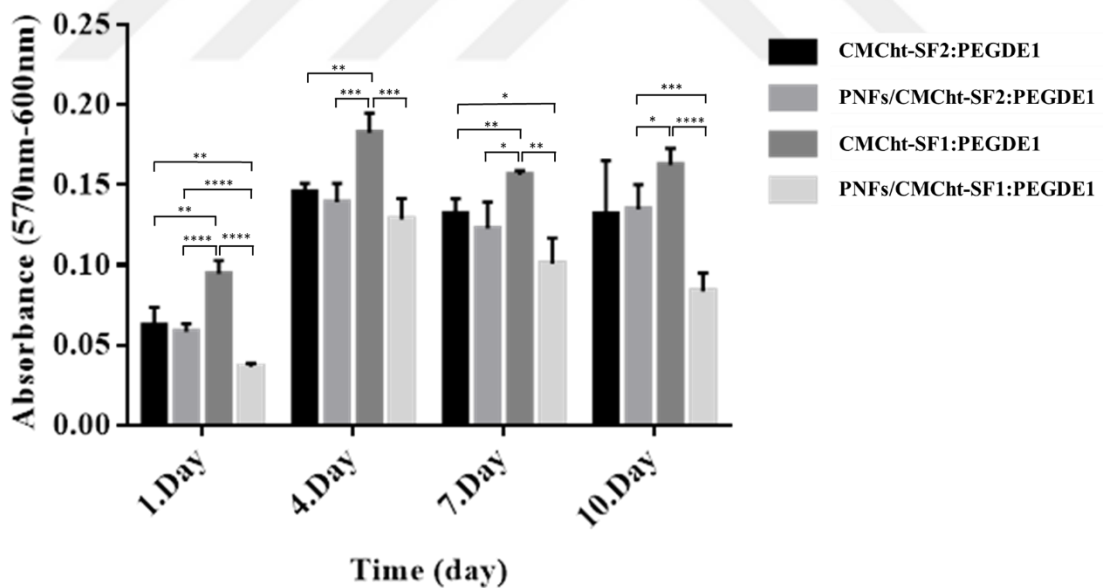
Figure 4.24 Cell viability on the scaffolds after 1, 4, 7 and 10 days of culture. The experiment was repeated in triplicate (n=3) for each sample. Data are shown as averages with the error bars indicating the standard deviation, (*p≤0.05, **p≤0.01, ***p≤0.001, ****p≤0.0001)

4.3.9.2 Cell Morphology

It is important to study the cell attachment and morphology in order to evaluate the suitability of the biomaterial toward cellular behavior in the culture condition. SEM images in Figure 4.25 show the attachment and spreading of BMSCs on the scaffolds during 1, 4, 7 and 10 days of culture. With the culture time, cells firmly attached and spread well on all the scaffolds, and at day 10, the cells nearly covered the surface. In the composite hydrogel scaffolds (PNFs/CMCht-SF2:PEGDE1 and PNFs/CMCht-SF1:PEGDE1), round cells displaying the features of the chondrocytes were clearly seen.
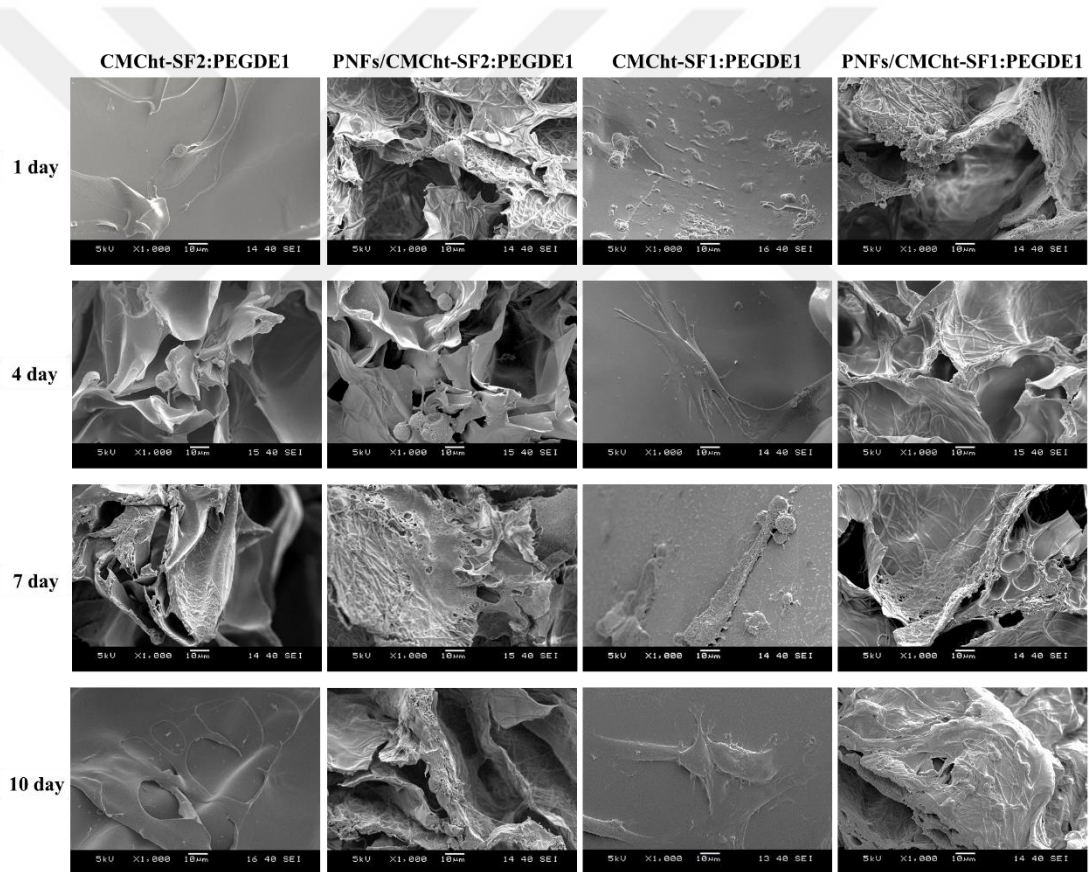
Figure 4.25 SEM images of the attachment and spreading of the BMSCs on the scaffolds after 1, 4, 7 and 10 days of culture (magnification=1000×, scale bar=10 μm)

4.3.9.3 Chondrogenic Differentiation

BMSC seeded scaffolds, which were allowed to undergo chondrogenic differentiation up to 21 days were analyzed histologically by alcian blue staining to show the distribution of GAGs within the scaffolds. Figure 4.26 shows the staining profiles for the histological sections of the scaffolds and polystyrene (PS) in control and chondrogenic mediums after 21 days of culture using alcian blue.

In the chondrogenic medium, all the scaffolds showed a positive staining indicating that the chondrocytes produced an extracellular matrix containing proteoglycans. However, in the fiber reinforced composite hydrogel scaffolds (PNFs/CMCht-SF2:PEGDE1 and PNFs/CMCht-SF1:PEGDE1) a significant increase in GAG accumulation was observed in comparision to the other scaffolds. PNFs/CMCht-SF1:PEGDE1 hydrogel scaffold showed the most intense staining.
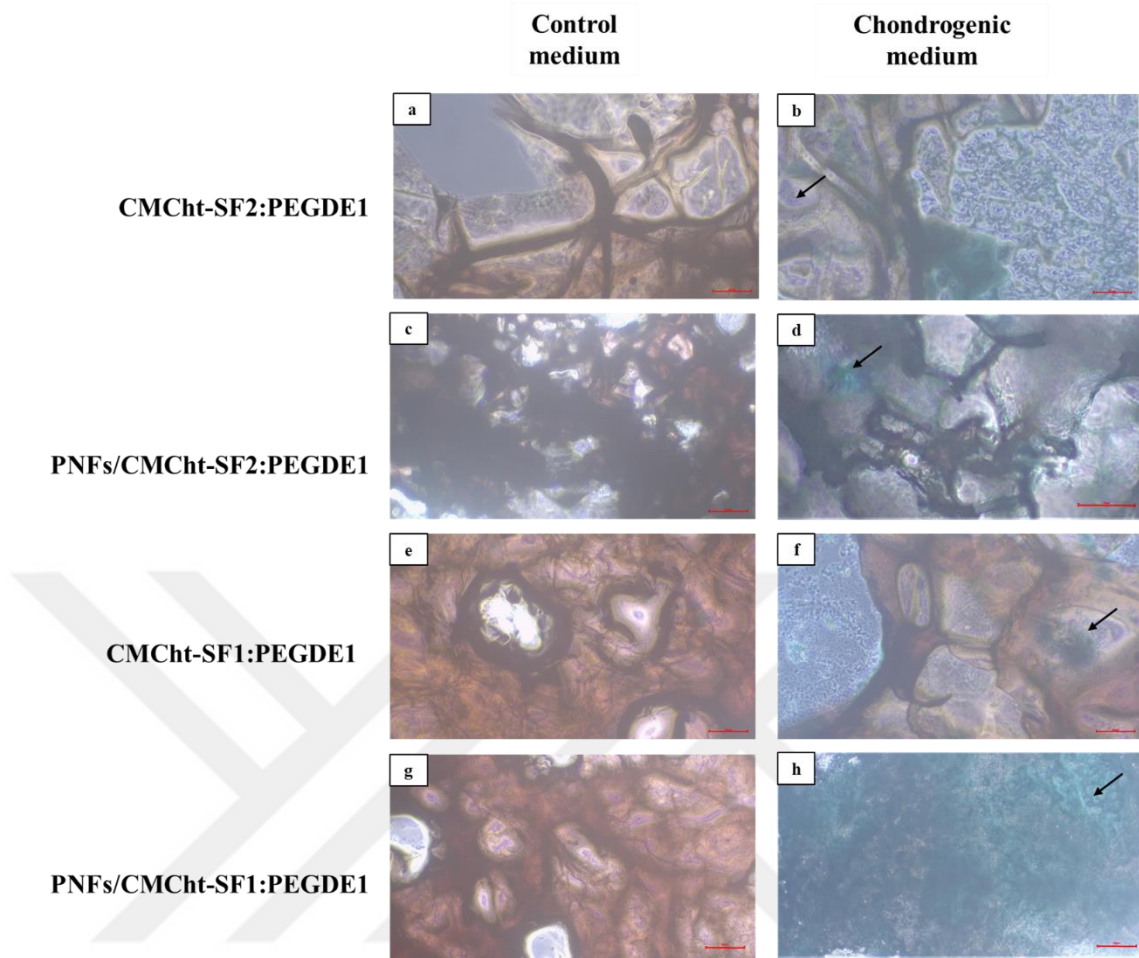
Figure 4.26 Light microscopy images of histology sections obtained from scaffolds after 21 days of cell culture stained with alcian blue in control medium (a, c, e, g) and chondrogenic medium (b, d, f, h) (Scale bar = 80 µm). Black arrows respresent the cells

4.4 Conclusion

In this part of the thesis, PHBV nanofiber reinforced CMCht - silk hydrogel scaffolds that were cross-linked by PEGDE at three different concentrations were prepared so as to mimic the composite structure of the cartilage ECM. SEM images showed that all the scaffolds have interconnnected microporous structure. In addition, PHBV nanofibers were well incorporated into the pore walls of the composite scaffolds. However, CMCht-SF1:PEGDE2 and PNFs/CMCht-SF1:PEGDE2 scaffolds could not maintain their dimensional stabilities as they collapsed after freeze-drying. Therefore, this cross-linking ratio was eliminated for further analyses. According to

DMA, thermal, mechanical and *in-vitro* test results PNFs/CMCht-SF1:PEGDE1 scaffold showed better properties in terms of damping capability, thermal stability, compressive strength, and chondrogenic differentiation. Consequently, this scaffold would be a promising candidate for cartilage tissue regeneration.

CHAPTER FIVE
WOUND HEALING STUDY

5.1 Introduction

The skin, which is the largest organ with 10% of the total body mass, acts as a protector against the environment by creating a barrier between the internal organs and external effects. In addition to this physical protective function, the skin is also responsible for fluid homeostasis, sensory detection and thermal isolation (Liu et al., 2018; Pinho & Soares, 2018). Since skin is constantly exposed to external atmosphere, wounds are formed by weakening and disruption of the normal anatomical structure and function of the skin (Boateng, Matthews, Stevens, & Eccleston, 2008; Pereira & Bartolo, 2016).

Wound healing is a complex process including hemostasis, inflammation, migration, proliferation and remodeling phases. The schematic illustration of these phases is seen in Figure 5.1. After skin is injured, bleeding occurs and it serves to flush out bacteria from the wound. Besides, it activates haemostasis which is initiated by the protein-rich liquid produced by the wound called exudate. Fibrinogen in the exudate reveals the clotting mechanism and stops bleeding by producing fibrin network. Therefore, haemostasis has a protective role in wound healing. The inflammatory phase occurs simultaneously with haemostasis. The releasing of exudate causes vasodilation and allows phagocytes to enter the wound where they cleared out the damaged and dead cells. In the migration phase, epithelial cells and fibroblasts move to the wounded area to replace damaged tissue. Proliferation phase occurs just after the migration phase. In this phase, the formation of granulation tissue by the in-growth of capillaries and lymphatic vessels, and the synthesis of collagen are occurred. In the last remodelling or maturation phase, cellular connective tissue is formed and the strength of the new epithelium increased by the rearrangement of the collagen fibers along tension lines. Even though, skin has an ability to restore the defects after injury, the healing process may be interrupted by a number of factors, including infection, age, stress, medication, and nutrition. Therefore, a great variety of wound care

products have been developed in order to restore the skin defects and improve the life quality of the people suffering from wounds (Boateng, Matthews, Stevens, & Eccleston, 2008; Liu et al., 2018).
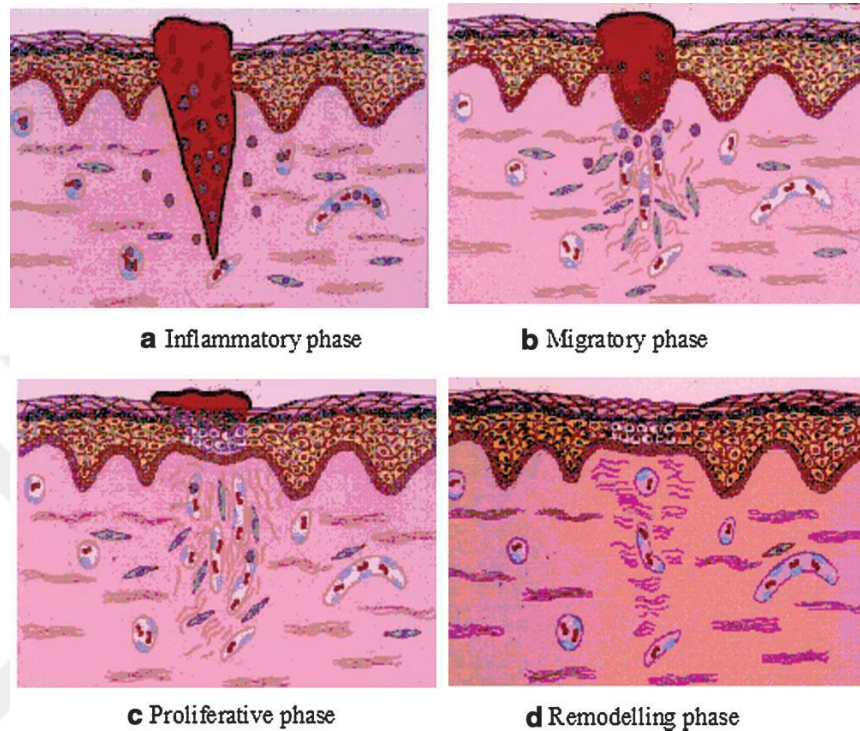
Figure 5.1 Schematic illustration of the wound healing phases (a) entering of the phagocytes to the wound area (b) movement of the epithelial cells (c) completely covering of the wound by epithelium (d) forming of the cellular connective tissue and disappearance of the capillaries and fibroblasts (Boateng, Matthews, Stevens, & Eccleston, 2008)

Wound dressings which are important parts of the worldwide medical and pharmaceutical wound care market have been used for many years to minimize the loss of function and protect the skin by covering the wounded area. Simply they can be classified as traditional or modern dressings. Traditional dressings are passive dressings, such as cotton, bandages and gauze and their aim is to cover the wound and keep it dry by absorbing the fluid released from the wound. However, traditional dressings have been replaced by modern dressings, since it has been shown that modern dressings can provide a humid wound environment which leads to faster and more successful wound healing (Boateng, Matthews, Stevens, & Eccleston, 2008; Mohandas, Deepthi, Biswas, & Jayakumar, 2017; Paul & Sharma, 2004).

For effective wound healing, there are some properties that the wound dressings should possess including high biocompatibility, high liquid absorption capacity to absorb excess exudate containing nutrients that increase the risk of bacterial growth, and sufficient water vapor transmission rate to provide a moist environment in the wound bed. Besides, in the last few years, since the number of patients with infection-related wounds increased considerably, it is important that the ideal wound dressing should be a barrier for the penetration of microorganisms and provide an antimicrobial activity (Mir et al., 2018; Naseri-Nosar & Ziora, 2018).

The use of wound dressings has started as a plain textile strip and today even if wound dressings are in film, sponge or gel form, textile materials are still among the most used materials for wound healing (Pinho & Soares, 2018). In the production of these materials, natural polymers are more preferred due to their high biocompatibility and environmentally friendly properties. Natural textile materials such as cotton, linen are used in the treatment of dry and orthopedic wounds because of their low cost, easy usage and manufacturing, absorbent capacity, air and moisture permeability, non-allergic and biocompatibility properties. However, these materials can cause wound dehydration and can cause pain and other lesions during replacement as they adhere strongly to the site of the wound. In addition, they are insufficient to prevent bacterial growth when used to treat wounds with a high volume of exudate (Koehler, Brandl, & Goepferich, 2018; Naseri-Nosar & Ziora, 2018; Pinho & Soares, 2018). Recently, in order to eliminate these disadvantages, the use of hydrogels in wound dressings has become very important. Hydrogel-based dressings absorb high amounts of water and provide a moist wound environment, control the loss of the fluid and reduce pain for treated patients by providing cooling effect and preventing adhesion to the wound area. In addition, hydrogel dressings are very suitable materials for the controlled delivery of growth factors, antimicrobial and anti-inflammatory agents. Polysaccharides as natural polymers are generally suitable for the design of hydrogels because their hydrophilic properties. Chitosan and alginate (Alg) are the most commonly used polysaccharides in preparing hydrogel dressings (Kamoun, Kenawy, & Chen, 2017; Pinho & Soares, 2018; Simões et al., 2018).

Chitosan has a very important role in wound treatment due to its low toxicity, high biodegradability and biocompatibility, antimicrobial and hemostatic properties. The reason of the antimicrobial character of chitosan is the interaction of the positively charged amino groups of chitosan with the negatively charged microbial cell membranes causing the intracellular components to leak out. However, the dissolution of the chitosan in the acidic environment limits its biological applications to a great extent. The carboxymethyl chitosan (CMCht), modified from chitosan, has the desired water solubility as well as the advantageous biological and antimicrobial properties of chitosan (Gonçalves, da Silva, Signini, & Naves, 2017; Paul & Sharma, 2004; Pranoto, Rakshit, & Salokhe, 2005).

Alginate is a highly biocompatible and non-toxic natural polymer extracted from brown seaweed. It forms physically cross-linked hydrogels in the presence of certain divalent cations (e.g., Ca^{2+}, Sr^{2+}, and Ba^{2+}) through the ionic interaction between the cation and the carboxyl functional group on the polymer chain. The gel-forming property of alginate helps to keep the wound moist, remove the dressing without excessive trauma and reduce the pain experienced by the patient during dressing changes. Alginate hydrogel dressings also reduce adverse allergic effects and exhibit hemostatic properties (D. Li & Xia, 2004; Lin & Yeh, 2004; Paul & Sharma, 2004).

In the literature, there are studies that produced alginate-chitosan hydrogels in wound treatment. For example; Murakami et al., 2010 produced alginate-chitin/chitosan-fucoidan composite hydrogel films and they observed significantly improved granulation tissue and capillary formation in wounds with healing disorders. Rudyardjo & Wijayanto, 2017 prepared alginate-chitosan hydrogels by the addition of lauric acid plasticizer and examined the effect of lauric acid on the mechanical properties of hydrogel and the water absorption capacity. Chen et al., 2017 produced an alginate-chitosan hydrogel loaded with gelatin microspheres containing tetracycline hydrochloride, an antibacterial agent, for use as a skin substitute and showed that the composite gel dressing inhibited the growth of *Escherichia coli* and *Staphylococcus aureus*.

The combination of hydrogels and textiles has been remarkable in recent years as it improves the mechanical properties of hydrogels and reduces the adhesion behavior of the textiles (Pinho & Soares, 2018). In the study of Anjum, Arora, Alam, & Gupta, 2016, antimicrobial and anti-scarring dressings were developed by coating cotton fabric with chitosan, polyethylene glycol and polyvinyl pyrrolidone blend. They also used tetracycline hydrochloride (antibiotic) as a model drug within the hydrogel matrix. They showed that the composite dressings with the drug demonstrated an antibacterial activity and faster wound healing with minimum scar formation.

Skin infections are the most common types of infections and can lead to serious life-threatening conditions depending on the severity of microbial invasion. In the early stage of the infection, gram-positive organisms especially *Staphylococcus aureus* (*S. aureus*) are the predominant organisms, whereas gram-negative organisms such as *Escherichia coli* (*E. coli*) are identified in 15% of skin tissue infections and they are more often seen in chronic wounds (Cardona & Wilson, 2015). In order to eliminate the infection problem, antimicrobial dressings have started to be developed. They can be produced with different strategies including surface functionalization of materials with different groups or incorporation of antimicrobial agents (antibiotics, nanoparticles and natural products) (Simões et al., 2018). Among these antibacterial agents, antimicrobial peptides (AMPs) are known as the evolutionarily protective products of the natural immune system. They are produced by tissues and cells in both plants and animals. Despite the difference in amino acid sequences, most of the AMPs have a cationic character. Thus, the mechanisms of antimicrobial action are due to electrostatic interactions of the microbial cell membrane with the anionic phospholipids resulting in cell death (Li et al., 2018; Mangoni, McDermott, & Zasloff, 2016).

Nisin is an antimicrobial polypeptide produced by Lactococcus lactis subsp.lactis and used as starter bacteria in the dairy industry. Nisin has an antimicrobial activity against a broad spectrum of gram-positive bacteria and it has been accepted as a food additive by both the US Food and Drug Administration (FDA) and the World Health Organization (WHO) (Pranoto, Rakshit, & Salokhe, 2005; Scannell et al., 2000). Zohri

et al., 2010 produced nisin-loaded chitosan/alginate nanoparticles, and they showed that antibacterial efficiency was increased compared to free nisin in dairy products. In the study of Li, Kennedy, Peng, Yie, & Xie, 2006, chitosan-nisin films containing glucomannan, known as a dietary fiber, were produced and the potential of using these films as antimicrobial packaging materials were shown. Bower et al., 2002 studied the antibacterial effect of nisin impregnated polymeric implantable materials. They concluded that nisin was able to adsorb to surfaces and had sufficient activity to inhibit pathogenic bacteria. Even though, nisin has also been evaluated as a promising antibacterial agent in clinical applications, no study has been reported yet on the use of nisin in wound dressing applications.

In this part of the thesis, antibacterial hydrogel composite wound dressings were produced by modifying the natural textile material, cotton. In line with this objective, the carboxymethyl chitosan-alginate polymers were integrated to the cotton and freeze-dried. Then, nisin was impregnated to the modified cotton and after the cross-linking reaction, antibacterial hydrogel composite wound dressings were obtained. Morphological, chemical structure and thermal behavior characterization of the wound dressings were performed by scanning electron microscopy, Fourier transform infrared spectroscopy, and differential/thermogravimetric analysis, respectively. Swelling ratios and water contents of the hydrogel wound dressings were evaluated. The viscoelastic properties of the hydrogel wound dressings were examined by dynamic mechanical analysis. Antibacterial activity of the hydrogel wound dressings was evaluated against gram-positive *S. aureus* and gram-negative *E. coli*.

5.2 Experimental

5.2.1 Materials

O-carboxymethylated CMCht with a deacetylation degree around 91% was obtained from Santa Cruz Biotechnology, USA. Sodium alginate and calcium chloride (CaCl$_2$) were supplied from Merck, Germany. Cotton fabrics were obtained from the

local markets in Turkey. Nisin from Lactococcus lactis (2.5% balance sodium chloride and denatured milk solids) was obtained from Sigma-Aldrich, USA.

5.2.2 Production of Hydrogel Composite Wound Dressings

Before the production of wound dressings, the formation of alginate and CMCht hydrogels were investigated in the presence of $CaCl_2$. CMCht and sodium alginate aqueous solutions at 1% (w/v) concentration were prepared individually by stirring at room temperature for 3 h. $CaCl_2$ was used as the cross-linker at three different concentrations (0.01, 0.005, and 0.0025 M). Physically cross-linked alginate hydrogels were successfully obtained by controlling the pH value. In the acidic environment (pH~3) the gelation process became quicker and controllable. Therefore, this pH value was chosen to control the cross-linking reaction for further experiments. However, the gelation of CMCht did not occur in the same conditions.

In order to produce hydrogel composite wound dressings, initially CMCht/Alg:$CaCl_2$ mixture at 2:2:1 v:v ratio was prepared by mixing for 1 h at room temperature. Then, 4 ml of this solution was impregnated to the cotton of 3 cm in diameter and 1 cm in thickness. After that, they were freeze-dried (TELSTAR – LyoQuest -85) at -25°C under 0.1 mbar pressure for 2 days. In order to obtain cross-linked structure, they were treated with 0.2 M acetic acid (pH~3). Hydrogel composite wound dressings were obtained after the second freeze-drying followed by washing with ethanol to remove acetic acid and drying in vacuum oven at 25°C.

5.2.3 Production of Antibacterial Hydrogel Composite Wound Dressings

According to the characterization results of the hydrogel composite wound dressings, 0.0025 M of $CaCl_2$ was chosen as the optimum value and this concentration of cross-linker was used in the production of antibacterial wound dressings. For the production of antibacterial hydrogel composite wound dressings, likewise as hydrogel composite wound dressing CMCht/Alg:$CaCl_2$ mixture at 2:2:1 v:v ratio was prepared, impregnated to the cotton and freeze-dried. However, in the cross-linking step

differently from the hydrogel composite wound dressings, 1, 5 and 7,5 mg/ml of nisin solutions in 0.2 M acetic acid were impregnated to the composite structures overnight. Finally, they were subjected to freeze-dry, washed with ethanol and dried.

5.2.4 Characterization of the Wound Dressings

5.2.4.1 SEM Analysis

The morphological analyses of the wound dressings were performed by SEM (JEOL JSM-6060) at an accelerating voltage of 5 kV. All the wound dressings were coated with a thin layer of gold/palladium prior to analysis.

5.2.4.2 ATR-FTIR Analysis

The chemical structures of the wound dressings were determined by ATR-FTIR (Perkin Elmer Spectrum BX). Each spectrum was obtained in the wavenumber range of 4000-650 cm^{-1} at a resolution of 4 cm^{-1}, and by scanning 25 times per sample.

5.2.4.3 Swelling Ratio Test

The swelling test of the wound dressings was performed in PBS solution. First, the dried scaffolds (n=3) were weighed (w_0), and then immersed in PBS at 37°C for 24 hours. After excess water was removed with a filter paper, scaffolds were weighed (w_s) again. Swelling ratio and water content values of the hydrogel wound dressings were calculated according to the following equations (5.1) and (5.2), respectively.

$$Swelling\ ratio\ (\%) = \left(\frac{w_s - w_0}{w_0}\right) x\ 100 \qquad (5.1)$$

$$Water\ content\ (\%) = \left(\frac{w_s - w_0}{w_s}\right) x\ 100 \qquad (5.2)$$

5.2.4.4 Viscoelastic Property Characterization

The viscoelastic measurements were performed using DMA (TA, Q800) equipped with the compression mode. The measurements were carried out using dynamic frequency sweep with frequencies ranging from 100 Hz to 0.1 Hz at 37°C under a constant strain amplitude (1%). The storage (E') and loss modules (E") of the samples were measured, and the tan delta (tan δ) values were calculated from the modules.

5.2.4.5 Antibacterial Studies

The antibacterial activity of the prepared hydrogel wound dressings was evaluated against gram-positive bacteria *S. aureus* and gram-negative bacteria *E. coli* using a modified AATCC Test Method 100-1999. Initially, each side of the wound dressings (n=3) with a diameter of 3 cm were sterilized by UV light for 15 minutes. Appropriate dilutions were made in trypticase soy broth and nutrient broth to obtain an inoculation solution containing 1.7×10^4 CFU/ml of *S. aureus* and 1.25×10^4 CFU/ml of *E. coli*, respectively. Then, 500 µl of the bacterial suspensions were added to the wound dressings into the conical flasks and they were incubated at 37°C for 24 h. After the incubation period, 20 ml of neutralizing solution was added to the flasks and each of the flask was subjected to mixing in an ultrasonic bath for one minute followed by vigorously shaking in a vortex mixer for another one minute. Finally, 100 µl of cultured media was spread over the trypticase soy and nutrient agar plates in duplicate. The plates were incubated at 37°C for 24 h and the bacterial colonies on the plates was counted visually.

5.2.4.6 DTA/TGA

DTA/TGA (Shimadzu DTG-60H) was used to determine the thermal properties of the wound dressings. Analyses were performed under a nitrogen atmosphere at a heating rate of 10°C/min and in the temperature range of 25-700ºC.

5.2.4.7 Elemental Analysis

In order to determine the presence of nisin in the wound dressings, elemental analyses of carbon, hydrogen, and nitrogen were performed on an Elemental Analyzer (LECO, CHNS-932) in the Central Laboratory of Middle East Technical University.

5.3 Results and Discussions

5.3.1 Production of the CMCht/Alginate Hydrogel Composite Wound Dressings

First of all, the cross-linker concentration and cross-linking parameters were optimized as the preliminary studies.

CMCht (1 % (w/v)), alginate (1 % (w/v)), and CMCht/Alg solutions (1:1 v:v) were prepared and subjected to cross-linking reaction in the presence of different molarities of $CaCl_2$ (0.01, 0.005, 0.0025 M). The polymer/cross-linker ratio was taken as 2:1 (v:v). Stable alginate hydrogels were immediately obtained by all the molarities of $CaCl_2$ in an acidic environment (pH~3) but hydrogel formation in a neutral environment took more than a day. Therefore, pH~3 was chosen as the cross-linking reaction for further productions. Even though CMCht hydrogels could not be produced by none of the $CaCl_2$ concentration at neither acidic nor neutral pH, CMCht/alginate hydrogels were produced by intermolecular interaction of both polymer and physically cross-linking of alginate with $CaCl_2$.

For the production of hydrogel composite wound dressings, initially CMCht/Alg:$CaCl_2$ mixture at 2:2:1 (v:v) ratio was prepared by mixing for 1 h at room temperature. Then, 4 ml of this solution was impregnated to the cotton (diameter: 3 cm, thickness: 1 cm) and allowed to penetrate overnight, and they were freeze-dried at -25°C for 2 days. In order to obtain cross-linked structure, they were treated with 0.2 M acetic acid and left overnight. After the second freeze-drying, they were washed with ethanol to remove acetic acid and dried in vacuum oven at 25°C.

116

The sample codes of the produced hydrogel composite wound dressings with or without nisin were given in Table 5.1. C and N in the codes refer to cotton and nisin, respectively. In order to obtain the optimum cross-linker concentration wound dressings were subjected to SEM and FTIR analysis as well as swelling and viscoelastic property measurements.

Table 5.1 The codes of hydrogel composite wound dressings

Sample Code	CMCht/Alg: CaCl$_2$ (v:v:v)	Molarity of CaCl$_2$ (M)	Nisin concentration (mg/ml)
C-CMCht/Alg:0.01CaCl$_2$	2:2:1	0.01	-
C-CMCht/Alg:0.005CaCl$_2$	2:2:1	0.005	-
C-CMCht/Alg:0.0025CaCl$_2$	2:2:1	0.0025	-
C-CMCht/Alg:0.0025CaCl$_2$_1N	2:2:1	0.0025	1
C-CMCht/Alg:0.0025CaCl$_2$_5N	2:2:1	0.0025	5
C-CMCht/Alg:0.0025CaCl$_2$_7.5N	2:2:1	0.0025	7.5

5.3.1.1 SEM Analysis

A three-dimensional and porous structure are very important for wound dressing in order to improve air and moisture permeability to provide a moist environment in the wound bed. Morphologies of the untreated cotton and hydrogel composite wound dressings were examined by SEM, and SEM images at different magnifications are shown in Figure 5.2. All the dressings maintained their three-dimensional porous structure. The pores between the cotton fibers were not fully closed after the impregnation of CMCht/Alg:CaCl$_2$.

Cotton

C-CMCht/Alg:0.01CaCl$_2$

C-CMCht/Alg:0.005CaCl$_2$

C-CMCht/Alg:0.0025CaCl$_2$
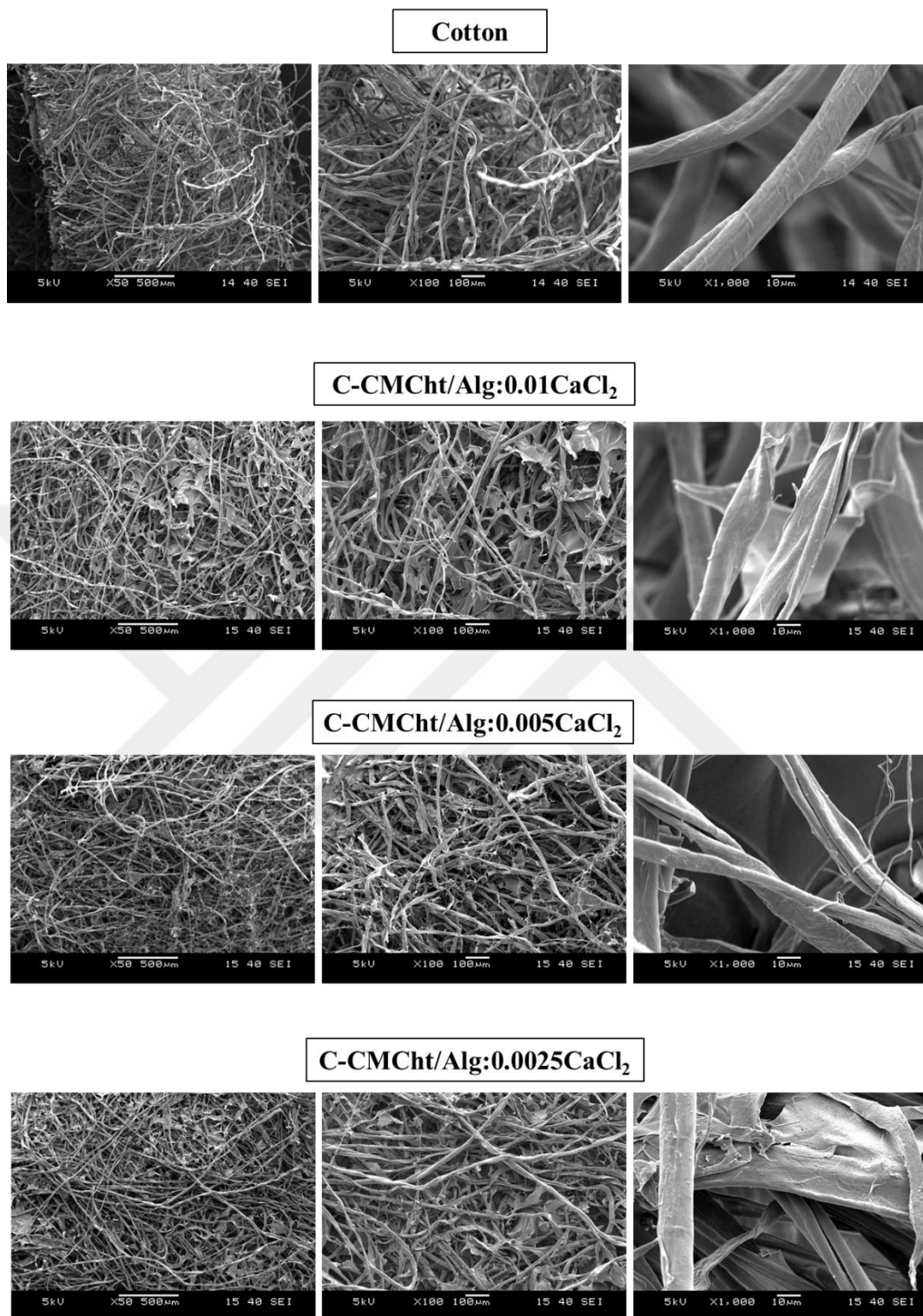
Figure 5.2 SEM images of the cotton and hydrogel composite wound dressings

FTIR analysis was carried out to investigate the chemical structure of the hydrogel composite wound dressings. FTIR spectra of the untreated cotton, sodium alginate, and CMCht are shown in Figure 5.3, Figure 5.4, and Figure 5.5 respectively.

FTIR spectra of cotton (Figure 5.3) showed strong and broad absorption at 3600–3000 cm^{-1} referred to the O–H stretching vibrations. This absorption band was composed of two vibrations located at 3336 cm^{-1} (attributed to intermolecular hydrogen bonds) and 3291 cm^{-1} (attributed to intra-molecular hydrogen bonds). C–H stretching vibration appeared at 2897 cm^{-1}. O-H bending vibration of adsorbed water molecules was located at 1658 cm^{-1}. The C–H bending vibrations are given by the peaks at 1428 and 1380 cm^{-1}. The band at 1332 cm^{-1} corresponded to the O-H bending of CH$_2$-OH group, and the bands at 1160 and 1109 cm^{-1} referred to the antisymmetric bridge stretching of C-O-C. The strong peak at around 1030 cm^{-1} is due to the presence of C-O-C pyranose ring vibration of the cellulose (Chung, Lee, & Choe, 2004; Santiago Cintrón et al., 2016; Tissera, Wijesena, Rathnayake, de Silva, & de Silva, 2018).

In the FTIR spectrum of alginate (Figure 5.4), strong and broad free stretching vibrations of O–H bonds appeared about 3600 cm^{-1}. Weak stretching vibrations of the C–H groups were observed at around 3000 cm^{-1}. The bands in 1603 and 1407 cm^{-1} were attributed to the asymmetric and symmetric stretching vibrations of the COO^{-} group, respectively. The bands around 1080 and 1030 cm^{-1} were attributed to the C-O-C stretching vibrations (Daemi & Barikani, 2012; Li, Dai, Zhang, Wang, & Wei, 2008).

In the FTIR spectrum of CMCht (Figure 5.5), the broad peak appeared at 3400–3200 cm^{-1} referred to both the O–H and N–H stretching vibrations. C–H stretching vibration was at ~2900 cm^{-1}. The peaks at 1587 and 1410 cm^{-1} were assigned to the asymmetric and symmetric stretching vibrations of the carboxy group, respectively. Besides, N-H bending vibration of the amine group overlapped with the asymmetric

vibration of the carboxy group. Also, the absorption peak of the secondary hydroxyl group appeared at 1053 cm^{-1} (Chen et al., 2017; Chen et al., 2015; Kumar Singh Yadav & Shivakumar, 2012).
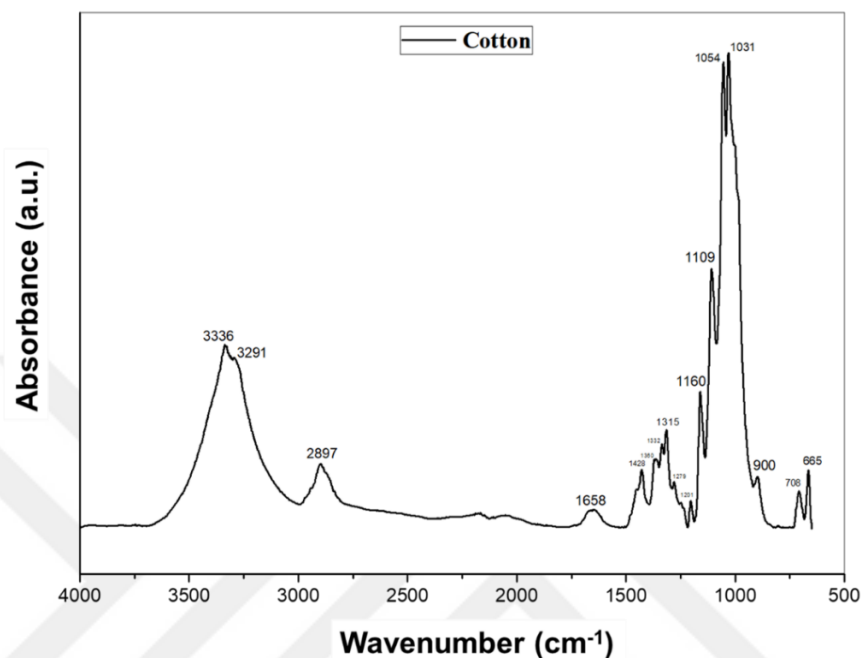
Figure 5.3 FTIR spectra of untreated cotton
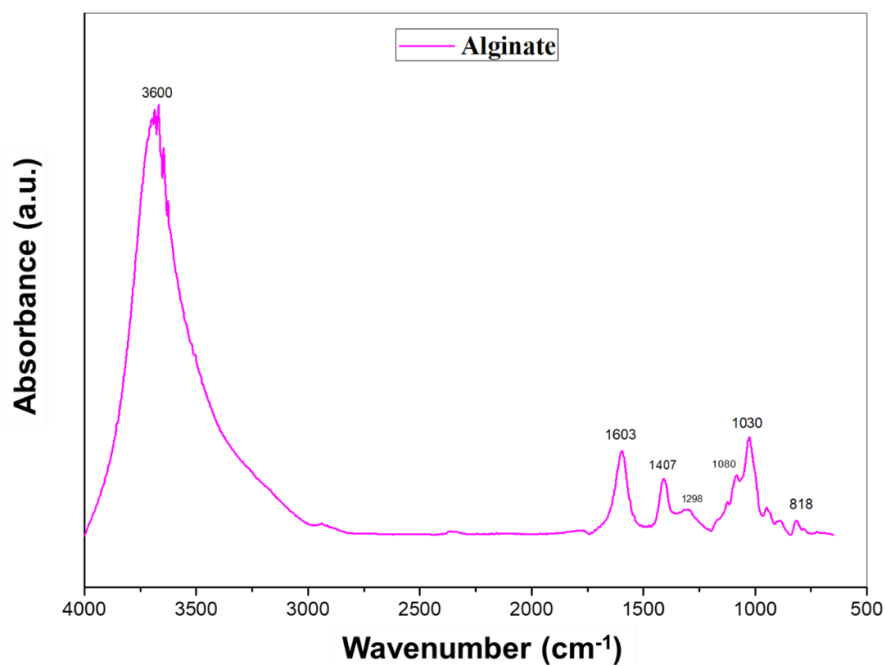
Figure 5.4 FTIR spectra of alginate powder

120
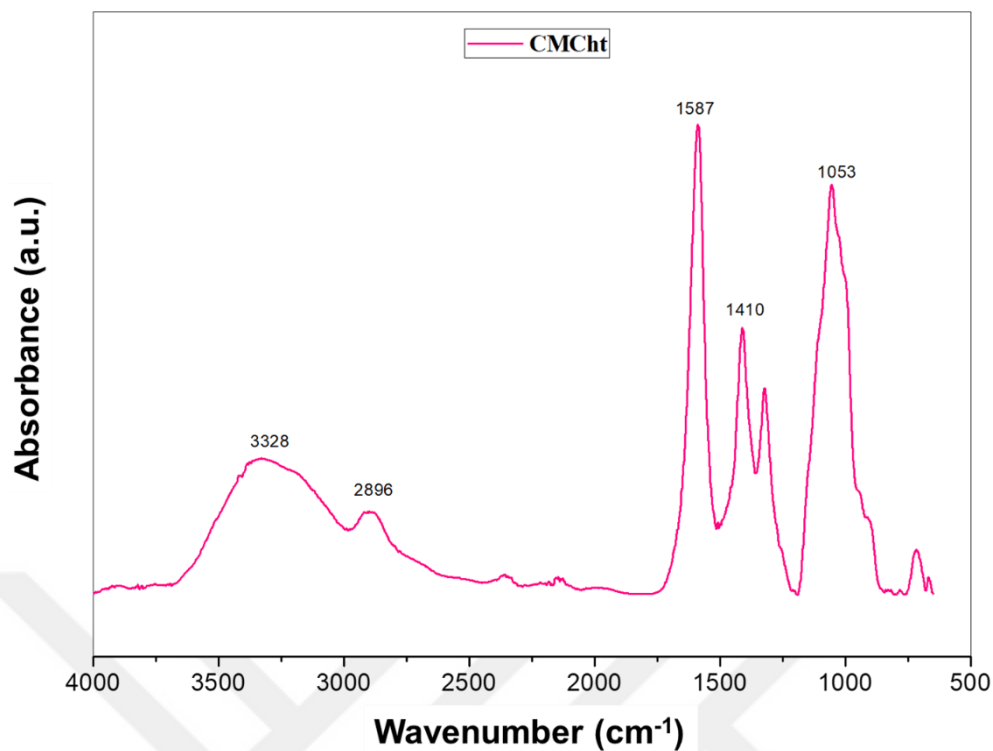
Figure 5.5 FTIR spectra of CMCht powder

In the FTIR spectra of the hydrogel wound dressings (Figure 5.6), O-H free stretching band of alginate was not observed, instead a new O-H stretching peak which was probably due to intermolecular hydrogen bonding between CMCht and alginate appeared at ~3280 cm^{-1}. Besides, after cross-linking reaction of alginate with CaCl$_2$, the peak at 1603 cm^{-1} of alginate shifted to lower wavenumbers. However, in this range CMCht had a strong absorption peak at 1587 cm^{-1} attributed to N-H bending; therefore, these two peaks merged at ~1595 cm^{-1}. In addition, it was proven that acetic acid was successfully removed from the dressings after ethanol treatment since the most intense band of the acetic acid (~1718 cm^{-1}, C = O stretching) was not observed (Colomer, 2013).
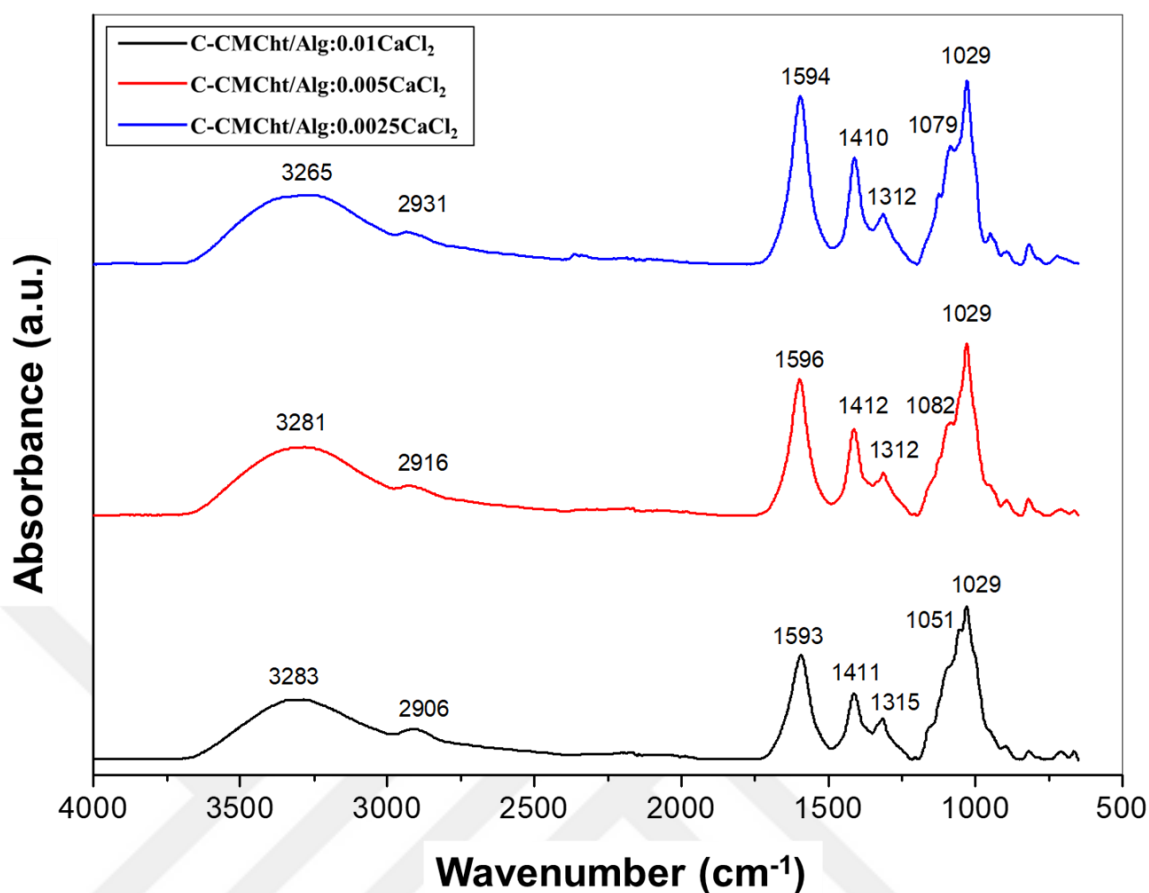
Figure 5.6 FTIR spectra of the produced hydrogel composite wound dressings

5.3.1.3 Swelling Behavior

It is very important and necessary that the wound dressing has high liquid absorption capacity to remove excess exudate which contains nutrients that increase the risk of bacterial growth from the wound bed in order to improve healing potential of the wound. Hydrogel dressings meet this requirement of the ideal wound dressing with their high-water content. Swelling ability of the produced hydrogel wound dressings as well as untreated cotton was evaluated by immersing the samples in PBS at 37°C for 24 h. The swelling ratio (eq. 5.1) and water content (eq. 5.2) of the samples were calculated from the formulas given in the experimental section. Figure 5.7 shows the swelling ratio values of the hydrogel wound dressings and cotton. The swelling ratio of the cotton was significantly different compared to dressings cross-linked with 0.005 and 0.01 M of CaCl$_2$, whereas cotton and the C-CMCht/Alg:0.0025CaCl$_2$ had

comparable swelling ratios (1394±92% and 1202±95%, respectively). As seen from the Table 5.2, all the hydrogel wound dressings had swelling ratio between 724-1202% and water content between 88-92%. Besides, both swelling ratios and the water content of the hydrogel wound dressings increased upon decreasing $CaCl_2$ content, as expected.
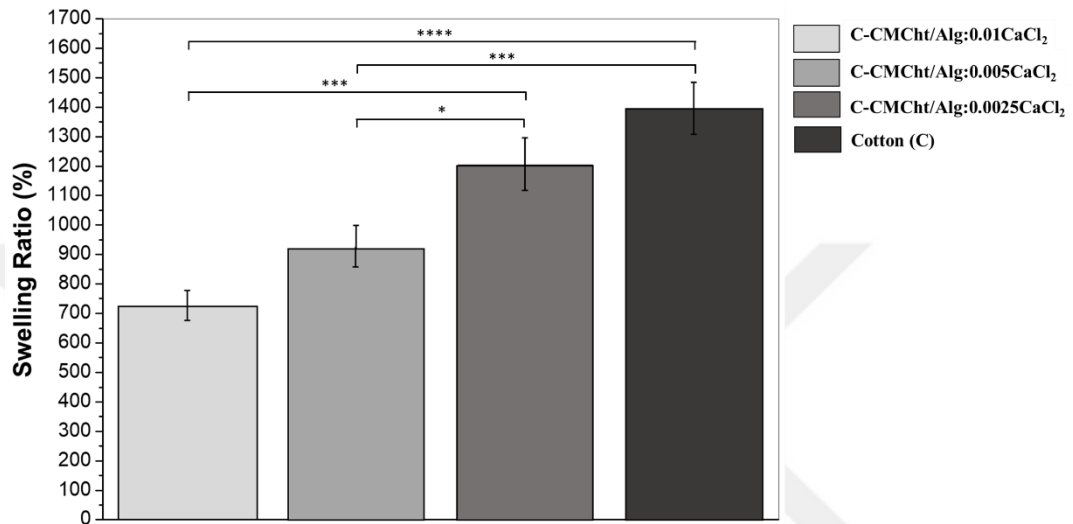
Figure 5.7 Swelling ratios of the cotton and hydrogel composite wound dressings (*p≤0.05, ***p≤0.001, ****p≤0.0001)

Table 5.2 Swelling ratio and water content values of the cotton and hydrogel wound dressings

	Swelling ratio (%)	Water content (%)
Cotton	1394±91.8	93.3±0.4
C-CMCht/Alg:0.0025CaCl$_2$	1202±94.9	92.3±0.5
C-CMCht/Alg:0.005CaCl$_2$	918.4±77.9	90.1±0.8
C-CMCht/Alg:0.01CaCl$_2$	724.0±50.6	87.8±0.7

5.3.1.4 Viscoelastic Properties

The viscoelastic properties of the hydrogel wound dressings were determined using DMA at 37°C. The measurements were carried out using a compression clamp and in dynamic frequency sweep mode with frequencies ranging from 0.1 Hz up to 100 Hz.

In Figure 5.8 storage and loss moduli of the hydrogel dressings are shown as functions of frequency. All the samples have E' >E" over the entire frequency range indicating an elastic solid behavior. Also, the E' and E" slightly increased as frequency increased, indicative of the structural relaxation of the network at higher frequencies. The storage moduli values enhanced upon increasing $CaCl_2$ concentration. Besides, a sharp decrease in the E' values of the hydrogels at higher frequencies can be ascribed to possible resonance and cavitation occurring in the hydrogels that result in micro-damage of the samples (Byju & Kulkarni, 2013).
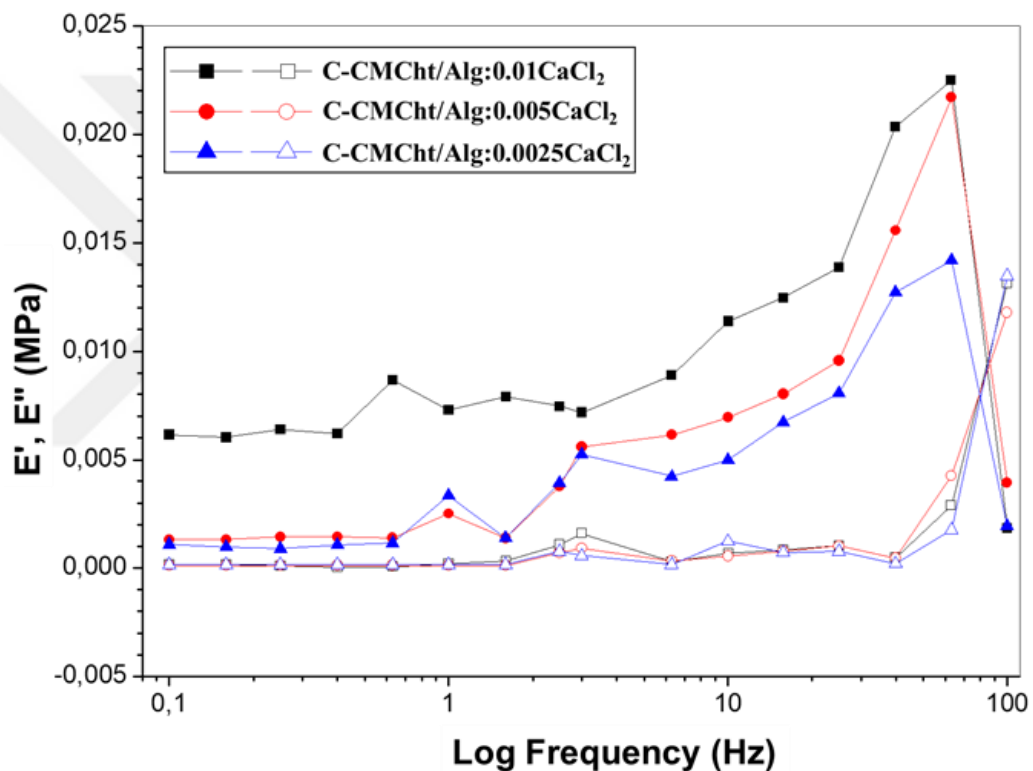
Figure 5.8 Storage (E', solid symbols) and loss modulus (E", hollow symbols) of the hydrogel composite wound dressings

Tan δ is determined by the ratio of loss modulus and storage modulus and provides information about the damping properties of the hydrogel wound dressings. Tan δ values of the wound dressings are shown in Figure 5.9. At some critical frequencies, relaxational process appears and tan δ pass through a maximum. Enhanced damping capability was obtained in hydrogel wound dressing cross-linked with 0.0025 M due

to its higher tan δ values and the presence of two maxima which were probably related to the α and β relaxations. A sharp increase in the tan δ values after 60 Hz was due to the decrease in storage moduli as the result of micro damages occurred within the samples.
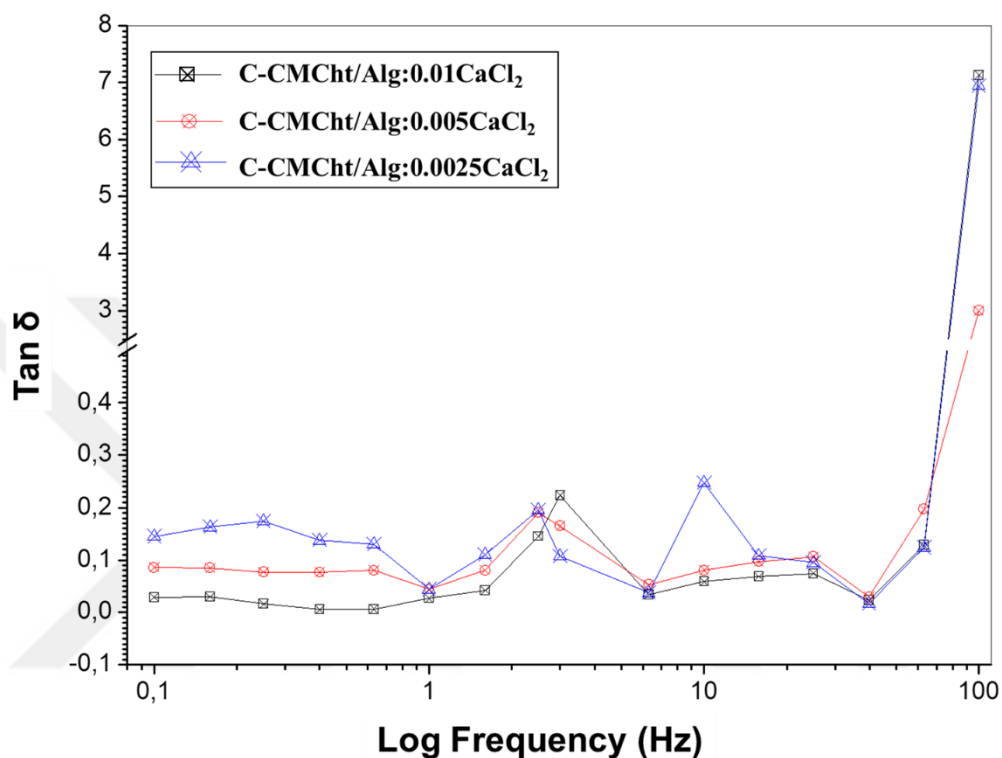
Figure 5.9 Tan δ values of the hydrogel composite wound dressings

5.3.2 Production of Antibacterial Nisin Incorporated CMCht/Alginate Hydrogel Composite Wound Dressings

For the production of antibacterial hydrogel wound dressings, 0.0025 M of $CaCl_2$ was chosen as an optimum cross-linker concentration according to its better viscoelastic nature and swelling capability. Nisin as the antibacterial polypeptide was incorporated to hydrogel wound dressings at different concentrations (1, 5 and 7.5 mg/ml). The codes of the produced antibacterial wound dressings were given in Table 5.1.

5.3.2.1 Antibacterial Studies

The antibacterial activities of the nisin incorporated hydrogel composite wound dressings were evaluated against *E. coli* (Gram-negative) and *S. aureus* (Gram-positive) bacteria. Cotton and hydrogel wound dressings without any nisin addition (C-CMCht/Alg:0.0025CaCl$_2$) was used as the control group. The bacterial suspensions (1.7x10^4 CFU/ml for *S. aureus* and 1.25x10^4 CFU/ml for *E.coli*) were added to the wound dressings and they were incubated at 37°C for 24 h. Then they were neutralized and cultured media was spread over the agar plates. After 24 h incubation at 37°C bacterial colonies were counted. Table 5.3 shows the number of bacterial colonies of the tested samples, and in Figure 5.10 the corresponding agar plates of the samples are given.

Table 5.3 The bacterial colonies of the hydrogel wound dressings

Sample	**Bacterial Colony (CFU/ml)**	
	S. aureus	*E. coli*
Cotton	>1.7x10^4	>1.25x10^4
CMCht/Alg:0.0025CaCl$_2$	>1.7x10^4	2.5
CMCht/Alg:0.0025CaCl$_2$_1N	5.0x10^3	>1.25x10^4
CMCht/Alg:0.0025CaCl$_2$_5N	6.5x10^2	>1.25x10^4
CMCht/Alg:0.0025CaCl$_2$_7.5N	0	>1.25x10^4

	S. aureus	*E. coli*
Cotton (C)	a	b
C-CMCht/Alg:0.0025CaCl$_2$	c	d
C-CMCht/Alg:0.0025CaCl$_2$-1N	e	f
C-CMCht/Alg:0.0025CaCl$_2$-5N	g	h
C-CMCht/Alg:0.0025CaCl$_2$-7.5N	i	j
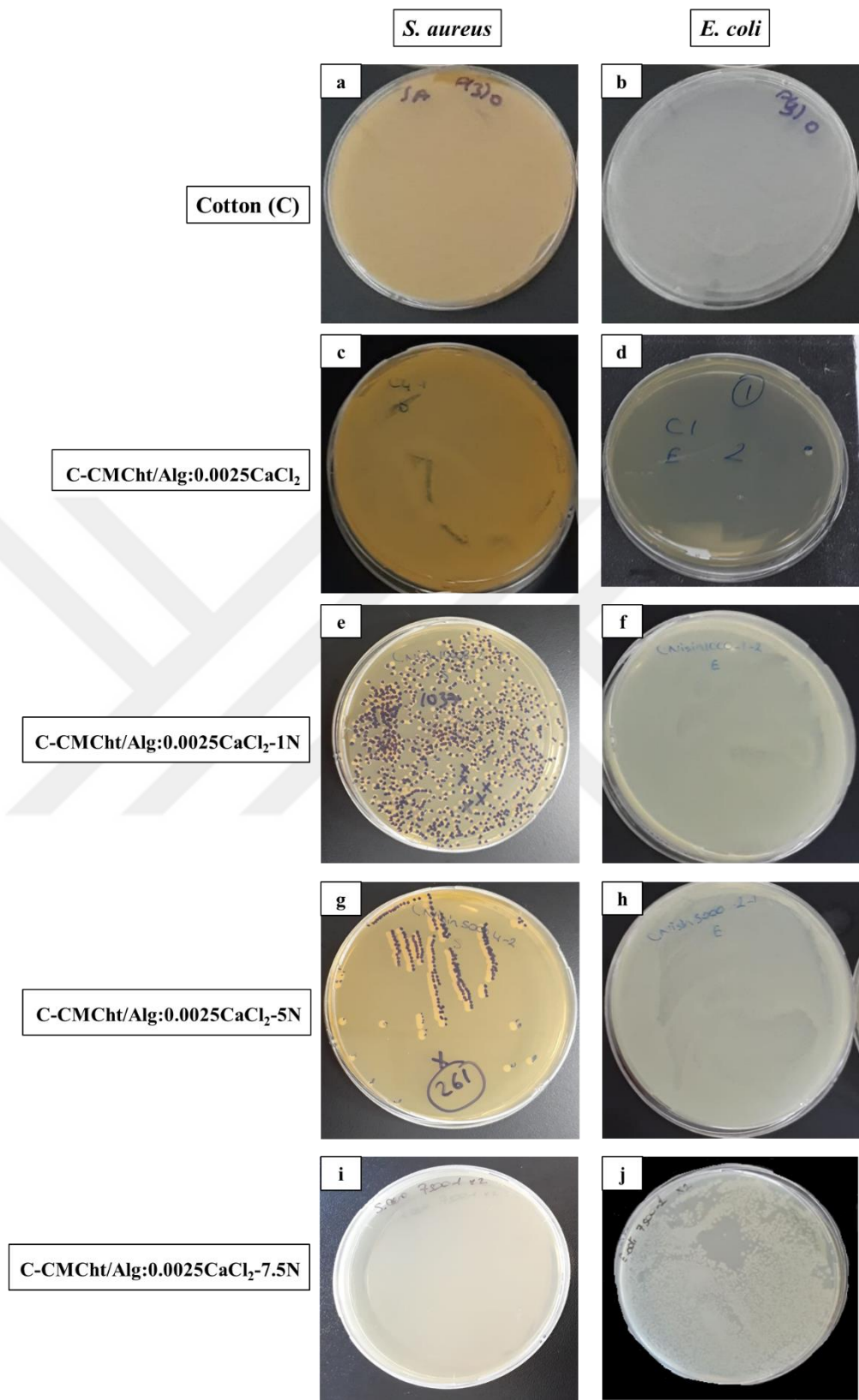
Figure 5.10 Representative agar plates after antibacterial tests against *S. aureus* (a, c, e, g, i) and *E. coli* (b, d, f, h, j)

The results suggested that cotton did not demonstrate any antibacterial activity against neither *E. coli* nor *S. aureus*. Hydrogel composite wound dressings without nisin incorporation (CMCht/Alg:0.0025CaCl$_2$) did not have antibacterial activity against *S. aureus*, whereas they demonstrated an antibacterial activity to *E. coli*. In the literature, it was stated that sodium alginate has no antibacterial activity against both gram-positive and negative bacteria (Alboofetileh, Rezaei, Hosseini, & Abdollahi, 2014; Tang, Pan, Sun, Cao, & Guo, 2017). On the other hand, Wahid et al., 2016 showed that CMCht had a slightly enhanced antibacterial activity against *E. coli* compared to *S. aureus*. They also demonstrated that CMCht hydrogels cross-linked with epichlorohydrin showed poor antibacterial activity against both bacteria. Therefore, it was concluded that the antibacterial activity to *E. coli* of the hydrogel composite wound dressings was due to the CMCht/alginate complex, which probably had a better interaction with the cell wall of gram-negative bacteria with an outer membrane containing lipopolysaccharide, lipoprotein, and phospholipids (Mohamed & Abd El-Ghany, 2017). However, in none of the nisin incorporated hydrogel composite wound dressings, no antibacterial effect against *E. coli* were observed. The hydrogel composite wound dressing comprising 1 mg/ml of nisin (CMCht/Alg:0.0025CaCl$_2$_1N) showed only bacteriostatic effect to *S. aureus*. Antibacterial activity of the hydrogel wound dressings enhanced upon increasing nisin concentration, and the wound dressing with 7.5 mg/ml of nisin (CMCht/Alg:0.0025CaCl$_2$_7.5N) exhibited bactericidal activity against *S. aureus*. Nisin has an antibacterial activity against broad spectrum of gram-positive bacteria by pore formation and inhibition of the cell wall synthesis *via* the electrostatic interaction between the positively charged surface of nisin and the negatively charged phosphate groups of the cell membrane. Pore formation causes the destruction of the barrier function and the reduction of the membrane potential. These pores allow the leaking of essential molecules (K$^+$, ATP, and amino acids) from the cell leading to cell death (Jozala, de Lencastre Novaes, & Junior, 2015). However, nisin does not show any antibacterial effect against gram negative bacteria as they have an extra lipopolysaccharide outer membrane which acts as a barrier and protects the membrane from the action of nisin (Vukomanović et al., 2017).

5.3.2.2 Morphological Characterization

Figure 5.11 shows the SEM images of the cotton, CMCht/Alg:$0.0025CaCl_2$ and CMCht/Alg:$0.0025CaCl_2$_7.5N wound dressings. The fiber surface of the hydrogel wound dressings (Figure 5.11 c-d and e-f) were rougher than that of cotton fibers due to the polymer impregnation. In addition, nisin incorporation did not affect the three-dimensional and porous structure of the dressing. The adsorption of nisin particles on the fibers were clearly seen in Figure 5.11 e and f.
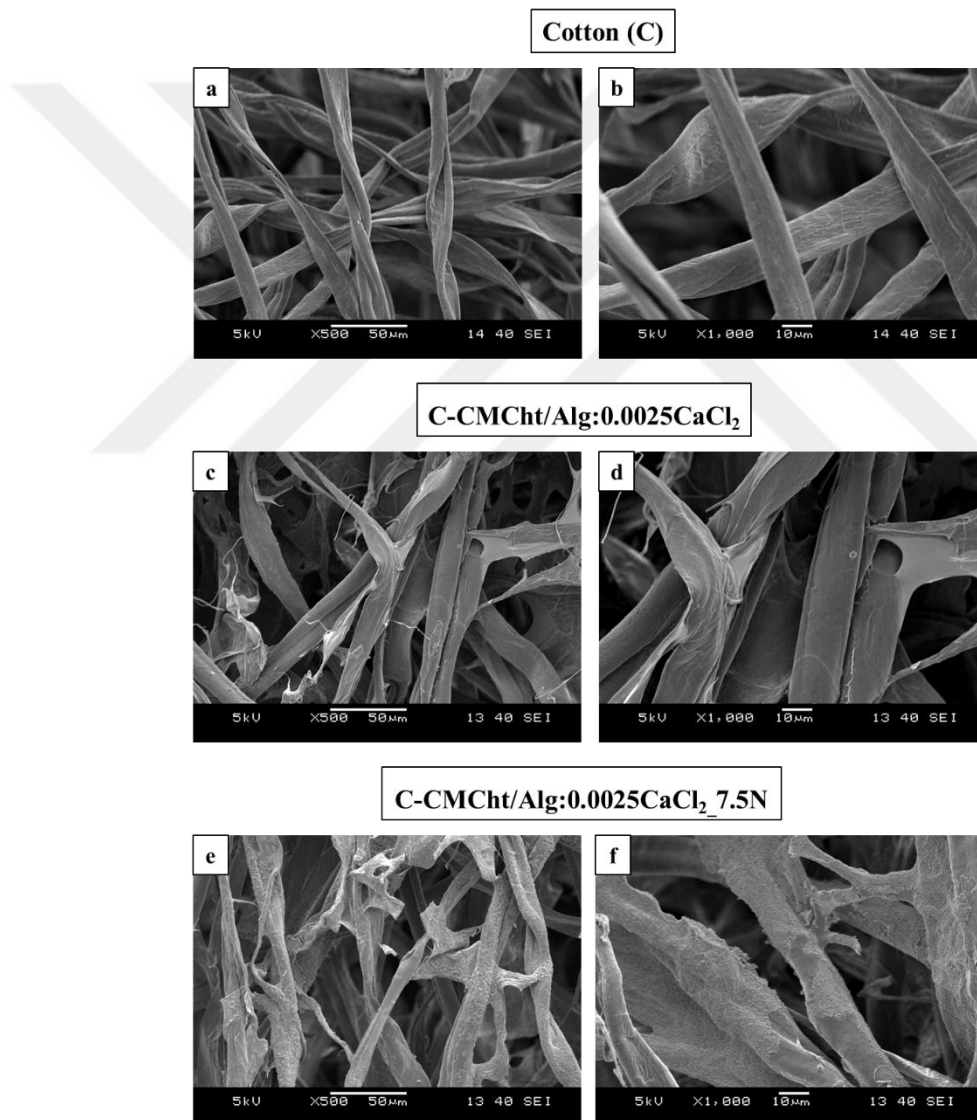
Figure 5.11 SEM images of the cotton, CMCht/Alg:$0.0025CaCl_2$ and CMCht/Alg:$0.0025CaCl_2$_7.5N wound dressings

5.3.2.3 ATR-FTIR Analysis

FTIR spectrum of the antibacterial hydrogel wound dressing (CMCht/Alg:0.0025CaCl$_2$_7.5N) is given in Figure 5.12 in comparison with CMCht/Alg:0.0025CaCl$_2$ hydrogel wound dressing. Two spectra showed very similar patterns as the characteristic bands of nisin (3288 cm^{-1}, O-H asymmetrical stretching; 3001 cm^{-1}, C-H symmetrical stretching; 1650 cm^{-1}, amide I; 1522 cm^{-1}, amide II) overlapped with the bands of the hydrogel wound dressing (Niaz et al., 2018). Therefore, the presence of nisin on the hydrogel wound dressing could not be determined *via* FTIR analysis.
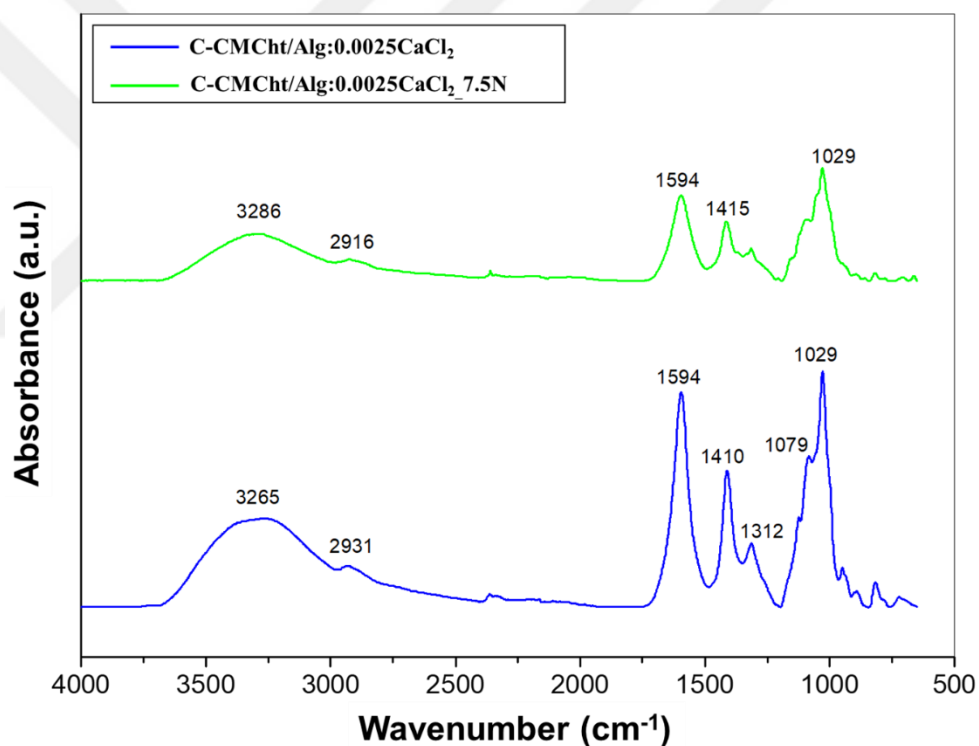
Figure 5.12 FTIR spectra of the CMCht/Alg:0.0025CaCl$_2$ and CMCht/Alg:0.0025CaCl$_2$_7.5N wound dressings

5.3.2.4 Elemental Analysis

Elemental analyzer determines the percentage of carbon, hydrogen and nitrogen elements of the organic samples chromatographically by burning them with a high

130

purity oxygen gas. The analyses of cotton, CMCht/Alg:0.0025CaCl$_2$ and CMCht/Alg:0.0025CaCl$_2$_7.5N wound dressings were performed and percentages of carbon, hydrogen, and nitrogen were obtained (Table 5.4). The nitrogen percentage of the CMCht/Alg:0.0025CaCl$_2$ sample which was due to CMCht, $(C_{10}H_{19}NO_6)_n$ with molecular weight of $(249.12)_n$, could not be detected due to the fact that the theoretically calculated nitrogen percentage (0.003 %) was far below the detection limit of the device. For the nisin incorporated hydrogel wound dressing (CMCht/Alg:0.0025CaCl$_2$_7.5N) the theoretical nitrogen percentage that came from nisin, $(C_{143}H_{230}N_{42}O_{37}S_7)$ and it was nearly same with calculated value indicating that nisin was successfully incorporated to the dressing.

Table 5.4 Elemental analysis results of the samples

Sample	C %	H %	N %
Cotton	41.63±0.62	6.66±0.24	-
CMCht/Alg:0.0025CaCl$_2$	37.54±0.62	6.12±0.20	< 0.5
CMCht/Alg:0.0025CaCl$_2$_7.5N	36.87±1.17	5.67±0.14	0.93±0.01

5.3.2.5 Swelling Properties

The swelling ability of the produced antibacterial hydrogel wound dressings was evaluated by immersing the samples in PBS at 37°C for 24 h, and the result was compared with the cotton as well as the hydrogel wound dressing without nisin. The swelling ratio (eq. 5.1) and water content (eq. 5.2) of the samples were calculated from the formulas given in the experimental section. Figure 5.13 shows the swelling ratio values of the samples. The cotton and C-CMCht/Alg:0.0025CaCl$_2$ had comparable swelling ratios (1394±92% and 1202±95%, respectively). On the other hand, the swelling ratio of the antibacterial hydrogel wound dressing (881±58%) showed a slight decrement with the incorporation of nisin. As seen from the Table 5.5, all the samples had a similar water content of 90-93%.
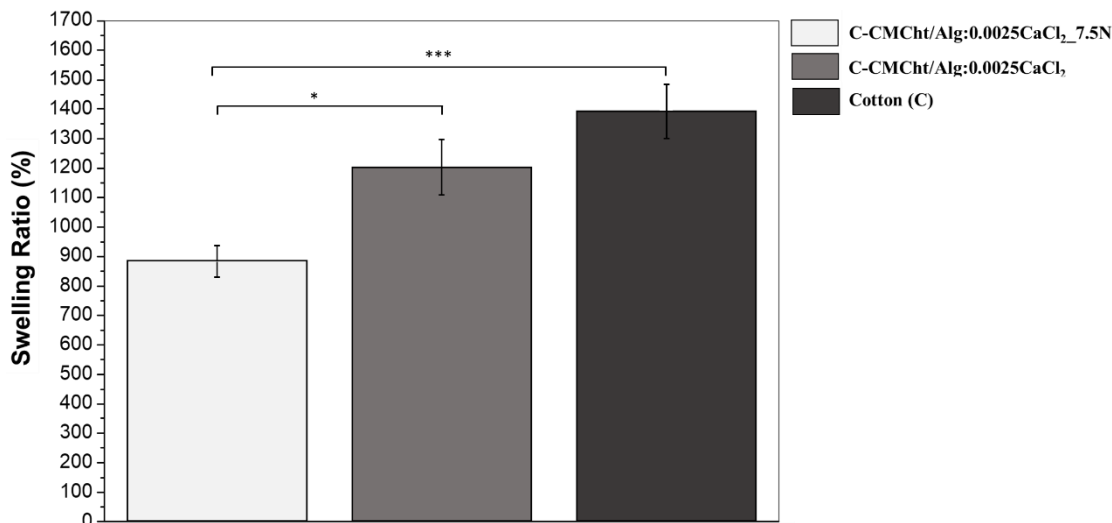
Figure 5.13 Swelling ratios of the cotton, CMCht/Alg:$0.0025CaCl_2$ and CMCht/Alg:$0.0025CaCl_2$_7.5N wound dressings (*$p \leq 0.05$, ***$p \leq 0.001$)

Table 5.5 Swelling ratio and water content values of the cotton and hydrogel wound dressings

	Swelling ratio (%)	Water content (%)
Cotton	1394±91.8	93.3±0.4
C-CMCht/Alg:$0.0025CaCl_2$	1202±94.9	92.3±0.5
C-CMCht/Alg:$0.0025CaCl_2$ _7.5N	881.2±53.0	89.8±0.6

5.3.2.6 DTA/TGA

Thermal properties of the cotton, CMCht/Alg:$0.0025CaCl_2$, and CMCht/Alg:$0.0025CaCl_2$_7.5N were examined by DTA/TGA. TGA curves of the samples are given in Figure 5.14. All of them exhibited two-stage decomposition. The first stage was assigned to the loss of adsorbed water around 100ºC. After that, the main thermal decomposition occurred. The onset decomposition temperatures of the cotton, CMCht/Alg:$0.0025CaCl_2$ and CMCht/Alg:$0.0025CaCl_2$_7.5N hydrogel wound dressings were 346, 264 and 275ºC respectively. The main thermal decay temperature of the cotton was the highest one with enhanced thermal stability, the onset decomposition temperatures of the hydrogel wound dressings with and without nisin were found to be similar. Besides, the char yield of the hydrogel wound dressing (15.7

%) was found to be higher than the cotton and with the addition of nisin the char yield increased to 20.5 wt. %.
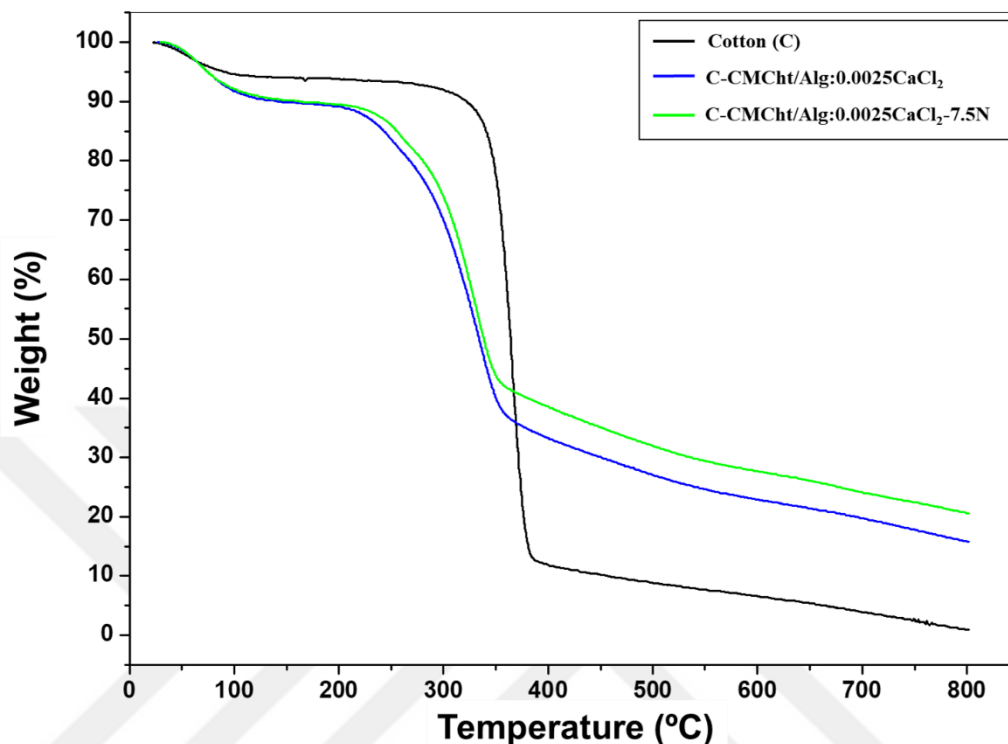
Figure 5.14 TGA curves of the cotton, CMCht/Alg:0.0025CaCl$_2$ and CMCht/Alg:0.0025CaCl$_2$_7.5N wound dressings

The DTA curves of the CMCht/Alg:0.0025CaCl$_2$ and CMCht/Alg:0.0025CaCl$_2$_7.5N hydrogel wound dressing are shown in Figure 5.15. All the samples presented an endothermic peak in the 75–100°C range, which was attributed to water loss. For cotton, the second endothermic peak observed at around 370°C was due to the decomposition of cellulose (Nada, Kamel, & El-Sakhawy, 2000). CMCht/Alg:0.0025CaCl$_2$ and CMCht/Alg:0.0025CaCl$_2$_7.5N hydrogel wound dressings showed an exothermic peak at 345°C and 349°C, respectively, due to the decomposition of the impregnated polymers. In addition, nisin incorporation did not affect the thermal profile of the hydrogel wound dressing.
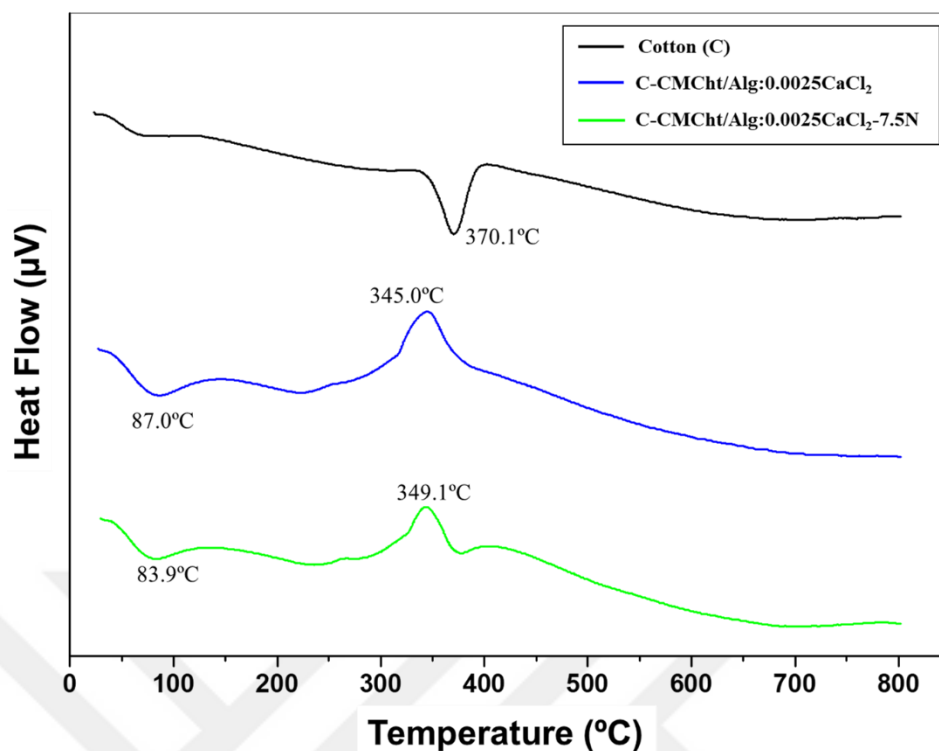
Figure 5.15 DTA curves of the cotton, CMCht/Alg:0.0025CaCl$_2$ and CMCht/Alg:0.0025CaCl$_2$_7.5N wound dressings

5.4 Conclusion

Three-dimensional, porous CMCht-alginate modified cotton hydrogel wound dressings were produced by cross-linking with different concentrations of CaCl$_2$ solution. SEM images showed that wound dressings maintained their porous structure after polymer impregnation. All the hydrogel wound dressings showed viscoelastic properties according to the DMA results and the dressing with the lowest CaCl$_2$ concentration had the best damping capability. Antibacterial hydrogel wound dressings with 7.5 mg/ml nisin showed an antibacterial activity against gram-positive *S. aureus*, however they did not have any antibacterial effect against gram-negative *E. coli*. On the other hand, wound dressing without nisin exhibited bactericidal property to *E. coli* only.

CHAPTER SIX
CONCLUSIONS AND FUTURE WORK

This thesis focuses on establishing fundamental scientific research to produce biomaterials with desired biocompatibility, biodegradability and antibacterial features for bone and cartilage tissue engineering and wound healing applications. For this purpose, the materials, as well as the production techniques, were specifically chosen for the intended uses.

In the first study for bone tissue engineering application, three dimensional and porous PHBV based nanofibrous cotton wool-like scaffolds with the average fiber diameter of 450-850 nm and an average porosity of 80-85% were produced by wet-electrospinning and freeze-drying techniques. Morphology of the scaffolds, which was suitable for tissue engineering applications favored osteoblast cell ingrowth and distribution within the scaffold. According to the biomineralization and *in-vitro* biocompatibility test results, HAP/PHBV-SF scaffold could be considered as a promising filling material for bone regeneration. However, the results showed that there was no statistically significant difference in the ALP values of the scaffolds during the 10 days of cell culture. Therefore, it is suggested to determine bone-forming ability of the scaffolds by long-term cell culture studies (at least 21 days) *via* ALP and osteocalcin assays. Besides, in order to enhance mineralization tendency of the scaffolds, different bioactive ceramics such as strontium-doped HAP or bioactive glass can be used.

In the cartilage tissue engineering study, PHBV nanofiber reinforced CMCht - silk hydrogel scaffolds that were cross-linked by PEGDE at three different concentrations were prepared so as to mimic the composite structure of the cartilage ECM. SEM images showed that all the scaffolds have interconnnected microporous structure. In addition, PHBV nanofibers were well incorporated into the pore walls of the composite scaffolds. However, CMCht-SF1:PEGDE2 and PNFs/CMCht-SF1:PEGDE2 scaffolds could not maintain their dimensional stabilities as they collapsed after freeze-drying. Therefore, this cross-linking ratio was eliminated for further analyses. According to

DMA, thermal, mechanical and *in-vitro* test results PNFs/CMCht-SF1:PEGDE1 scaffold showed better properties in terms of damping capability, thermal stability, compressive strength, and chondrogenic differentiation. Consequently, this scaffold would be a promising candidate for cartilage tissue regeneration. Even though, CMCht, silk and PHBV are considered as biodegradable polymers, it is suggested to perform the biodegradability studies of the produced scaffolds to estimate the degradation time and behavior.

Lastly, in the wound healing study, three-dimensional, porous CMCht-alginate modified cotton hydrogel wound dressings were produced by cross-linking with different concentrations of $CaCl_2$ solution. SEM images showed that wound dressings maintained their porous structure after polymer impregnation. All the hydrogel wound dressings showed viscoelastic properties according to the DMA results and the dressing with the lowest $CaCl_2$ concentration had the best damping capability. Antibacterial hydrogel wound dressings with 7.5 mg/ml nisin showed an antibacterial activity against gram-positive *S. aureus*, however they did not have any antibacterial effect against gram-negative *E. coli*. On the other hand, wound dressing without nisin exhibited bactericidal property to *E. coli* only. In order to understand how long the antibacterial effect is sustained, it is recommended to perform a releasing study followed by an antibacterial test. In addition, wound dressings should have sufficient water vapor transmission rate to provide a moist environment in the wound bed; therefore, water vapor permeability test can be performed. It is also recommended to determine the strength and elasticity of the wound dressings.

REFERENCES

Achilias, D. S., Karabela, M. M., Varkopoulou, E. A., & Sideridou, I. D. (2012). Cure kinetics study of two epoxy systems with fourier tranform infrared spectroscopy (FTIR) and differential scanning calorimetry (DSC). *Journal of Macromolecular Science, Part A, 49* (8), 630-638.

Ahmadi, F., Giti, R., Mohammadi-Samani, S., & Mohammadi, F. (2017). Biodegradable Scaffolds for Cartilage Tissue Engineering. *Galen Medical Journal*, *6* (2), 70-80.

Ahmed, E. M. (2015). Hydrogel: Preparation, characterization, and applications: A review. *Journal of Advanced Research, 6* (2), 105-121.

Ai, J., Heidari, K. S., Ghorbani, F., Ejazi, F., Biazar, E., Asefnejad, A., et al. (2011). Fabrication of coated-collagen electrospun PHBV nanofiber film by plasma method and its cellular study. *Journal of Nanomaterials*, 2011, 1-8.

Ainola, M., Tomaszewski, W., Ostrowska, B., Wesolowska, E., Wagner, H. D., Swieszkowski, W., et al. (2016). A bioactive hybrid three-dimensional tissue-engineering construct for cartilage repair. *Journal of Biomaterials Applications*, *30* (6), 873-885.

Akbarzadeh, R., & Yousefi, A. M. (2014). Effects of processing parameters in thermally induced phase separation technique on porous architecture of scaffolds for bone tissue engineering. *Journal of Biomedical Materials Research Part B*: *Applied Biomaterials*, *102* (6), 1304-1315.

Alboofetileh, M., Rezaei, M., Hosseini, H., & Abdollahi, M. (2014). Antimicrobial activity of alginate/clay nanocomposite films enriched with essential oils against three common foodborne pathogens. *Food Control*, *36* (1), 1-7.

Altman, G. H., Diaz, F., Jakuba, C., Calabro, T., Horan, R. L., Chen, J., et al. (2003). Silk-based biomaterials. *Biomaterials*, *24* (3), 401-416.

Andiappan, M., Sundaramoorthy, S., Panda, N., Meiyazhaban, G., Winfred, S. B., Venkataraman, G., & Krishna, P. (2013). Electrospun eri silk fibroin scaffold coated with hydroxyapatite for bone tissue engineering applications. *Progress in Biomaterials*, *2* (6), 1-11.

Anjum, S., Arora, A., Alam, M., & Gupta, B. (2016). Development of antimicrobial and scar preventive chitosan hydrogel wound dressings. *International Journal of Pharmaceutics*, *508* (1-2), 92-101.

Armentano, I., Dottori, M., Fortunati, E., Mattioli, S., & Kenny, J. (2010). Biodegradable polymer matrix nanocomposites for tissue engineering: a review. *Polymer Degradation and Stability*, *95* (11), 2126-2146.

Armiento, A., Stoddart, M., Alini, M., & Eglin, D. (2017). Biomaterials for articular cartilage tissue engineering: Learning from biology. *Acta Biomaterialia*, *65*, 1-20.

Avalle, M., Belingardi, G., & Montanini, R. (2001). Characterization of polymeric structural foams under compressive impact loading by means of energy-absorption diagram. *International Journal of Impact Engineering*, *25* (5), 455-472.

Badr, M., Amer, A., & Shehat, A. (2010). Synthesis and characterization of waterborne epoxy resins for coating application. *Australian Journal of Basic and Applied Science*, *4* (6), 1376-1382.

Bartnikowski, M., Wellard, R., Woodruff, M., & Klein, T. (2015). Tailoring hydrogel viscoelasticity with physical and chemical crosslinking. *Polymers*, *7* (12), 2650-2669.

Barud, H. O., Barud, H. d. S., Cavicchioli, M., do Amaral, T. S., de Oliveira Junior, O. B., Santos, D. Met al. (2015). Preparation and characterization of a bacterial cellulose/silk fibroin sponge scaffold for tissue regeneration. *Carbohydrate Polymers*, *128,* 41-51.

Bas, O., De-Juan-Pardo, E. M., Meinert, C., D'Angella, D., Baldwin, J. G., Bray, L. J., et al (2017). Biofabricated soft network composites for cartilage tissue engineering. *Biofabrication, 9* (2), 025014.

Basha, R. Y., & Doble, M. (2015). Design of biocomposite materials for bone tissue regeneration. *Materials Science and Engineering: C*, *57*, 452-463.

Bhardwaj, N., & Kundu, S. C. (2010). Electrospinning: a fascinating fiber fabrication technique. *Biotechnology Advances*, *28* (3), 325-347.

Bhattarai, N., Gunn, J., & Zhang, M. (2010). Chitosan-based hydrogels for controlled, localized drug delivery. *Advanced Drug Delivery Reviews*, *62* (1), 83-99.

Boateng, J. S., Matthews, K. H., Stevens, H. N., & Eccleston, G. M. (2008). Wound healing dressings and drug delivery systems: a review. *Journal of Pharmaceutical Sciences*, *97* (8), 2892-2923.

Bower, C., Parker, J., Higgins, A., Oest, M., Wilson, J., Valentine, B., et al. (2002). Protein antimicrobial barriers to bacterial adhesion: *in-vitro* and *in-vivo* evaluation of nisin-treated implantable materials. *Colloids and Surfaces B: Biointerfaces*, *25* (1), 81-90.

Butcher, A. L., Offeddu, G. S., & Oyen, M. L. (2014). Nanofibrous hydrogel composites as mechanically robust tissue engineering scaffolds. *Trends in Biotechnology*, *32* (11), 564-570.

Byju, A. G., & Kulkarni, A. (2013). Mechanics of Gelatin and Elastin based hydrogels as Tissue Engineered Constructs. *13th International Conference on Fracture*. Beijing, China, 1-10.

Cao, Y., Ding, Y., Zhang, L., Shi, G., Sang, X., & Ni, C. (2018). Preparation of surface-modified, micrometer-sized carboxymethyl chitosan drug-loaded microspheres. *Journal of Applied Polymer Science*, *135* (4), 1-7.

Cardona, A. F., & Wilson, S. E. (2015). Skin and soft-tissue infections: a critical review and the role of telavancin in their treatment. *Clinical Infectious Diseases*, *61 (suppl_2),* S69-S78.

Chan, B., & Leong, K. (2008). Scaffolding in tissue engineering: general approaches and tissue-specific considerations. *European Spine Journal*, *17* (4), 467-479.

Chang, H.-I., & Wang, Y. (2011). *Cell responses to surface and architecture of tissue engineering scaffolds Regenerative medicine and tissue engineering-cells and biomaterials*. London: InTech.

Chapekar, M. S. (2000). Tissue engineering: challenges and opportunities. *Journal of Biomedical Materials Research Part A*, *53* (6), 617-620.

Chen, C.-Y., Ke, C.-J., Yen, K.-C., Hsieh, H.-C., Sun, J.-S., & Lin, F.-H. (2015). 3D porous calcium-alginate scaffolds cell culture system improved human osteoblast cell clusters for cell therapy. *Theranostics*, *5* (6), 643-655.

Chen, G., Ushida, T., & Tateishi, T. (2002). Scaffold design for tissue engineering. *Macromolecular Bioscience*, *2* (2), 67-77.

Chen, H., Xing, X., Tan, H., Jia, Y., Zhou, T., Chen, Y., et al. (2017). Covalently antibacterial alginate-chitosan hydrogel dressing integrated gelatin microspheres

containing tetracycline hydrochloride for wound healing. *Materials Science and Engineering: C*, *70*, 287-295.

Chen, K., Zhang, D., Yang, X., Zhang, X., & Wang, Q. (2016). Research on viscoelastic behavior and mechanism of hydrogel grafted with UHMWPE. *Soft Materials*, *14* (4), 244-252.

Chen, Y., Wang, H., Yu, J., Wang, Y., Zhu, J., & Hu, Z. (2017). Mechanically strong and pH-responsive carboxymethyl chitosan/graphene oxide/polyacrylamide nanocomposite hydrogels with fast recoverability. *Journal of Biomaterials Science, Polymer Edition*, *28* (16), 1899-1917.

Chen, Z., Cao, S., Wang, H., Li, Y., Kishen, A., Deng, X., et al. (2015). Biomimetic remineralization of demineralized dentine using scaffold of CMC/ACP nanocomplexes in an *in-vitro* tooth model of deep caries. *PloS One*, *10* (1), e0116553.

Cheng, M.-L., & Sun, Y.-M. (2009). Relationship between free volume properties and structure of poly (3-hydroxybutyrate-co-3-hydroxyvalerate) membranes *via* various crystallization conditions. *Polymer*, *50* (22), 5298-5307.

Chung, C., Lee, M., & Choe, E. K. (2004). Characterization of cotton fabric scouring by FT-IR ATR spectroscopy. *Carbohydrate Polymers*, *58* (4), 417-420.

Coburn, J. M., Gibson, M., Monagle, S., Patterson, Z., & Elisseeff, J. H. (2012). Bioinspired nanofibers support chondrogenesis for articular cartilage repair. *Proceedings of the National Academy of Sciences*, *109* (25), 10012-10017.

Colomer, M. (2013). Straightforward synthesis of Ti-doped YSZ gels by chemical modification of the precursors alkoxides. *Journal of Sol-Gel Science and Technology*, *67* (1), 135-144.

Colpankan Gunes, O., Unalan, I., Cecen, B., Ziylan Albayrak, A., Havitcioglu, H., Ustun, O., & Ergur, B. U. (2019). Three-dimensional silk impregnated HAp/PHBV nanofibrous scaffolds for bone regeneration. *International Journal of Polymeric Materials and Polymeric Biomaterials*, *68* (5), 214-228.

da Silva, T. L., Vidart, J. M. M., da Silva, M. G. C., Gimenes, M. L., & Vieira, M. G. A. (2017). *Alginate and Sericin: environmental and pharmaceutical applications. Biological activities and application of marine polysaccharides*. London: InTech.

Daemi, H., & Barikani, M. (2012). Synthesis and characterization of calcium alginate nanoparticles, sodium homopolymannuronate salt and its calcium nanoparticles. *Scientia Iranica*, *19* (6), 2023-2028.

De Mori, A., Peña Fernández, M., Blunn, G., Tozzi, G., & Roldo, M. (2018). 3D printing and electrospinning of composite hydrogels for cartilage and bone tissue engineering. *Polymers*, *10* (3), 285.

Dhandayuthapani, B., Yoshida, Y., Maekawa, T., & Kumar, D. S. (2011). Polymeric scaffolds in tissue engineering application: a review. *International Journal of Polymer Science*, 1-19.

Díez-Pascual, A. M., & Díez-Vicente, A. L. (2016). Electrospun fibers of chitosan-grafted polycaprolactone/poly(3-hydroxybutyrate-co-3-hydroxyhexanoate) blends. *Journal of Materials Chemistry B*, *4* (4), 600-612.

Dimida, S., Barca, A., Cancelli, N., De Benedictis, V., Raucci, M. G., & Demitri, C. (2017). Effects of Genipin Concentration on Cross-Linked Chitosan Scaffolds for Bone Tissue Engineering: Structural Characterization and Evidence of Biocompatibility Features. *International Journal of Polymer Science*, 2017, 1-8.

Ebnesajjad, S. (2012). *Handbook of biopolymers and biodegradable plastics: properties, processing and applications*. New York: William Andrew.

Eslahi, N., Simchi, A., Mehrjoo, M., Shokrgozar, M. A., & Bonakdar, S. (2016). Hybrid cross-linked hydrogels based on fibrous protein/block copolymers and layered silicate nanoparticles: tunable thermosensitivity, biodegradability and mechanical durability. *RSC Advances*, *6* (67), 62944-62957.

Ferreira, P., Calvinho, P., Cabrita, A. S., Schacht, E., & Gil, M. H. (2006). Synthesis and characterization of new methacrylate based hydrogels. *Revista Brasileira de Ciências Farmacêuticas*, *42* (3), 419-427.

Fouchal, F., Knight, J., & Dickens, P. M. (2004). Monitoring the polymerization of a diglycidyl ether bisphenol-A/2, 2′-dimethyl-4, 4′-methylenebis (cyclohexylamine) matrix with a Fourier transform infrared optical fibre sensor. *Proceedings of the Institution of Mechanical Engineers, Part L: Journal of Materials: Design and Applications*, *218* (4), 331-342.

Fox, S. A. J., Bedi, A., & Rodeo, S. A. (2009). The basic science of articular cartilage: structure, composition, and function. *Sports Health*, *1* (6), 461-468.

Frantz, C., Stewart, K. M., & Weaver, V. M. (2010). The extracellular matrix at a glance. *Journal of Cell Science*, *123* (24), 4195-4200.

Gámiz-González, M. A., Edlund, U., Vidaurre, A., & Gomez Ribelles, J. L. (2017). Synthesis of highly swellable hydrogels of water-soluble Carboxymethyl chitosan and Poly (ethylene glycol). *Polymer International*, *66,* 1624–1632.

Gang, E. H., Ki, C. S., Kim, J. W., Lee, J., Cha, B. G., Lee, K. H., & Park, Y. H. (2012). Highly porous three-dimensional poly (lactide-co-glycolide) (PLGA) microfibrous scaffold prepared by electrospinning method: A comparison study with other PLGA type scaffolds on its biological evaluation. *Fibers and Polymers*, *13* (6), 685-691.

Gonçalves, R. C., da Silva, D. P., Signini, R., & Naves, P. L. F. (2017). Inhibition of bacterial biofilms by carboxymethyl chitosan combined with silver, zinc and copper salts. *International Journal of Biological Macromolecules*, *105*, 385-392.

González, M. G., Cabanelas, J. C., & Baselga, J. (2012). *Infrared Spectroscopy-Materials Science, Engineering and Technology*. London: InTech.

Greiner, A., & Wendorff, J. H. (2007). Electrospinning: a fascinating method for the preparation of ultrathin fibers. *Angewandte Chemie International Edition*, *46* (30), 5670-5703.

Gugjoo, M., Amarpal, G., Aithal, H., & Kinjavdekar, P. (2016). Cartilage tissue engineering: Role of mesenchymal stem cells along with growth factors & scaffolds. *The Indian Journal of Medical Research*, *144* (3), 339-347.

Gunatillake, P. A., & Adhikari, R. (2003). Biodegradable synthetic polymers for tissue engineering. *European Cell & Materials*, *5* (1), 1-16.

Haugh, M. G., Murphy, C. M., & O'Brien, F. J. (2009). Novel freeze-drying methods to produce a range of collagen–glycosaminoglycan scaffolds with tailored mean pore sizes. *Tissue Engineering Part C: Methods*, *16* (5), 887-894.

Holzwarth, J. M., & Ma, P. X. (2011a). 3D nanofibrous scaffolds for tissue engineering. *Journal of Materials Chemistry*, *21* (28), 10243-10251.

Holzwarth, J. M., & Ma, P. X. (2011b). Biomimetic nanofibrous scaffolds for bone tissue engineering. *Biomaterials*, *32* (36), 9622-9629.

Hong, Z., Qiu, X., Sun, J., Deng, M., Chen, X., & Jing, X. (2004). Grafting polymerization of L-lactide on the surface of hydroxyapatite nano-crystals. *Polymer*, *45* (19), 6699-6706.

Huang, Z.-M., Zhang, Y.-Z., Kotaki, M., & Ramakrishna, S. (2003). A review on polymer nanofibers by electrospinning and their applications in nanocomposites. *Composites Science and Technology*, *63* (15), 2223-2253.

Hurler, J., Engesland, A., Poorahmary Kermany, B., & Škalko-Basnet, N. (2012). Improved texture analysis for hydrogel characterization: gel cohesiveness, adhesiveness, and hardness. *Journal of Applied Polymer Science*, *125* (1), 180-188.

Iwasaki, N., Kasahara, Y., Yamane, S., Igarashi, T., Minami, A., & Nisimura, S.-i. (2010). Chitosan-based hyaluronic acid hybrid polymer fibers as a scaffold biomaterial for cartilage tissue engineering. *Polymers*, *3* (1), 100-113.

Jang, J.-H., Castano, O., & Kim, H.-W. (2009). Electrospun materials as potential platforms for bone tissue engineering. *Advanced Drug Delivery Reviews*, *61* (12), 1065-1083.

Jones, D. S., Woolfson, A. D., & Djokic, J. (1996). Texture profile analysis of bioadhesive polymeric semisolids: mechanical characterization and investigation of interactions between formulation components. *Journal of Applied Polymer Science*, *61* (12), 2229-2234.

Jozala, A. F., de Lencastre Novaes, L. C., & Junior, A. P. (2015). *Nisin Concepts, Compounds and the Alternatives of Antibacterials*. London: InTech.

Kamoun, E. A., Kenawy, E.-R. S., & Chen, X. (2017). A review on polymeric hydrogel membranes for wound dressing applications: PVA-based hydrogel dressings. *Journal of Advanced Research*, *8* (3), 217-233.

Kanoujia, J., Singh, M., Singh, P., & Saraf, S. A. (2016). Novel genipin crosslinked atorvastatin loaded sericin nanoparticles for their enhanced antihyperlipidemic activity. *Materials Science and Engineering: C*, *69*, 967-976.

Kasuga, T., Obata, A., Maeda, H., Ota, Y., Yao, X., & Oribe, K. (2012). Siloxane-poly (lactic acid)-vaterite composites with 3D cotton-like structure. *Journal of Materials Science: Materials in Medicine*, *23* (10), 2349-2357.

Katti, D. S., Robinson, K. W., Ko, F. K., & Laurencin, C. T. (2004). Bioresorbable nanofiber-based systems for wound healing and drug delivery: Optimization of fabrication parameters. *Journal of Biomedical Materials Research Part B: Applied Biomaterials*, *70* (2), 286-296.

Kim, B.-S., Park, I.-K., Hoshiba, T., Jiang, H.-L., Choi, Y.-J., Akaike, T., & Cho, C.-S. (2011). Design of artificial extracellular matrices for tissue engineering. *Progress in Polymer Science*, *36* (2), 238-268.

Kim, H., Che, L., Ha, Y., & Ryu, W. (2014). Mechanically-reinforced electrospun composite silk fibroin nanofibers containing hydroxyapatite nanoparticles. *Materials Science and Engineering: C*, *40,* 324-335.

Kim, H. W., Lee, H. H., & Knowles, J. (2006). Electrospinning biomedical nanocomposite fibers of hydroxyapatite/poly (lactic acid) for bone regeneration. *Journal of Biomedical Materials Research Part A*, *79* (3), 643-649.

Kim, M. S., & Kim, G. (2014). Three-dimensional electrospun polycaprolactone (PCL)/alginate hybrid composite scaffolds. *Carbohydrate Polymers*, *114,* 213-221.

Kim, M. S., & Kim, G. H. (2014). Highly porous electrospun 3D polycaprolactone/β-TCP biocomposites for tissue regeneration. *Materials Letters*, *120*, 246-250.

Kim, S. H., Nam, Y. S., Lee, T. S., & Park, W. H. (2003). Silk fibroin nanofiber. Electrospinning, properties, and structure. *Polymer Journal*, *35* (2), 185-190.

Koehler, J., Brandl, F. P., & Goepferich, A. M. (2018). Hydrogel wound dressings for bioactive treatment of acute and chronic wounds. *European Polymer Journal*, *100,* 1-11.

Kokubo, T., & Takadama, H. (2006). How useful is SBF in predicting in vivo bone bioactivity?. *Biomaterials*, *27* (15), 2907-2915.

Kostakova, E., Seps, M., Pokorny, P., & Lukas, D. (2014). Study of polycaprolactone wet electrospinning process. *eXPRESS Polymer Letters*, *8* (8), 554-564.

Król, Ż., Malik, M., Marycz, K., & Jarmoluk, A. (2016). Physicochemical properties of biopolymer hydrogels treated by direct electric current. *Polymers*, *8* (7), 248.

Kumar Singh Yadav, H., & Shivakumar, H. (2012). *In-vitro* and *in-vivo* evaluation of pH-sensitive hydrogels of carboxymethyl chitosan for intestinal delivery of theophylline. *ISRN Pharmaceutics*, 2012.

Kumbar, S., James, R., Nukavarapu, S., & Laurencin, C. (2008). Electrospun nanofiber scaffolds: engineering soft tissues. *Biomedical Materials*, *3* (3), 034002.

Kundu, B., Rajkhowa, R., Kundu, S. C., & Wang, X. (2013). Silk fibroin biomaterials for tissue regenerations. *Advanced Drug Delivery Reviews*, *65* (4), 457-470.

Lawless, B. M., Sadeghi, H., Temple, D. K., Dhaliwal, H., Espino, D. M., & Hukins, D. W. (2017). Viscoelasticity of articular cartilage: Analysing the effect of induced stress and the restraint of bone in a dynamic environment. *Journal of the Mechanical Behavior of Biomedical Materials*, *75,* 293-301.

Lee, C.-T., Kung, P.-H., & Lee, Y.-D. (2005). Preparation of poly (vinyl alcohol)-chondroitin sulfate hydrogel as matrices in tissue engineering. *Carbohydrate Polymers*, *61* (3), 348-354.

Lee, K. Y., & Mooney, D. J. (2012). Alginate: properties and biomedical applications. *Progress in Polymer Science*, *37* (1), 106-126.

Lewandowska-Łańcucka, J., Mystek, K., Mignon, A., Van Vlierberghe, S., Łatkiewicz, A., & Nowakowska, M. (2017). Alginate-and gelatin-based bioactive photocross-linkable hybrid materials for bone tissue engineering. *Carbohydrate Polymers*, *157*, 1714-1722.

Li, B., Kennedy, J., Peng, J., Yie, X., & Xie, B. (2006). Preparation and performance evaluation of glucomannan–chitosan–nisin ternary antimicrobial blend film. *Carbohydrate Polymers*, *65* (4), 488-494.

Li, C., Vepari, C., Jin, H.-J., Kim, H. J., & Kaplan, D. L. (2006). Electrospun silk-BMP-2 scaffolds for bone tissue engineering. *Biomaterials*, *27* (16), 3115-3124.

Li, D., & Xia, Y. (2004). Electrospinning of nanofibers: reinventing the wheel? *Advanced Materials*, *16* (14), 1151-1170.

Li, P., Dai, Y.-N., Zhang, J.-P., Wang, A.-Q., & Wei, Q. (2008). Chitosan-alginate nanoparticles as a novel drug delivery system for nifedipine. *International Journal of Biomedical Science*, *4* (3), 221.

Li, S., Dong, S., Xu, W., Tu, S., Yan, L., Zhao, C., et al. (2018). Antibacterial Hydrogels. *Advanced Science*, *5* (5), 1700527.

Li, W. J., Laurencin, C. T., Caterson, E. J., Tuan, R. S., & Ko, F. K. (2002). Electrospun nanofibrous structure: a novel scaffold for tissue engineering. *Journal of Biomedical Materials Research*, *60* (4), 613-621.

Li, Y., Hu, W., Han, G., Lu, W., Jia, D., Hu, M., & Wang, D. (2018). Involvement of bone morphogenetic protein–related pathways in the effect of aucubin on the

promotion of osteoblast differentiation in MG63 cells. *Chemico-Biological Interactions*, *283*, 51-58.

Li, Z., Yang, J., & Loh, X. J. (2016). Polyhydroxyalkanoates: opening doors for a sustainable future. *NPG Asia Materials*, *8* (4), e265.

Lin, H. R., & Yeh, Y. J. (2004). Porous alginate/hydroxyapatite composite scaffolds for bone tissue engineering: preparation, characterization, and *in-vitro* studies. *Journal of Biomedical Materials Research Part B: Applied Biomaterials*, *71* (1), 52-65.

Liu, C., Xia, Z., & Czernuszka, J. (2007). Design and development of three-dimensional scaffolds for tissue engineering. *Chemical Engineering Research and Design*, *85* (7), 1051-1064.

Liu, H., Wang, C., Li, C., Qin, Y., Wang, Z., Yang, F., et al. (2018). A functional chitosan-based hydrogel as a wound dressing and drug delivery system in the treatment of wound healing. *RSC Advances*, *8* (14), 7533-7549.

Liu, M., Zeng, X., Ma, C., Yi, H., Ali, Z., Mou, X., et al. (2017). Injectable hydrogels for cartilage and bone tissue engineering. *Bone Research*, *5*, 17014.

Liu, X., & Ma, P. X. (2004). Polymeric scaffolds for bone tissue engineering. *Annals of Biomedical Engineering*, *32* (3), 477-486.

Liu, Y., & Chan-Park, M. B. (2009). Hydrogel based on interpenetrating polymer networks of dextran and gelatin for vascular tissue engineering. *Biomaterials*, *30* (2), 196-207.

Liu, Y., Lim, J., & Teoh, S.-H. (2013). Development of clinically relevant scaffolds for vascularised bone tissue engineering. *Biotechnology Advances*, *31* (5), 688-705.

LogithKumar, R., KeshavNarayan, A., Dhivya, S., Chawla, A., Saravanan, S., & Selvamurugan, N. (2016). A review of chitosan and its derivatives in bone tissue engineering. *Carbohydrate Polymers*, *151*, 172-188.

Lu, T., Li, Y., & Chen, T. (2013). Techniques for fabrication and construction of three-dimensional scaffolds for tissue engineering. *International Journal of Nanomedicine*, *8*, 337.

Lu, X., Xu, Y., Zheng, C., Zhang, G., & Su, Z. (2006). Ethylene glycol diglycidyl ether as a protein cross-linker: a case study for cross-linking of hemoglobin. *Journal of Chemical Technology and Biotechnology*, *81* (5), 767-775.

Ma, P. X. (2004). Scaffolds for tissue fabrication. *Materials Today*, *7* (5), 30-40.

Ma, P. X. (2008). Biomimetic materials for tissue engineering. *Advanced Drug Delivery Reviews*, *60* (2), 184-198.

Ma, P. X., & Zhang, R. (1999). Synthetic nano-scale fibrous extracellular matrix. *Journal of Biomedical Materials Research*, *46* (1), 60-72.

Maji, S., Agarwal, T., Das, J., & Maiti, T. K. (2018). Development of gelatin/carboxymethyl chitosan/nano-hydroxyapatite composite 3D macroporous scaffold for bone tissue engineering applications. *Carbohydrate Polymers*, *189*, 115-125.

Mangoni, M. L., McDermott, A. M., & Zasloff, M. (2016). Antimicrobial peptides and wound healing: biological and therapeutic considerations. *Experimental Dermatology*, *25* (3), 167-173.

Martina, M., & Hutmacher, D. W. (2007). Biodegradable polymers applied in tissue engineering research: a review. *Polymer International*, *56* (2), 145-157.

Martins, A., Reis, R., & Neves, N. (2008). Electrospinning: processing technique for tissue engineering scaffolding. *International Materials Reviews*, *53* (5), 257-274.

McGaw, L. J., Elgorashi, E. E., & Eloff, J. N. (2014). *Toxicological Survey of African Medicinal Plants*. Amsterdam: Elsevier.

Meli, L., Miao, J., Dordick, J. S., & Linhardt, R. J. (2010). Electrospinning from room temperature ionic liquids for biopolymer fiber formation. *Green Chemistry*, *12* (11), 1883-1892.

Mikos, A. G., & Temenoff, J. S. (2000). Formation of highly porous biodegradable scaffolds for tissue engineering. *Electronic Journal of Biotechnology*, *3* (2), 23-24.

Mir, M., Ali, M. N., Barakullah, A., Gulzar, A., Arshad, M., Fatima, S., & Asad, M. (2018). Synthetic polymeric biomaterials for wound healing: a review. *Progress in Biomaterials*, *7*, 1-21.

Mirahmadi, F., Tafazzoli-Shadpour, M., Shokrgozar, M. A., & Bonakdar, S. (2013). Enhanced mechanical properties of thermosensitive chitosan hydrogel by silk fibers for cartilage tissue engineering. *Materials Science and Engineering: C*, *33* (8), 4786-4794.

Mohamed, N. A., & Abd El-Ghany, N. A. (2017). Pyromellitimide benzoyl thiourea cross-linked carboxymethyl chitosan hydrogels as antimicrobial agents. *International Journal of Polymeric Materials and Polymeric Biomaterials*, *66* (17), 861-870.

Mohandas, A., Deepthi, S., Biswas, R., & Jayakumar, R. (2017). Chitosan based metallic nanocomposite scaffolds as antimicrobial wound dressings. *Bioactive Materials*, *3*, 267-277.

Mooney, D. J., Baldwin, D. F., Suh, N. P., Vacanti, J. P., & Langer, R. (1996). Novel approach to fabricate porous sponges of poly (D, L-lactic-co-glycolic acid) without the use of organic solvents. *Biomaterials*, *17* (14), 1417-1422.

Moonsri, P., Watanesk, R., Watanesk, S., Niamsup, H., & Deming, R. L. (2008). Fibroin membrane preparation and stabilization by polyethylene glycol diglycidyl ether. *Journal of Applied Polymer Science*, *108* (3), 1402-1406.

Moraes, M. A. d., Nogueira, G. M., Weska, R. F., & Beppu, M. M. (2010). Preparation and characterization of insoluble silk fibroin/chitosan blend films. *Polymers*, *2* (4), 719-727.

Murakami, K., Aoki, H., Nakamura, S., Nakamura, S.-i., Takikawa, M., Hanzawa, M., et al. (2010). Hydrogel blends of chitin/chitosan, fucoidan and alginate as healing-impaired wound dressings. *Biomaterials*, *31* (1), 83-90.

Nada, A.-A. M., Kamel, S., & El-Sakhawy, M. (2000). Thermal behaviour and infrared spectroscopy of cellulose carbamates. *Polymer Degradation and Stability*, *70* (3), 347-355.

Nair, L. S., & Laurencin, C. T. (2007). Biodegradable polymers as biomaterials. *Progress in Polymer Science*, *32* (8-9), 762-798.

Nam, Y. S., & Park, T. G. (1999). Porous biodegradable polymeric scaffolds prepared by thermally induced phase separation. *Journal of Biomedical Materials Research*, *47* (1), 8-17.

Naseri-Nosar, M., & Ziora, Z. M. (2018). Wound dressings from naturally-occurring polymers: A review on homopolysaccharide-based composites. *Carbohydrate Polymers*, *189*, 379-398.

Neri-Numa, I. A., Pessoa, M. G., Paulino, B. N., & Pastore, G. M. (2017). Genipin: A natural blue pigment for food and health purposes. *Trends in Food Science & Technology*, *67*, 271-279.

Niaz, T., Shabbir, S., Noor, T., Abbasi, R., Raza, Z. A., & Imran, M. (2018). Polyelectrolyte multicomponent colloidosomes loaded with nisin Z for enhanced antimicrobial activity against foodborne resistant pathogens. *Frontiers in Microbiology*, *8*, 1-19.

O'brien, F. J. (2011). Biomaterials & scaffolds for tissue engineering. *Materials Today*, *14* (3), 88-95.

Okamoto, M., & John, B. (2013). Synthetic biopolymer nanocomposites for tissue engineering scaffolds. *Progress in Polymer Science*, *38* (10), 1487-1503.

Paşcu, E. I., Stokes, J., & McGuinness, G. B. (2013). Electrospun composites of PHBV, silk fibroin and nano-hydroxyapatite for bone tissue engineering. *Materials Science and Engineering: C*, *33* (8), 4905-4916.

Patel, N. R., & Gohil, P. P. (2012). A review on biomaterials: scope, applications & human anatomy significance. *International Journal of Emerging Technology and Advanced Engineering*, *2* (4), 91-101.

Paul, W., & Sharma, C. P. (2004). Chitosan and alginate wound dressings: a short review. *Trends in Biomaterials and Artificial Organs*, *18* (1), 18-23.

Pereira, R. F., & Bartolo, P. J. (2016). Traditional therapies for skin wound healing. *Advances in Wound Care*, *5* (5), 208-229.

Perinelli, D. R., Fagioli, L., Campana, R., Lam, J. K., Baffone, W., Palmieri, G. F., et al. (2018). Chitosan-based nanosystems and their exploited antimicrobial activity. *European Journal of Pharmaceutical Sciences*, *117*, 8-20.

Pham, Q. P., Sharma, U., & Mikos, A. G. (2006). Electrospinning of polymeric nanofibers for tissue engineering applications: a review. *Tissue Engineering*, *12* (5), 1197-1211.

Pinho, E., & Soares, G. (2018). Functionalization of cotton cellulose for improved wound healing. *Journal of Materials Chemistry B*, *6* (13), 1887-1898.

Placet, V., & Foltête, E. (2010). Is Dynamic Mechanical Analysis (DMA) a non-resonance technique? *14th International Conference on Experimental Mechanics*. Politiers, France.

Pranoto, Y., Rakshit, S., & Salokhe, V. (2005). Enhancing antimicrobial activity of chitosan films by incorporating garlic oil, potassium sorbate and nisin. *LWT-Food Science and Technology*, *38* (8), 859-865.

Puppi, D., Chiellini, F., Piras, A., & Chiellini, E. (2010). Polymeric materials for bone and cartilage repair. *Progress in Polymer Science*, *35* (4), 403-440.

Raghunath, J., Rollo, J., Sales, K. M., Butler, P. E., & Seifalian, A. M. (2007). Biomaterials and scaffold design: key to tissue-engineering cartilage. *Biotechnology and Applied Biochemistry*, *46* (2), 73-84.

Ramakrishna, S. (2005). *An introduction to electrospinning and nanofibers*. Washington: World Scientific.

Reis, R. L., & Cohn, D. (2012). *Polymer based systems on tissue engineering, replacement and regeneration*. Berlin: Springer Science & Business Media.

Rosenthal, A. J. (2010). Texture profile analysis–how important are the parameters?. *Journal of Texture Studies*, *41* (5), 672-684.

Rudyardjo, D. I., & Wijayanto, S. (2017). The synthesis and characterization of hydrogel chitosan-alginate with the addition of plasticizer lauric acid for wound dressing application. *Journal of Physics: Conference Series*, *853* (1), 012042.

Sachlos, E., & Czernuszka, J. (2003). Making tissue engineering scaffold work: review on the application of SFF technology to the production of tissue engineering scaffolds. *European Cells and Materials*, *5*, 29-40.

Sahithi, K., Swetha, M., Ramasamy, K., Srinivasan, N., & Selvamurugan, N. (2010). Polymeric composites containing carbon nanotubes for bone tissue engineering. *International Journal of Biological Macromolecules*, *46* (3), 281-283.

Saladino, S., Di Leonardo, E., Salamone, M., Mercuri, D., Segatti, F., & Ghersi, G. (2014). Formulation of Different Chitosan Hydrogels for Cartilage Tissue Repair. *Chemical Engineering Transactions*, *38*, 505-510.

Sangkert, S., Meesane, J., Kamonmattayakul, S., & Chai, W. L. (2016). Modified silk fibroin scaffolds with collagen/decellularized pulp for bone tissue engineering in cleft palate: morphological structures and biofunctionalities. *Materials Science and Engineering: C*, *58*, 1138-1149.

Santiago Cintrón, M., Montalvo, J., Von Hoven, T., Rodgers, J., Hinchliffe, D., Madison, C., et al. (2016). Infrared imaging of cotton fiber bundles using a focal plane array detector and a single reflectance accessory. *Fibers*, *4* (4), 27.

Scannell, A. G., Hill, C., Ross, R., Marx, S., Hartmeier, W., & Arendt, E. K. (2000). Development of bioactive food packaging materials using immobilised bacteriocins Lacticin 3147 and Nisaplin®. *International Journal of Food Microbiology*, *60* (2-3), 241-249.

Seol, Y. J., Park, J. Y., Jeong, W., Kim, T. H., Kim, S. Y., & Cho, D. W. (2015). Development of hybrid scaffolds using ceramic and hydrogel for articular cartilage

tissue regeneration. *Journal of Biomedical Materials Research Part A*, *103* (4), 1404-1413.

Sharma, C., Gautam, S., Dinda, A. K., & Mishra, N. C. (2011). Cartilage tissue engineering: current scenario and challenges. *Advanced Materials Letters*, *2*, 90-99.

Shin, H., Jo, S., & Mikos, A. G. (2003). Biomimetic materials for tissue engineering. *Biomaterials*, *24* (24), 4353-4364.

Shoulders, M. D., & Raines, R. T. (2009). Collagen structure and stability. *Annual Review of Biochemistry, 78*, 929-958.

Sill, T. J., & von Recum, H. A. (2008). Electrospinning: applications in drug delivery and tissue engineering. *Biomaterials*, *29* (13), 1989-2006.

Simões, D., Miguel, S. P., Ribeiro, M. P., Coutinho, P., Mendonça, A. G., & Correia, I. J. (2018). Recent advances on antimicrobial wound dressing: a review. *European Journal of Pharmaceutics and Biopharmaceutics*, *127*, 130-141.

Smith, L. A., Liu, X., & Ma, P. X. (2008). Tissue engineering with nano-fibrous scaffolds. *Soft Materials*, *4* (11), 2144-2149.

Song, J.-H., Kim, H.-E., & Kim, H.-W. (2008). Electrospun fibrous web of collagen–apatite precipitated nanocomposite for bone regeneration. Journal of Materials Science: *Materials in Medicine*, *19* (8), 2925-2932.

Song, X., Ling, F., Ma, L., Yang, C., & Chen, X. (2013). Electrospun hydroxyapatite grafted poly (L-lactide)/poly (lactic-co-glycolic acid) nanofibers for guided bone regeneration membrane. *Composites Science and Technology*, *79*, 8-14.

Stiers, P.-J., van Gastel, N., & Carmeliet, G. (2016). Targeting the hypoxic response in bone tissue engineering: a balance between supply and consumption to improve bone regeneration. *Molecular and Cellular Endocrinology*, *432*, 96-105.

Sultana, N., & Wang, M. (2008). Fabrication of HA/PHBV composite scaffolds through the emulsion freezing/freeze-drying process and characterisation of the scaffolds. *Journal of Materials Science: Materials in Medicine*, *19* (7), 2555-2561.

Sun, B., Long, Y., Zhang, H., Li, M., Duvail, J., Jiang, X., & Yin, H. (2014). Advances in three-dimensional nanofibrous macrostructures *via* electrospinning. *Progress in Polymer Science*, *39* (5), 862-890.

Sun, F., Zhou, H., & Lee, J. (2011). Various preparation methods of highly porous hydroxyapatite/polymer nanoscale biocomposites for bone regeneration. *Acta Biomaterialia*, *7* (11), 3813-3828.

Swetha, M., Sahithi, K., Moorthi, A., Srinivasan, N., Ramasamy, K., & Selvamurugan, N. (2010). Biocomposites containing natural polymers and hydroxyapatite for bone tissue engineering. *International Journal of Biological Macromolecules*, *47* (1), 1-4.

Tamayol, A., Akbari, M., Annabi, N., Paul, A., Khademhosseini, A., & Juncker, D. (2013). Fiber-based tissue engineering: progress, challenges, and opportunities. *Biotechnology Advances*, *31* (5), 669-687.

Tang, Q., Pan, D., Sun, Y., Cao, J., & Guo, Y. (2017). Preparation, Characterization and Antimicrobial Activity of Sodium Alginate Nanobiocomposite Films Incorporated with E-Polylysine and Cellulose Nanocrystals. *Journal of Food Processing and Preservation*, *41* (5), e13120.

Taskin, M. B., Xu, R., Gregersen, H., Nygaard, J. V., Besenbacher, F., & Chen, M. (2016). Three-Dimensional Polydopamine Functionalized Coiled Microfibrous

Scaffolds Enhance Human Mesenchymal Stem Cells Colonization and Mild Myofibroblastic Differentiation. *ACS Applied Materials & Interfaces*, *8* (25), 15864-15873.

Temple, D. K., Cederlund, A. A., Lawless, B. M., Aspden, R. M., & Espino, D. M. (2016). Viscoelastic properties of human and bovine articular cartilage: a comparison of frequency-dependent trends. *BMC Musculoskeletal Disorders*, *17* (1), 419.

Thein-Han, W., Kitiyanant, Y., & Misra, R. (2008). Chitosan as scaffold matrix for tissue engineering. *Materials Science and Technology*, *24* (9), 1062-1075.

Thiré, R. M. d. S. M., Arruda, L. C., & Barreto, L. S. (2011). Morphology and thermal properties of poly (3-hydroxybutyrate-co-3-hydroxyvalerate)/attapulgite nanocomposites. *Materials Research*, *14* (3), 340-344.

Tissera, N. D., Wijesena, R. N., Rathnayake, S., de Silva, R. M., & de Silva, K. N. (2018). Heterogeneous in situ polymerization of polyaniline (PANI) nanofibers on cotton textiles: improved electrical conductivity, electrical switching, and tuning properties. *Carbohydrate Polymers*, *186*, 35-44.

Tuzlakoglu, K., Bolgen, N., Salgado, A., Gomes, M. E., Piskin, E., & Reis, R. (2005). Nano-and micro-fiber combined scaffolds: a new architecture for bone tissue engineering. *Journal of Materials Science: Materials in Medicine*, *16* (12), 1099-1104.

Unalan, I., Colpankan, O., Albayrak, A. Z., Gorgun, C., & Urkmez, A. S. (2016). Biocompatibility of plasma-treated poly (3-hydroxybutyrate-co-3-hydroxyvalerate) nanofiber mats modified by silk fibroin for bone tissue regeneration. *Materials Science and Engineering: C*, *68*, 842-850.

Ünalan, İ. (2015). *Production of biodegredable and biocompatible polymeric tissue scaffolds with different surface charges and evaluation of cell -scaffold interactions*. Master Thesis, Dokuz Eylül University, Izmir.

Varaprasad, K., Raghavendra, G. M., Jayaramudu, T., Yallapu, M. M., & Sadiku, R. (2017). A mini review on hydrogels classification and recent developments in miscellaneous applications. *Materials Science and Engineering: C*, *79,* 958-971.

Vargas, G., Acevedo, J., López, J., & Romero, J. (2008). Study of cross-linking of gelatin by ethylene glycol diglycidyl ether. *Materials Letters*, *62* (21-22), 3656-3658.

Vasita, R., & Katti, D. S. (2006). Nanofibers and their applications in tissue engineering. *International Journal of Nanomedicine*, *1* (1), 15.

Vepari, C., & Kaplan, D. L. (2007). Silk as a biomaterial. *Progress in Polymer Science*, *32* (8), 991-1007.

Vert, M., Doi, Y., Hellwich, K.-H., Hess, M., Hodge, P., Kubisa, P., et al. (2012). Terminology for biorelated polymers and applications (IUPAC Recommendations 2012). *Pure and Applied Chemistry*, *84* (2), 377-410.

Vishwanath, V., Pramanik, K., & Biswas, A. (2016). Optimization and evaluation of silk fibroin-chitosan freeze-dried porous scaffolds for cartilage tissue engineering application. *Journal of Biomaterials Science, Polymer Edition*, *27* (7), 657-674.

Vukomanović, M., Žunič, V., Kunej, Š., Jančar, B., Jeverica, S., & Suvorov, D. (2017). Nano-engineering the antimicrobial spectrum of lantibiotics: activity of nisin against gram negative bacteria. *Scientific Reports*, *7* (1), 4324.

Wahid, F., Yin, J.-J., Xue, D.-D., Xue, H., Lu, Y.-S., Zhong, C., & Chu, L.-Q. (2016). Synthesis and characterization of antibacterial carboxymethyl Chitosan/ZnO

nanocomposite hydrogels. *International Journal of Biological Macromolecules*, *88,* 273-279.

Wang, L., Wang, Y., Qu, J., Hu, Y., You, R., & Li, M. (2013). The cytocompatibility of genipin-crosslinked silk fibroin films. *Journal of Biomaterials and Nanobiotechnology*, *4* (03), 213.

Wei, Y., Sun, D., Yi, H., Zhao, H., & Wang, J. (2014). Preparation and characterization of PEGDE crosslinked silk fibroin film. *Journal of Wuhan University of Technology-Material Science Edition*, *29* (5), 1083-1089.

Weigel, T., Schinkel, G., & Lendlein, A. (2006). Design and preparation of polymeric scaffolds for tissue engineering. *Expert Review of Medical Devices*, *3* (6), 835-851.

Xu, H., Cai, S., Xu, L., & Yang, Y. (2014). Water-stable three-dimensional ultrafine fibrous scaffolds from keratin for cartilage tissue engineering. *Langmuir*, *30* (28), 8461-8470.

Yan, J., Miao, Y., Tan, H., Zhou, T., Ling, Z., Chen, Y., et al. (2016). Injectable alginate/hydroxyapatite gel scaffold combined with gelatin microspheres for drug delivery and bone tissue engineering. *Materials Science and Engineering: C*, *63,* 274-284.

Yan, L. P., Wang, Y. J., Ren, L., Wu, G., Caridade, S. G., Fan, J. B., et al. (2010). Genipin-cross-linked collagen/chitosan biomimetic scaffolds for articular cartilage tissue engineering applications. *Journal of Biomedical Materials Research Part A*, *95* (2), 465-475.

Yang, D., Wang, Y., Zhang, D., Liu, Y., & Jiang, X. (2009). Control of the morphology of micro/nanostructures of polycarbonate *via* electrospinning. *Chinese Science Bulletin*, *54* (17), 2911-2917.

Yang, J., Zhang, Y. S., Yue, K., & Khademhosseini, A. (2017). Cell-laden hydrogels for osteochondral and cartilage tissue engineering. *Acta Biomaterialia*, *57,* 1-25.

Yang, Q., Li, Z., Hong, Y., Zhao, Y., Qiu, S., Wang, C., & Wei, Y. (2004). Influence of solvents on the formation of ultrathin uniform poly (vinyl pyrrolidone) nanofibers with electrospinning. *Journal of Polymer Science Part B: Polymer Physics*, *42* (20), 3721-3726.

Yang, S. Y., Hwang, T. H., Che, L., Oh, J. S., Ha, Y., & Ryu, W. (2015). Membrane-reinforced three-dimensional electrospun silk fibroin scaffolds for bone tissue engineering. *Biomedical Materials*, *10* (3), 035011.

Yang, Z., Wu, Y., Li, C., Zhang, T., Zou, Y., Hui, J. H., et al. (2011). Improved mesenchymal stem cells attachment and *in-vitro* cartilage tissue formation on chitosan-modified poly (L-lactide-co-epsilon-caprolactone) scaffold. *Tissue Engineering Part A*, *18* (3-4), 242-251.

Yodmuang, S., McNamara, S. L., Nover, A. B., Mandal, B. B., Agarwal, M., Kelly, T.-A. N., et al. (2015). Silk microfiber-reinforced silk hydrogel composites for functional cartilage tissue repair. *Acta Biomaterialia*, *11,* 27-36.

Yokoyama, Y., Hattori, S., Yoshikawa, C., Yasuda, Y., Koyama, H., Takato, T., & Kobayashi, H. (2009). Novel wet electrospinning system for fabrication of spongiform nanofiber 3-dimensional fabric. *Materials Letters*, *63* (9), 754-756.

Zhang, H., Liu, X., Yang, M., & Zhu, L. (2015). Silk fibroin/sodium alginate composite nano-fibrous scaffold prepared through thermally induced phase-separation (TIPS) method for biomedical applications. *Materials Science and Engineering: C*, *55,* 8-13.

Zhang, Y., Venugopal, J. R., El-Turki, A., Ramakrishna, S., Su, B., & Lim, C. T. (2008). Electrospun biomimetic nanocomposite nanofibers of

hydroxyapatite/chitosan for bone tissue engineering. *Biomaterials*, *29* (32), 4314-4322.

Zhao, L., Gwon, H.-J., Lim, Y.-M., Nho, Y.-C., & Kim, S. Y. (2014). Hyaluronic acid/chondroitin sulfate-based hydrogel prepared by gamma irradiation technique. *Carbohydrate Polymers*, *102,* 598-605.

Zhou, H., & Lee, J. (2011). Nanoscale hydroxyapatite particles for bone tissue engineering. *Acta Biomaterialia*, *7* (7), 2769-2781.

Zhu, N., & Chen, X. (2013). Biofabrication of tissue scaffolds *Advances in Biomaterials Science and Biomedical Applications*. London: InTech.

Zohri, M., Alavidjeh, M. S., Haririan, I., Ardestani, M. S., Ebrahimi, S. E. S., Sani, H. T., & Sadjadi, S. K. (2010). A comparative study between the antibacterial effect of nisin and nisin-loaded chitosan/alginate nanoparticles on the growth of *Staphylococcus aureus* in raw and pasteurized milk samples. *Probiotics and Antimicrobial Proteins*, *2* (4), 258-266.

Zong, X., Kim, K., Fang, D., Ran, S., Hsiao, B. S., & Chu, B. (2002). Structure and process relationship of electrospun bioabsorbable nanofiber membranes. *Polymer*, *43* (16), 4403-4412.